CAPITAL UNIVERSITY OF SCIENCE AND TECHNOLOGY, ISLAMABAD

The Impact of Cattaneo-Christov Double Diffusion, Thermal Radiation on a Rotating Flow of Casson Nanofluid

by

Muhammad Samiullah

A thesis submitted in partial fulfillment for the degree of Master of Philosophy

in the

Faculty of Computing
Department of Mathematics

2023

*I dedicate my dissertation work to my **family** and dignified **teachers**. A special feeling of gratitude to my loving parents who have supported me in my studies.*

CERTIFICATE OF APPROVAL

The Impact of Cattaneo-Christov Double Diffusion, Thermal Radiation on a Rotating Flow of Casson Nanofluid

by

Muhammad Samiullah

(MMT213008)

THESIS EXAMINING COMMITTEE

(a)	External Examiner	Dr. Bilal Ahmed	University of Wah
(b)	Internal Examiner	Dr. Muhammad Sabeel Khan	CUST, Islamabad
(c)	Supervisor	Dr. Muhammad Sagheer	CUST, Islamabad

Dr. Muhammad Sagheer
Thesis Supervisor
September 2023

Dr. Muhammad Sagheer	Dr. M. Abdul Qadir
Head	Dean
Dept. of Mathematics	Faculty of Computing
September, 2023	September, 2023

Author's Declaration

I, **Muhammad Samiullah**, hereby state that my MPhil thesis titled "**The Impact of Cattaneo-Christov Double Diffusion, Thermal Radiation on a Rotating Flow of Casson Nanofluid**" is my own work and has not been submitted previously by me for taking any degree from Capital University of Science and Technology, Islamabad or anywhere else in the country/abroad.

At any time if my statement is found to be incorrect even after my graduation, the University has the right to withdraw my MPhil Degree.

(Muhammad Samiullah)

Registration No: MMT213008

Plagiarism Undertaking

I solemnly declare that research work presented in this thesis titled “**The Impact of Cattaneo-Christov Double Diffusion, Thermal Radiation on a Rotating Flow of Casson Nanofluid**” is solely my research work with no significant contribution from any other person. Small contribution/help wherever taken has been dully acknowledged and that complete thesis has been written by me.

I understand the zero tolerance policy of the HEC and Capital University of Science and Technology towards plagiarism. Therefore, I as an author of the above titled thesis declare that no portion of my thesis has been plagiarized and any material used as reference is properly referred/cited.

I undertake that if I am found guilty of any formal plagiarism in the above titled thesis even after award of MPhil Degree, the University reserves the right to withdraw my MPhil degree and that HEC and the University have the right to publish my name on the HEC/University website on which names of students are placed who submitted plagiarized work.

(Muhammad Samiullah)
Registration No: MMT213008

Acknowledgement

I got no words to articulate my cordial sense of gratitude to **Almighty Allah** who is the most merciful and most beneficent to his creation.

I also express my gratitude to the last prophet of **Almighty Allah, Prophet Muhammad (PBUH)** the supreme reformer of the world and knowledge for human being.

I would like to be thankful to all those who provided support and encouraged me during this work.

I would like to be grateful to my thesis supervisor **Dr. Muhammad Sagheer**, the Head of the Department of Mathematics, for guiding and encouraging towards writing this thesis. It would have remained incomplete without his endeavours. Due to his efforts I was able to write and complete this dissertation.

I would like to pay great tribute to my **parents**, for their prayers, moral support, encouragment and appreciation.

Last but not the least, I want to express my gratitude to my **friends** who helped me throughout in my MPhil degree.

(Muhammad Samiullah)

Abstract

The theoretical and numerical investigation of viscous dissipation and thermal radiation effects on Casson nanofluid flow over a stretching sheet has been carried out through the utilization of the shooting method. The primary objective of the current research is to comprehensively analyze the influence of viscous dissipation and thermal radiation, while incorporating the Cattaneo-Christov double diffusion model. Additionally, this study takes into account factors such as thermophoresis, diffusion, Brownian motion, thermal diffusivity, and chemical reaction, in the context of a Casson nanofluid flowing over an extensible sheet. The similarity transformations have been employed to convert the nonlinear partial differential equations into a set of ordinary differential equations. Tables and graphs vividly illustrate the impact of various parameters, including the magnetic field parameter, heat generation parameter, Prandtl number, thermophoresis parameter, Brownian motion parameter, and chemical reaction parameter. The findings indicate that as the rotation parameter increases, both the velocity and temperature profiles exhibit a decrease. As the Casson parameter β values increase, there is a decrease in the local Nusselt number values and a simultaneous increase in the Sherwood number.

Contents

List of Figures

List of Tables

Abbreviations

IVPs	Initial value problems
MHD	Magnetohydrodynamics
ODEs	Ordineary differential equations
PDEs	Partial differential equations
RK	Runge-Kutta

Symbols

μ	Viscosity
ρ	Density
ν	Kinematic viscosity
τ	Stress tensor
k	Thermal conductivity
α	Thermal diffisuitivity
σ	Electrical conductivity
u	x-component of fluid velocity
v	y-component of fluid velocity
w	z-component of fluid velocity
B_0	Magnetic field constant
Γ_c	relaxation time for mass flux
Γ_e	relaxation time for heat flux
Ω	angular velocity
a	Stretching constant
T_w	Temperature of the wall
T_∞	Ambient temperature of the nanofluid
T	Temperature
C_w	Concentration of the wall
C_∞	Ambient concentration of the nanofluid
C	Concentration
ρ_f	Density of the fluid
μ_f	Viscosity of the fluid

ν_f	Kinematic viscosity of the base fluid
ρ_{nf}	Density of the nanofluid
μ_{nf}	Viscosity of the nanofluid
q_r	Radiative heat flux
q	Heat generation constant
q_w	Heat flux
q_m	Mass flux
σ^*	Stefan Boltzmann constant
k^*	Absorption coefficient
ψ	Stream function
θ	Stream function
ϕ	Stream function
η	Similarity variable
χ	Similarity variable
C_{fx}	Skin friction coefficient along x direction
C_{fy}	Skin friction coefficient along y direction
Nu	Nusselt number
Nu_x	Local Nusselt number
Sh	Sherwood number
Sh_x	Local Sherwood number
Re	Reynolds number
Re_x	Local Reynolds number
ϕ	Nanoparticle volume fraction
Nb	Brownian motion parameter
Nt	Thermophoresis parameter
M	Magnetic parameter
α_f	Thermal diffusivity
λ_C	relaxation time Parameter of concentration
λ_E	relaxation time Parameter of temperature
Ec	Eckert number
Pr	Prandtl number

ϵ	heat generation/absorption parameter
Q	heat generation/absorption coefficient
Bi	Biot number
Sc	Schmidt number
K_c^*	rate of chemical reaction
K_c	Chemical reaction parameter
γ_1	rotation parameter
ρ_f	Density of the pure fluid
μ_{nf}	Viscosity of the nanofluid
μ_f	Viscosity of the base fluid
$(\rho c_p)_f$	Heat capacitance of fluid
σ_f	Electrical conductivity of the fluid
κ_f	Thermal conductivity of the fluid
D_T	Thermophortic diffusion coefficient
D_B	Brownian diffusion coefficient
f	Dimensionless velocity
g	Dimensionless velocity
θ	Dimensionless temperature
ϕ	Dimensionless concentration

Chapter 1

Introduction

A specific branch in the study of fluid mechanics that focuses on delineating the fluids motion, like gases and liquids is said to be fluid dynamics. Within the widely acknowledged field of fluid mechanics, distinct branches such as aerodynamics and hydrodynamics are notable components of fluid dynamics. This encompasses a diverse range of practical applications, including the computation of forces and moments, estimation of oil mass flow rates in pipelines, prediction of weather patterns, exploration of interstellar nebulae, and the practice of modeling. Zhao and Collins [1] were the first who introduced fluid dynamics through their experimental work. This innovation paved the way for additional research and offered humanity a platform to extract further advancements from it. The initial contributions to the field of fluid dynamics had been done by Li et al. [2], Eisazadeh et al. [3] and Wang et al. [4] etc.

The introduction of colloidal suspensions of nanoparticles into base fluids has introduced a novel category of fluids known as nanofluids. Nanofluids exhibit extraordinary properties that the conventional fluids were unlikely to achieve through traditional means of technology. When conventional fluids are infused with nano-sized particles, they demonstrate improved strength, chemical reactivity, electrical conductivity, supermagnetic attributes, and notably, enhanced heat transfer and thermal conductivity. The utilization of nanofluids in sectors such as aeronautics, medicine, pharmaceutics, and photoelectricity has yielded remarkable advancements. For instance, applications like brake fluids, nuclear reactions, enhancements in cooling transformer oil, and power plant efficiency improvements have showcased notable breakthroughs. The term "nanofluids" was introduced through experimental work conducted by Choi and Eastman [5]. The foundational research on nanofluids was conducted by Wang and Majumdar [6], Yang et al. [7], and Jahani et al. [8].

A fluid that exhibits shear-thinning behavior, with a theoretical infinite viscosity at zero shear rate and a viscosity of zero at an infinite shear rate, is referred to as a Casson nanofluid. In comparison to Newtonian-based nanofluid flow, Casson nanofluids are more advantageous as cooling and friction-reducing agents. Casson fluids include various examples such as honey, jelly, sauce, and soup etc. Applications of Casson nanofluids span various sectors, including heat transfer and cooling systems, biomedical and pharmaceutical, food industry, cosmetics and personal care, oil and gas industrial processing and automotive. The earliest work on Casson nanofluid was done by Casson et al. [9] to forecast fluid attributes bearing similarity to printing ink. A series-based remedy to tackle heat and mass transfer occurences for a non Newtonian fluid is examined by Nadeem et al. [10]. According to their findings, variations in the Casson parameter, whether positive or negative, give rise to relocations of the stagnation point concerning its initial position. The study by Butt et al. [11] focused on elucidating the heat transfer properties in the context of boundary layer flow for a Casson rotating fluid on a extending surface.

The research conducted by Gorla et al. [12] delved into the analysis of flow in boundary layer for nanofluids, incorporating the buoyancy force impacts. Shehzad et al. [13] investigated various types of nanoparticles in order to examine the peristaltic transport behavior of nanofluids. Additionally, they introduced two models, namely Maxwell and Hamilton Crosser, to facilitate a comparative analysis of their findings. Sheikholeslami et al. [14–18] investigated the heat transfer behaviours and flow patterens of a nanofluid across diverse geometric setups while considering a variety of boundary conditions. Hayat et al. [19] introduced the concept of Newtonian mass flux condition within the context of nanofluid flow around a permeable stretching cylinder. Presently, numerous researchers are integrating magnetohydrodynamic flow into their studies, motivated by its broad industrial use in applications involving solar atmosphere and laboratory plasmas.

The examination of fluid motion with rotation that gives rise to the Coriolis force finds noteworthy applications in a range of disciplines, including astrophysics, oceanography, and various geophysical situations. Moreover, this specific flow pattern over a stretching surface is employed across various domains. Wang [20] considered a two-dimensional stretchable surface to investigate the issue of rotating fluid flow. Moreover, when the rotational parameter outran unity, he gained a precise solution through analytical means, afterward contrasting it with the numerical technique. Zaimi et al. [21] employed the Keller-box method to analyze the rotating flow due to a stretching surface by considering a non-Newtonian viscoelastic fluid.

Rashidi et al. [22] employed the law of increased Entropy to present an analysis of Entropy generation in the context of rotating nanofluid flow. Mabood et al. [23] conducted an investigation into the impact of Brownian motion and thermophoresis on the flow of rotating nanofluid. This analysis was carried out considering the presence of magnetic fields, radiation, viscous dissipation effects, heat source etc. The research executed by Das et al. [24] centered on investigating how transient hydromagnetic Couette flow of a viscous fluid is influenced by both magnetic fields and rotation. The study revealed a substantial alteration in fluid velocity resulting from the combined effects. Ali et al. [25] investigated various types of nanoparticles to analyze how magnetic fields within a rotational setup modifies Couette flow.

Radiation heat transfer plays a peripheral role in numerous engineering processes that take place under high-temperature conditions. A significant quantity of both experimental and theoretical research has been undertaken by numerous scholars to explore the impact of radiation effects [26–29]. Hayat et al. [30] introduced a novel boundary condition known as zero nanoparticle mass flux. This condition was put into practice to inspect the impact in viscoelastic fluid for three-dimensional flow due to thermal radiations act as nonlinear.

1.1 Thesis Contributions

Within the thesis, comprehensive examine a specific rotating nanofluid flow presented by Archana et al. [31] through a review study. The ongoing study is directed towards conducting a theoritical and numerical analysis of the Cattaneo-Christov double diffusion within a rotating flow of Casson nanofluid over a stretching sheet, incorporating the impact of inclined magnetic field, porous medium, chemical reaction and heat source/sink which has not yet been explored. The current research aims to address this research gap, and the outcomes of the present study present a novel contribution to the existing literature. Throughout the procedure, nonlinear partial differential equations (PDEs) have been transformed using similarity transformations into a system of dimensionless ordinary differential equations (ODEs), and the outcomes have been generated through the shooting method. The numerical outcomes are visually derived with the assistance of MATLAB. The influence of key parameters on velocity distributions $f'(\eta)$ and $g(\eta)$, temperature distribution $\theta(\eta)$, concentration distribution $\phi(\eta)$, skin friction coefficients Cf_x and Cf_y, local Nusselt number Nu_x and local Sherwood number Sh_x has been examined through graphical representations and tabular presentations.

1.2 Layout of Thesis

The following is a quick summary about thesis contents.

Chapter 2 covers fundamental definitions along definite nomenclature which would be imperative and dicussed afterward.

Chapter 3 provides the proposed analytical evaluation of a Casson nanofluid flow on a stretching surface effected by thermal radiation with magnetic field effect and shooting methodology is used to generate the numerical solutions of the governing flow model.

Chapter 4 extends the proposed model flow mentioned in Chapter 3 by including the Cattaneo-Christov double diffusion, Casson nanofluid and chemical reaction effects.The shooting methodology is used to generate the numerical solutions of the governing flow model.

Chapter 5 serves the section in which thesis concludes.

The **Biblography** provides all the refrences which are utilized in the thesis.

Chapter 2

Preliminaries

The present chapter outlines crucial definitions and governing laws, that will serve as a foundation in forthcoming chapters.

2.1 Some Fundamental Terminologies

Definition 2.1.1 (Fluid)
"A substance that cannot keep its own shape but instead adopts that of its container is referred to as a fluid." [32]

Definition 2.1.2 (Fluid Mechanics)
"The fluid mechanics is defined as the science that deals with the behavior of fluids at rest or in motion, and the interaction of fluids with solids or other fluids at the boundaries." [33]

Definition 2.1.3 (Fluid Dynamics)
"The study of fluid if the pressure forces are also considered for the fluids in motion, that branch of science is called fluid dynamics." [33]

Definition 2.1.4 (Fluid Statics)
"The study of fluid at rest is called fluid statics." [33]

Definition 2.1.5 (Viscosity)

"Viscosity is defined as the property of a fluid which offers resistance to the movement of one layer of fluid over another adjacent layer of the fluid. Mathematically,

$$\mu = \frac{\tau}{\frac{\partial u}{\partial y}},$$

where μ is viscosity coefficient, τ is shear stress and $\frac{\partial u}{\partial y}$ represents the velocity gradient." [33]

Definition 2.1.6 (Kinematic Viscosity)

"It is defined as the ratio between the dynamic viscosity and density of fluid. It is denoted by symbol ν called **'nu'**. Mathematically,

$$\nu = \frac{\mu}{\rho}.\text{" [33]}$$

Definition 2.1.7 (Thermal Conductivity)

"The Fourier heat conduction law states that the heat flow is proportional to the temperature gradient. The coefficient of proportionality is a material parameter known as the thermal conductivity which may be a function of a number of variables." [34]

Definition 2.1.8 (Thermal Diffusivity)

"The rate at which heat diffuses by conducting through a material depends on the thermal diffusivity. It can be defined as,

$$\alpha = \frac{k}{\rho C_p},$$

where α is the thermal diffusivity, k is the thermal conductivity, ρ is the density and C_p is the specifc heat at constant pressure." [34]

2.2 Types of Fluid

Definition 2.2.1 (Ideal Fluid)

"A fluid, which is incompressible and has no viscosity, is known as an ideal fluid. Ideal fluid is only an imaginary fluid as all the fluids, which exist, have some viscosity." [33]

Definition 2.2.2 (Real Fluid)

"A fluid, which possesses viscosity, is known as a real fluid. In actual practice, all the fluids are real fluids." [33]

Definition 2.2.3 (Newtonian Fluid)

"A real fluid, in which the shear stress is directly proportional to the rate of shear strain (or velocity gradient), is known as a Newtonian fluid." Examples are water and alcohol." [33]

Definition 2.2.4 (Non-Newtonian Fluid)

"A real fluid in which the shear stress is not directly proportional to the rate of shear strain (or velocity gradient), is known as a non-Newtonian fluid." Non-Newtonian fluids include substances like toothpaste and honey."

$$\tau_{xy} \propto \left(\frac{du}{dy}\right)^m, \qquad m \neq 1$$
$$\tau_{xy} = \mu\left(\frac{du}{dy}\right)^m \quad [33]$$

Definition 2.2.5 (Magnetohydrodynamics)

"Magnetohydrodynamics(MHD) is concerned with the mutual interaction of fluid flow and magnetic fields. The fluids in question must be electrically conducting and non-magnetic, which limits us to liquid metals, hot ionised gases (plasmas) and strong electrolytes." [35]

2.3 Types of Flow

Definition 2.3.1 (Rotational Flow)

"Rotational flow is that type of flow in which the fluid particles while flowing along stream-lines, also rotate about their own axis." [33]

Definition 2.3.2 (Irrotational Flow)

"Irrotational flow is that type of flow in which the fluid particles while flowing along stream-lines, do not rotate about their own axis then this type of flow is called irrotational flow." [33]

Definition 2.3.3 (Compressible Flow)

"Compressible flow is that type of flow in which the density of the fluid changes from point to point or in other words the density (ρ) is not constant for the fluid, Mathematically,

$$\rho \neq k,$$

where k is constant." [33]

Definition 2.3.4 (Incompressible Flow)

"Incompressible flow is that type of flow in which the density is constant for the fluid. Liquids are generally incompressible while gases are compressible, Mathematically,

$$\rho = k,$$

where k is constant." [33]

Definition 2.3.5 (Steady Flow)

"Steady flow is defined as that type of flow in which the fluid characteristics like velocity, pressure, density, etc., at a point do not change with time. Thus for steady flow, Mathematically we have,

$$\frac{\partial Q}{\partial t} = 0,$$

where Q is any fluid property." [33]

Definition 2.3.6 (Unsteady Flow)
"Unsteady flow is defined as that type of flow in which the fluid characteristics like velocity, pressure, density, etc., at a point do change with time. Thus for Unsteady flow, Mathematically, we have,

$$\frac{\partial Q}{\partial t} \neq 0,$$

where Q is any fluid property." [33]

Definition 2.3.7 (Laminar Flow)
"Laminar flow is defined as that type of flow in which the fluid particles move along well-defined paths or stream lines and all the stream-lines are straight and parallel." [32]

Definition 2.3.8 (Turbulent Flow)

"Turbulent flow is that type of flow in which the fluid particles move in a zig-zag way." [32]

2.4 Kinds of Heat Transfer

Definition 2.4.1 (Heat Transfer)
"Heat transfer is a branch of engineering that deals with the transfer of thermal energy from one point to another within a medium or from one medium to another due to the occurrence of a temperature difference. For example, heat is transferred from stove to the cooking pan." [34]

Definition 2.4.2 (Conduction)
"The transfer of heat within a medium due to a diffusion process is called conduction. The Fourier heat conduction law states that the heat flow is proportional to the temperature gradient." Examples are during the ironing process, heat is

transferred from the iron to the fabric. Chocolate candy in a hand will eventually melt as heat is conducted from a hand to the chocolate" [34]

Definition 2.4.3 (Convection)
"Convection heat transfer is usually defined as energy transport effected by the motion of a fluid. The convection heat transfer between two dissimilar media is governed by Newton's law of cooling. It states that the heat flow is proportional to the difference of the temperatures of the two media. The proportionality coefficient is called the convection heat transfer coefficient." Examples are heating water on the stove and air Conditioner" [34]

Definition 2.4.4 (Thermal Radiation)
"Thermal radiation is defined as radiant (electromagnetic) energy emitted by a medium and is solely to the temperature of the medium. Sometimes radiant energy is taken to be transported by electromagnetic wave while at other times it is supposed to be transported by particle like photons. " [34]

2.5 Dimensionless Numbers

Definition 2.5.1 (Eckert Number)

"It is the dimensionless number used in continuum mechanics. It describes the relation between flows and the boundary layer enthalpy difference and it is used for characterized heat dissipation. Mathematically,

$$Ec = \frac{u^2}{C_p \nabla T}$$

where C_p denotes the specific heat." [32]

Definition 2.5.2 (Prandtl Number)

"It is the ratio between the momentum diffusivity ν and thermal diffusivity α. Mathematically, it can be defined as

$$Pr = \frac{\nu}{\alpha} = \frac{\frac{\mu}{\rho}}{\frac{k}{C_p \rho}} = \frac{\mu C_p}{k}$$

where μ represents the dynamic viscosity, Cp denotes the specific heat and k stands for thermal conductivity. The relative thickness of thermal and momentum boundary layer is controlled by Prandtl number. For small Pr, heat distributed rapidly corresponds to the momentum." [32]

Definition 2.5.3 (Skin Friction Coefficient)
"The steady flow of an incompressible gas or liquid in a long pipe of internal D. The mean velocity is denoted by u_w. The skin friction coefficient can be defined as

$$C_f = \frac{2\tau_0}{\rho u_w^2}$$

where τ_0 denotes the wall shear stress and ρ is the density." [36]

Definition 2.5.4 (Nusselt Number)
"The hot surface is cooled by a cold fluid stream. The heat from the hot surface, which is maintained at a constant temperature, is diffused through a boundary layer and convected away by the cold stream. Mathematically,

$$Nu = \frac{qL}{k}$$

where q stands for the convection heat transfer, L for the characteristic length and k stands for thermal conductivity." [37]

Definition 2.5.5 (Sherwood Number)
"It is the nondimensional quantity which show the ratio of the mass transport by convection to the transfer of mass by diffusion. Mathematically:

$$Sh = \frac{kL}{D}$$

here L is characteristics length, D is the mass diffusivity and k is the mass transfer" coeffcient." [38]

Definition 2.5.6 (Reynolds Number)

"It is defined as the ratio of inertia force of a flowing fluid and the viscous force of the fluid. Mathematically,

$$Re = \frac{VL}{\nu},$$

where V denotes the free stream velocity, L is the characteristic length and ν stands for kinematic viscosity." [33]

2.6 Governing Laws

Definition 2.6.1 (Continuity Equation)

"The principle of conservation of mass can be stated as the time rate of change of mass is fixed volume is equal to the net rate of flow of mass across the surface. Mathematically, it can be written as"

$$\frac{\partial \rho}{\partial t} + \nabla.(\rho \mathbf{u}) = 0 \text{ [34]}$$

Definition 2.6.2 (Momentum Equation)

"The momentum equation states that the time rate of change of linear momentum of a given set of particles is equal to the vector sum of all the external forces acting on the particles of the set, provided Newton's Third Law of action and reaction governs the internal forces. Mathematically, it can be written as":

$$\frac{\partial}{\partial t}(\rho \mathbf{u}) + \nabla.[(\rho \mathbf{u})\mathbf{u}] = \nabla.\mathbf{T} + \rho g. \text{ [34]}$$

Definition 2.6.3 (Energy Equation)

"The law of conservation of energy states that the time rate of change of the total energy is equal to the sum of the rate of work done by the applied forces and change of heat content per unit time.

$$\frac{\partial \rho}{\partial t} + \nabla.\rho\mathbf{u} = -\nabla.\mathbf{q} + Q + \phi,$$

where ϕ is the dissipation function." [34]

Definition 2.6.4 (Conservation Equation)

"The principle of conservation of mass can be stated as the time rate of change of mass is fixed volume is equal to the net rate of flow of mass across the surface. Mathematically, it can be written as:

$$\frac{\partial \rho}{\partial t} + \nabla.(\rho\mathbf{u}) = 0,$$

where t is time, the fluid density is ρ, and the fluid velocity is u." [34]

2.7 Shooting Method

It is a numerical approach for resolving boundary value problems expressed in the form of nonlinear ordinary differential equations. Initially, the higher-order nonlinear ordinary differential equations (ODEs) are converted into a system of first-order ODEs. The missing initial conditions are guessed to have a complete initial value problem (IVP). To explain the detailed computational procedure, consider the classical Blausius problem in the dimensionless form governed by he following ODEs along with the relavant boundary conditions:

$$\left.\begin{aligned} &2f'''(x) + f(x)f''(x) \\ &f(0) = 0 = f'(0), \quad f' \to 1 \quad as \quad x \to \infty. \end{aligned}\right\} \tag{2.1}$$

Introduce the following notations to reduce the order of the above boundary value problem.

$$\left.\begin{aligned} f &= z_1, \\ f' &= z_1' = z_2, \\ f'' &= z_2' = z_3. \end{aligned}\right\} \tag{2.2}$$

As a result, (2.1) is transformed into the following system of first order ODEs:

$$z_1' = z_2, \qquad z_1(0) = 0. \tag{2.3}$$

$$z_2' = z_3, \qquad z_2(0) = 1. \tag{2.4}$$

$$z_3' = -\frac{1}{2}(z_1 z_3), \qquad z_3(0) = h. \tag{2.5}$$

where h is the missing initial condition which will be guessed to initialize the computational problem.

The RK-4 method will be used for the numerical solution of the provided initial value problem (IVP). The choice of "h" should be made to meet this condition:

$$z_2(x, h) = 1. \tag{2.6}$$

For convenience, now onward $z_2(x, h)$ will be denoted by $z_2(h)$. Let us further denote $z_2(h) - 1$ by $\phi(h)$, so that

$$\phi(h) = 0. \tag{2.7}$$

The iterative formula detailed below allows us to implement Newton's method as a solution approach for the previously discussed equation:

$$\begin{aligned} h_{n+1} &= h_n - \frac{\phi(h_n)}{\left(\frac{\partial \phi(h)}{\partial h}\right)_{h=h_n}}, \\ h_{n+1} &= h_n - \frac{z_2(h_n) - 1}{\left(\frac{\partial z_2(h)}{\partial t}\right)_{h=h_n}}. \end{aligned} \tag{2.8}$$

For $\frac{\partial z_2(h)}{\partial h}$, we introduce the following notations:

$$\frac{\partial z_1}{\partial h} = z_4, \quad \frac{\partial z_2}{\partial h} = z_5, \quad \frac{\partial z_3}{\partial h} = z_6. \tag{2.9}$$

With the use of these notations, representation for iterative scheme of Newton is:

$$h_{n+1} = h_n - \frac{z_2(h_n) - 1}{z_5(h_n)}. \tag{2.10}$$

Differentiating the first-order ODEs (2.3)-(2.4) with respect to 'h', we derive a different system of ODEs as below:

$$z_4' = z_5, \qquad z_4(0) = 0. \tag{2.11}$$

$$z_5' = z_6, \qquad z_5(0) = 0. \tag{2.12}$$

$$z_6' = -\frac{1}{2}\big[z_1 z_6 + z_3 z_4\big], \qquad z_6(0) = 1. \tag{2.13}$$

Writing all the four ODEs (2.3), (2.4), (2.10) and (2.11) together, we have the following IVP.

$$\begin{aligned}
z_1' &= z_2, && z_1(0) = 0.\\
z_2' &= z_3, && z_2(0) = 1.\\
z_3' &= -\frac{1}{2}\big[z_1 z_3\big], && z_3(0) = h.\\
z_4' &= z_5, && z_4(0) = 0.\\
z_5' &= z_6, && z_5(0) = 0.\\
z_6' &= -\frac{1}{2}\big[z_1 z_6 + z_3 z_4\big], && z_6(0) = 1.
\end{aligned}$$

To solve the above IVP, we will apply the fourth-order Runge-Kutta numerical method.

The stopping criteria for the shooting technique is established as:

$$\mid z_2(h) - 1 \mid < \epsilon,$$

where ϵ is an arbitrarily small positive number.

Chapter 3

A Casson Nanofluid Flow on a Stretching Surface Effected by Thermal Radiation

3.1 Introduction

The primary focus of this chapter has been about the numerical inspection of a Casson nanofluid rotating flow when subjected to the impact of a magnetic field, viscous dissipation, Joule heating and nonlinear thermal radiation. This model was proposed and numerically computed by Archana et al. [31] by utilizing shooting method together with Runge-Kutta the fourth order method. The conversion of the governing nonlinear PDEs into a set of dimensionless ODEs is a prerequisite for implementing the shooting method. To conclude that, result from numerical analysis for various parameters is debated for the dimensionless velocity f', temperature distribution θ and concentration distribution ϕ. The obtained numerical results have been presented through tables and graphs.

3.2 Mathematical Modeling

Consider a three-dimensional steady, laminar flow of an incompressible Casson nanofluid through a stretching sheet surface. The fluid has been assumed to rotate about z-axis with an angular velocity Ω, where the domain of flow is $z \geq 0$. Suppose that the sheet has been stretched with velocity $U_w(x)=ax$. In the z-direction, a constant magnetic field of strength B_0 is applied. Suppose C_w represents the wall concentration and T_w signifies the wall temperature. While $C_\infty < C_w$ and $T_\infty < T_w$ are ambient concentartion and temperature respectively. A dimensionless parameter, temperature ratio θ_w is defined as, $\theta_w=\frac{T_w}{T_\infty}> 1$.

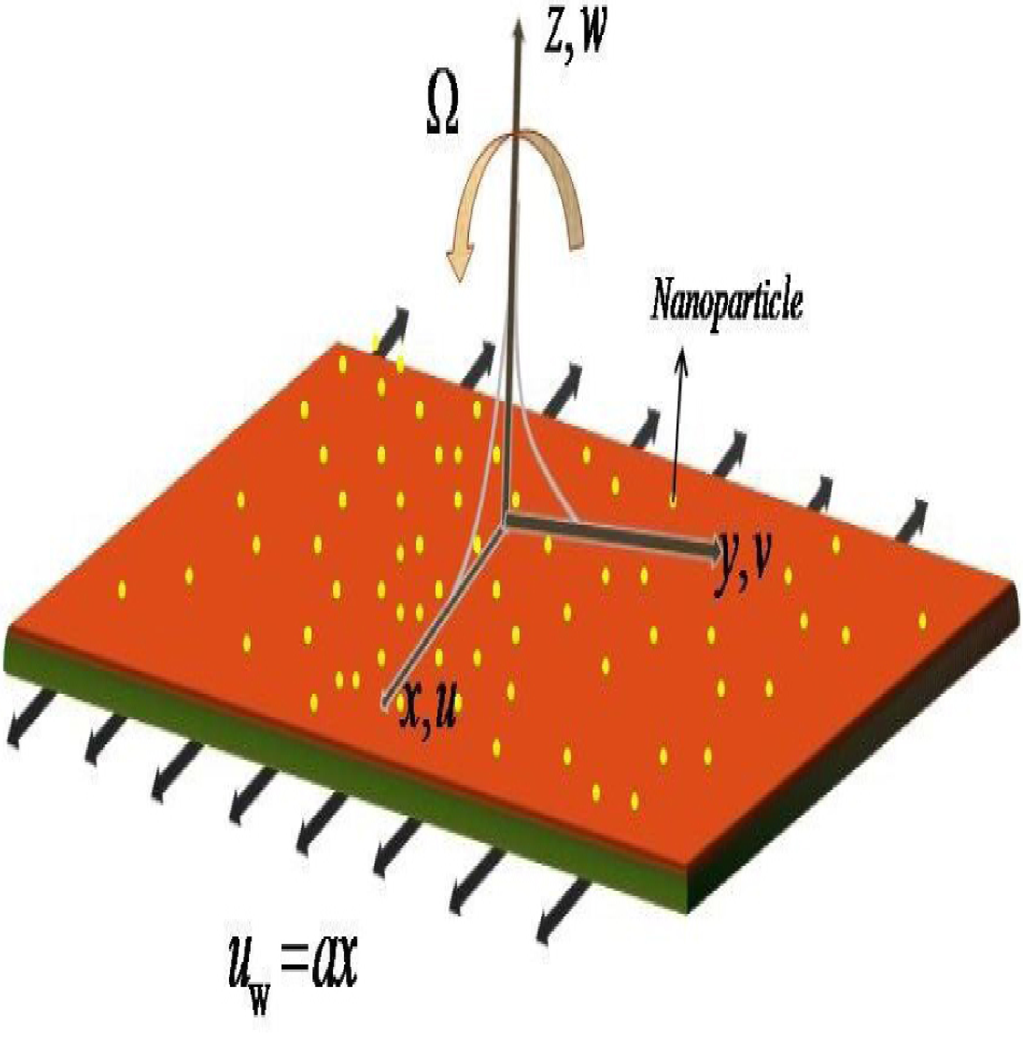

FIGURE 3.1: Methodical presentation of the tangible system.

The set of equations describing the flow are:

$$\frac{\partial u}{\partial x}+\frac{\partial v}{\partial y}+\frac{\partial w}{\partial z}=0, \tag{3.1}$$

$$u\frac{\partial u}{\partial x}+v\frac{\partial u}{\partial y}+w\frac{\partial u}{\partial z}-2\Omega v=\nu\left(1+\frac{1}{\beta}\right)\frac{\partial^2 u}{\partial z^2}-\frac{\sigma B_0^2}{\rho_f}u, \tag{3.2}$$

$$u\frac{\partial v}{\partial x}+v\frac{\partial v}{\partial y}+w\frac{\partial v}{\partial z}+2\Omega v=\nu\left(1+\frac{1}{\beta}\right)\frac{\partial^2 v}{\partial z^2}-\frac{\sigma B_0^2}{\rho_f}v, \tag{3.3}$$

$$\begin{aligned}u\frac{\partial T}{\partial x}+v\frac{\partial T}{\partial y}+w\frac{\partial T}{\partial z}&=\frac{\partial}{\partial z}\left[\left(\alpha+\frac{16\sigma^*T^3}{3K^*\left(\rho c_p\right)_f}\right)\frac{\partial T}{\partial z}\right]\\&+\tau\left[D_B\frac{\partial T}{\partial z}\frac{\partial C}{\partial z}+\frac{D_T}{T_\infty}\left(\frac{\partial T}{\partial z}\right)^2\right]\\&+\frac{\mu}{\left(\rho c_p\right)_f}\left(1+\frac{1}{\beta}\right)\left(\left(\frac{\partial u}{\partial z}\right)^2+\left(\frac{\partial v}{\partial z}\right)^2\right)+\frac{\sigma B_0^2}{\left(\rho c_p\right)_f}\left(u^2+v^2\right),\end{aligned} \tag{3.4}$$

$$u\frac{\partial C}{\partial x}+v\frac{\partial C}{\partial y}+w\frac{\partial C}{\partial z}=\frac{\partial}{\partial z}=D_B\frac{\partial^2 C}{\partial z^2}+\frac{D_T}{T_\infty}\frac{\partial^2 T}{\partial z^2}. \tag{3.5}$$

The associated BCs have been taken as:

$$\left.\begin{aligned}&u=U_w(x),\quad v=0,\quad w=0,\quad T=T_w,\quad C=C_w\quad at\quad z=0,\\&u\to 0,\quad v\to 0\quad T\to T_\infty,\quad C\to C_\infty\quad as\quad z\to\infty.\end{aligned}\right\} \tag{3.6}$$

With the utilization of the Rosseland approximation for radiation, q_r is introduced as the radiative heat flux:

$$q_r=-\frac{4\sigma^*}{3k^*}\frac{\partial T^4}{\partial y},$$

where σ^* represents the Stefan-Boltzmann constant, and k^* denotes the absorption coefficient. If the difference of temperature is relatively minor, then the temperature T^4 can be expanded about T_∞ using Taylor series, as follows.

$$T^4=T_\infty^4+4T_\infty^3(T-T_\infty)+6T_\infty^2(T-T_\infty)^2+...$$

Ignoring the terms with higher order, we write:

$$T^4=T_\infty^4+4T_\infty^3(T-T_\infty)$$

$$
\begin{aligned}
&= T_\infty^4 + 4T_\infty^3 T - 4T_\infty^4 \\
&= -3T_\infty^4 + 4T_\infty^3 T \\
&= 4T_\infty^3 T - 3T_\infty^4.
\end{aligned}
$$

To transform the equations (3.1)-(3.5) into a set of ODEs, we have taken into consideration the subsequent similarity transformations.

$$
\left.
\begin{aligned}
&u = axf^{'}, \quad v = axg, \quad w = -\sqrt{a\nu}f, \\
&T = T_\infty \left(1 + (\theta_w - 1)\theta\right), \quad \phi = \frac{C - C_\infty}{C_w - C_\infty}, \quad \eta = z\sqrt{\frac{a}{\nu}}.
\end{aligned}
\right\} \tag{3.7}
$$

where $\theta_w{=}\frac{T_w}{T_\infty} > 1$ denotes the temperature ratio parameter.
The detailed method for converting equations (3.1)-(3.5) into dimensionless form is discussed below:

$$
\begin{aligned}
&\frac{\partial u}{\partial x} = \frac{\partial}{\partial x} axf^{'} = af^{'} \\
&\frac{\partial v}{\partial y} = \frac{\partial}{\partial y}(axg) = 0 \\
&\frac{\partial w}{\partial z} = \frac{\partial}{\partial z}(-\sqrt{a\nu}f) = -\sqrt{a\nu}f'\sqrt{\frac{a}{\nu}} = -af'.
\end{aligned}
$$

The satisfaction of Equation (3.1) by using the above results, as follows:

$$
\frac{\partial u}{\partial x} + \frac{\partial v}{\partial y} + \frac{\partial w}{\partial z} = af' - af' = 0. \tag{3.8}
$$

Below derivatives are determined from equation (3.2) as:

$$
\begin{aligned}
&\frac{\partial \eta}{\partial z} = \sqrt{\frac{a}{\nu}}. \\
&\frac{\partial u}{\partial z} = \frac{\partial}{\partial z}(axf') = axf''\sqrt{\frac{a}{\nu}}. \\
&\frac{\partial^2 u}{\partial z^2} = axf^{'''}\frac{a}{\nu} = \frac{a^2}{\nu}xf^{'''}. \\
&u\frac{\partial u}{\partial x} = a^2 xf'^2.
\end{aligned}
$$

$$\begin{aligned}
w\frac{\partial u}{\partial z} &= axf''\sqrt{\frac{a}{\nu}}(-\sqrt{a\nu})f = -a^2xff''.\\
\frac{\partial u}{\partial y} &= \frac{\partial}{\partial y}(axf^{'}) = 0.
\end{aligned}$$

The left side of (3.2) becomes, by using above derivatives:

$$u\frac{\partial u}{\partial x} + v\frac{\partial u}{\partial y} + w\frac{\partial u}{\partial z} - 2\Omega v = a^2xf'^2 - a^2xff'' - 2\gamma_1 a^2xg. \tag{3.9}$$

Similarly, right side of (3.2) turns into:

$$\nu\left(1+\frac{1}{\beta}\right)\frac{\partial^2 u}{\partial z^2} - \frac{\sigma B_0^2}{\rho_f}u = \nu\left(1+\frac{1}{\beta}\right)\left(\frac{a^2}{\nu}xf^{'''}\right) - \frac{a^2x\sigma B_0^2 f^{'}}{a\rho_f}. \tag{3.10}$$

The dimensionless form of (3.2) is, by comparing (3.9)-(3.10) as follows:

$$\begin{aligned}
&a^2xf'^2 - a^2xff'' - 2\gamma_1 a^2xg = \nu\left(1+\frac{1}{\beta}\right)\left(\frac{a^2}{\nu}xf^{'''}\right) - \frac{a^2x\sigma B_0^2 f^{'}}{a\rho_f}.\\
\Rightarrow &f'^2 - ff'' - 2\gamma_1 g = \nu\left(1+\frac{1}{\beta}\right)\left(\frac{1}{\nu}f^{'''}\right) - \frac{\sigma B_0^2 f^{'}}{a\rho_f}.\\
\Rightarrow &\left(1+\frac{1}{\beta}\right)f^{'''} - f'^2 + ff^{''} + 2\gamma_1 g - Mf' = 0.
\end{aligned} \tag{3.11}$$

The following dimensionless parameters are used in equation (3.11):

$$\gamma_1 = \tfrac{\Omega}{a}, \qquad M = \tfrac{\sigma B_0^2}{\rho a}$$

For the momentum equation (3.3), we must compute the following derivatives:

$$\begin{aligned}
\frac{\partial v}{\partial x} &= \frac{\partial}{\partial x}(axg) = ag.\\
u\frac{\partial v}{\partial x} &= a^2xf^{'}g.\\
\frac{\partial v}{\partial y} &= \frac{\partial}{\partial y}(axg) = 0.\\
\frac{\partial v}{\partial z} &= axg'\sqrt{\frac{a}{\nu}}.\\
w\frac{\partial v}{\partial z} &= -a^2xg'f.
\end{aligned}$$

$$\frac{\partial^2 v}{\partial z^2} = \frac{a^2}{\nu} x g''.$$

The left side of (3.3) becomes, by using above derivatives:

$$u\frac{\partial v}{\partial x} + v\frac{\partial v}{\partial y} + w\frac{\partial v}{\partial z} + 2\Omega u = a^2 x f' g - a^2 x g' f + 2\gamma_1 a^2 x f'. \tag{3.12}$$

Similarly, the right side of (3.3) becomes:

$$\nu\left(1+\frac{1}{\beta}\right)\frac{\partial^2 v}{\partial z^2} - \frac{\sigma B_0^2}{\rho_f} v = \nu\left(1+\frac{1}{\beta}\right)\left(\frac{a^2}{\nu} x g''\right) - \frac{a^2 x \sigma B_0^2 g}{a\rho_f}. \tag{3.13}$$

The dimensionless form of (3.3) is, by comparing (3.12)-(3.13) as below:

$$\begin{aligned}
&a^2 x f' g - a^2 x g' f + 2\gamma_1 a^2 x f' = \nu\left(1+\frac{1}{\beta}\right)\left(\frac{a^2}{\nu} x g''\right) - \frac{a^2 x \sigma B_0^2 g}{a\rho_f}.\\
&\Rightarrow f' g - g' f + 2\gamma_1 f' = \nu\left(1+\frac{1}{\beta}\right)\left(\frac{1}{\nu} g''\right) - \frac{\sigma B_0^2 g}{a\rho_f}.\\
&\Rightarrow \left(1+\frac{1}{\beta}\right) g'' + f g' - f' g - 2\gamma_1 f' - M g = 0. \qquad (3.14)
\end{aligned}$$

Now, for the conversion of energy equation (3.4), the following procedure has been carried out.

$$\begin{aligned}
\theta &= \frac{T - T_\infty}{T_w - T_\infty}.\\
&= T_\infty + (T_w - T_\infty)\theta\\
&= T_\infty + T_\infty\left(\frac{T_w}{T_\infty} - 1\right)\theta\\
&= T_\infty\left(1 + (\theta_w - 1)\theta\right).\\
\theta_w &= \frac{T_w}{T_\infty}.\\
\frac{\partial T}{\partial z} &= \left((T_w - T_\infty)\theta' \sqrt{\frac{a}{\nu}}\right).\\
w\frac{\partial T}{\partial z} &= \left(-a f (T_w - T_\infty)\theta'\right).\\
u\frac{\partial T}{\partial x} &= 0 = v\frac{\partial T}{\partial y}.
\end{aligned}$$

The governing equation for the conservation of energy is

$$
\begin{aligned}
& u\frac{\partial T}{\partial x}+v\frac{\partial T}{\partial y}+w\frac{\partial T}{\partial z}=\frac{\partial}{\partial z}\left[\left(\alpha+\frac{16\sigma^{*}T^{3}}{3k^{*}\left(\rho c_{p}\right)_{f}}\right)\frac{\partial T}{\partial z}\right] \\
& +\tau\left[D_{B}\frac{\partial T}{\partial z}\frac{\partial C}{\partial z}+\frac{D_{T}}{T_{\infty}}\left(\frac{\partial T}{\partial z}\right)^{2}\right]+\frac{\mu}{\left(\rho c_{p}\right)_{f}}\left(1+\frac{1}{\beta}\right)\left(\left(\frac{\partial u}{\partial z}\right)^{2}+\left(\frac{\partial v}{\partial z}\right)^{2}\right) \\
& +\frac{\sigma B_{0}^{2}}{(\rho c_{p})_{f}}(u^{2}+v^{2}). \\
\Rightarrow & -af(T_{w}-T_{\infty})\theta^{'}=\frac{\partial}{\partial z}\left[\alpha\sqrt{\frac{a}{\nu}}(T_{w}-T_{\infty})\theta^{''}\right. \\
& \left.+Rd\alpha\sqrt{\frac{a}{\nu}}(T_{w}-T_{\infty})\theta^{'}\left(1+(\theta_{w}-1)\theta\right)^{3}\right] \\
& +\tau\left[D_{B}\left((T_{w}-T_{\infty})\theta^{'}(\sqrt{\frac{a}{\nu}})\right)\left(C_{w}-C_{\infty}\right)\phi^{'}(\sqrt{\frac{a}{\nu}})\right. \\
& \left.+\frac{D_{T}}{T_{\infty}}\left((T_{w}-T_{\infty})\theta^{'}(\sqrt{\frac{a}{\nu}})\right)^{2}\right]+\frac{\mu}{(\rho c_{p})_{f}}\left(1+\frac{1}{\beta}\right)\left[\left(axf^{''}\sqrt{\frac{a}{\nu}}\right)^{2}\right. \\
& \left.+\left(axg^{\prime}\sqrt{\frac{a}{\nu}}\right)^{2}\right]+\frac{\sigma B_{0}^{2}}{(\rho c_{p})_{f}}\left[\left(axf^{\prime}\right)^{2}+\left(axg\right)^{2}\right]. \\
\Rightarrow & -af(T_{w}-T_{\infty})\theta^{'}=\frac{\alpha a}{\nu}\left[(T_{w}-T_{\infty})\theta^{''}+Rd(T_{w}-T_{\infty})\theta^{'}\left(1+(\theta_{w}-1)\theta\right)^{3}\right. \\
& \left.+3Rd(\theta_{w}-1)(T_{w}-T_{\infty})\theta^{\prime 2}\left(1+(\theta_{w}-1)\theta\right)^{2}\right]+aN_{b}(T_{w}-T_{\infty})\theta^{'}\phi^{'} \\
& +aN_{t}(T_{w}-T_{\infty})\theta^{\prime 2}+\frac{aU_{w}^{2}}{(c_{p})_{f}}\left(1+\frac{1}{\beta}\right)\left(f^{''2}+g^{\prime 2}\right)+\frac{a\sigma B_{0}^{2}U_{w}^{2}}{a(\rho c_{p})_{f}}\left(f^{'2}+g^{2}\right). \\
\Rightarrow & -Prf\theta^{'}=\theta^{''}+Rd\theta^{''}\left(1+(\theta_{w}-1)\theta\right)^{3}+3Rd(\theta_{w}-1)\theta^{\prime 2}\left(1+(\theta_{w}-1)\theta\right)^{2} \\
& +PrN_{b}\theta^{'}\phi^{'}+PrN_{t}\theta^{\prime 2}+PrEc\left(1+\frac{1}{\beta}\right)\left(f^{''2}+g^{\prime 2}\right)+PrEcM\left(f^{'2}+g^{2}\right) \\
\Rightarrow & \left(\left(1+Rd\left(1+(\theta_{w}-1)\theta\right)^{3}\right)\theta^{'}\right)^{'}+Pr\left[+Prf\theta^{'}N_{b}\theta^{'}\phi^{'}+N_{t}\theta^{\prime 2}\right. \\
& \left.+Ec\left(\left(1+\frac{1}{\beta}\right)\left(f^{''2}+g^{'2}\right)+M\left(f^{'2}+g^{2}\right)\right)\right]=0. \qquad (3.15)
\end{aligned}
$$

The dimensionless parameters used in equation (3.15) are:

$$
M=\frac{\sigma B_0^2}{\rho a}, \quad Rd=\frac{16\sigma^* T_\infty^3}{3kk^*}, \quad Pr=\frac{\nu}{\alpha}, \quad Nb=\frac{\tau D_B (C_w-C_\infty)}{\nu},
$$

$$
Nt=\frac{\tau D_T (T_w-T_\infty)}{\nu T_\infty}, \qquad Ec=\frac{U_w^2}{(c_p)_f (T_w-T_\infty)}.
$$

Now, for the conversion of concentration equation (3.5), the following process is carried out:

$$\begin{aligned}
\phi &= \frac{C - C_\infty}{C_w - C_\infty}.\\
\Rightarrow \ \frac{\partial C}{\partial z} &= (C_w - C_\infty)\phi'\sqrt{\frac{a}{\nu}}.\\
\Rightarrow w\frac{\partial C}{\partial z} &= -af(C_w - C_\infty)\phi'.\\
\frac{\partial^2 C}{\partial z^2} &= \Big(C_w - C_\infty)\phi'\frac{a}{\nu}.\\
\frac{\partial T}{\partial z} &= \left((T_w - T_\infty)\theta'\sqrt{\frac{a}{\nu}}\right).\\
\Rightarrow \ \frac{\partial^2 T}{\partial z^2} &= \left((T_w - T_\infty)\theta'\frac{a}{\nu}\right).\\
\frac{\partial C}{\partial x} &= \frac{\partial C}{\partial y} = 0.
\end{aligned}$$

The governing equation of concentration is converted into dimensionless form as:

$$\begin{aligned}
&u\frac{\partial C}{\partial x} + v\frac{\partial C}{\partial y} + w\frac{\partial C}{\partial z} = D_B\frac{\partial^2 C}{\partial z^2} + \frac{D_T}{T_\infty}\frac{\partial^2 T}{\partial z^2}.\\
&\Rightarrow -af\Big(C_w - C_\infty\Big)\phi' = D_B\Big(C_w - C_\infty\Big)\phi'\frac{a}{\nu} + \frac{D_T}{T_\infty}\left((T_w - T_\infty)\theta'\frac{a}{\nu}\right).\\
&\Rightarrow -f\phi' = \frac{D_B}{\nu}\phi' + \frac{D_T}{\nu T_\infty}\left(\frac{T_w - T_\infty}{C_w - C_\infty}\theta'\right).\\
&\Rightarrow \phi'' + Scf\phi' + \frac{Nt}{Nb}\theta'' = 0. \qquad (3.16)
\end{aligned}$$

The dimensionless parameters used in equation (3.16) are:

$$Nb = \tfrac{\tau D_B(C_w - C_\infty)}{\nu}, \quad Nt = \tfrac{\tau D_T(T_w - T_\infty)}{\nu T_\infty}, \quad Sc = \tfrac{\nu}{D_B}.$$

The governing model's ultimate dimensionless form is:

$$\left(1 + \frac{1}{\beta}\right)f''' - f'^2 + ff'' + 2\gamma_1 g - Mf' = 0. \qquad (3.17)$$

$$\left(1 + \frac{1}{\beta}\right)g'' + fg' - f'g - 2\gamma_1 f' - Mg = 0. \qquad (3.18)$$

$$\left(\left(1+Rd\left(1+(\theta_w-1)\theta\right)^3\right)\theta'\right)'+Pr\Big[Prf\theta'+N_b\theta'\phi'$$
$$+N_t\theta'^2+Ec\left(\left(1+\frac{1}{\beta}\right)\left(f''^2+g'^2\right)+M\left(f'^2+g^2\right)\right)\Big]=0. \tag{3.19}$$
$$\phi''+Scf\phi'+\frac{Nt}{Nb}\theta''=0. \tag{3.20}$$

The transformation of corresponding BCs into the non-dimensional form is given below:

$$
\begin{aligned}
& u=U_w(x), && at \quad z=0.\\
\Rightarrow\quad & axf'(\eta)=ax, && at \quad \eta=0.\\
\Rightarrow\quad & f'(0)=1, && \\
& v=0, && at \quad z=0.\\
\Rightarrow\quad & axg(\eta)=0, && at \quad \eta=0.\\
\Rightarrow\quad & g(0)=0, && \\
& w=0, && at \quad z=0.\\
\Rightarrow\quad & -\sqrt{a\nu}f(\eta)=0, && at \quad \eta=0.\\
\Rightarrow\quad & f(0)=0, && \\
& T=T_w, && at \quad z=0.\\
\Rightarrow\quad & \theta(\eta)(T_w-T_\infty)+T_\infty=T_w, && at \quad \eta=0.\\
\Rightarrow\quad & \theta(\eta)(T_w-T_\infty)=(T_w-T_\infty), && at \quad \eta=0.\\
\Rightarrow\quad & \theta(0)=1, && \\
& C=C_w, && at \quad z=0.\\
\Rightarrow\quad & \phi(\eta)(C_w-C_\infty)=(C_w-C_\infty), && at \quad \eta=0.\\
\Rightarrow\quad & \phi(0)=1, && \\
& u\to 0, && as \quad z\to\infty.\\
\Rightarrow\quad & f'(\eta)\to 0, && as \quad \eta\to\infty.\\
& v\to 0, && as \quad z\to\infty.\\
\Rightarrow\quad & g(\eta)\to 0, && as \quad \eta\to\infty.
\end{aligned}
$$

$$
\begin{aligned}
& w \to 0, && as \quad z \to \infty. \\
\Rightarrow \quad & f(\eta) \to 0, && as \quad \eta \to \infty. \\
& T \to T_\infty, && as \quad z \to \infty. \\
\Rightarrow \quad & \theta(\eta) \to 0, && as \quad \eta \to \infty. \\
& C \to C_\infty, && as \quad z \to \infty. \\
\Rightarrow \quad & \phi(\eta) \to 0, && as \quad \eta \to \infty.
\end{aligned}
$$

The dimensionless form of associated BCs (3.6) are:

$$
\left.\begin{aligned}
& f(0) = 0, \quad g(0) = 0, \quad f'(0) = 1, \quad \theta(0) = 0, \quad \phi(0) = 0, \quad as \quad \eta \to 0 \\
& f^{'} \to 0, \quad g \to 0, \quad \theta \to 0, \quad \phi \to 0 \quad as \quad \eta \to \infty.
\end{aligned}\right\} \tag{3.21}
$$

The skin friction coefficients, are given as follows:

$$
C_{fx} = \frac{\tau_{wx}}{\rho_f U_w^2}, \tag{3.22}
$$

where

$$
\tau_{wx} = \left(\mu_B + \frac{1}{\beta}\right)\left(\frac{\partial u}{\partial z}\right)_{z=0}, \tag{3.23}
$$

and

$$
C_{fy} = \frac{\tau_{wy}}{\rho_f U_w^2}, \tag{3.24}
$$

where

$$
\tau_{wy} = \left(\mu_B + \frac{1}{\beta}\right)\left(\frac{\partial v}{\partial z}\right)_{z=0}, \tag{3.25}
$$

Therefore

$$
C_{fx} = \frac{\mu_B\left(1 + \frac{1}{\beta}\right)\left(\frac{\partial u}{\partial z}\right)_{z=0}}{\rho_f U_w^2}
$$

$$
\begin{aligned}
&= \frac{\mu_B\left(1+\frac{1}{\beta}\right)\left(axf''(0)\sqrt{\frac{a}{\nu}}\right)}{\rho_f U_w^2} \\
&= \frac{\nu\ U_w}{U_w^2}\sqrt{\frac{a}{\nu}}\left(1+\frac{1}{\beta}\right)f''(0) \\
&= \frac{\sqrt{a}\sqrt{\nu}}{\sqrt{U_w^2}}\left(1+\frac{1}{\beta}\right)f''(0) \\
&= \frac{1}{\sqrt{Re_x}}\left(1+\frac{1}{\beta}\right)f''(0). \\
\Rightarrow\quad (Re_x)^{1/2}C_{fx} &= \left(1+\frac{1}{\beta}\right)f''(0).
\end{aligned}
\tag{3.26}
$$

Similarly

$$
\begin{aligned}
C_{fy} &= \frac{\mu_B\left(1+\frac{1}{\beta}\right)\left(\frac{\partial v}{\partial z}\right)_{z=0}}{\rho_f U_w^2} \\
&= \frac{\mu_B\left(1+\frac{1}{\beta}\right)\left(axg'(0)\sqrt{\frac{a}{\nu}}\right)}{\rho_f U_w^2} \\
&= \frac{\nu\ U_w}{U_w^2}\sqrt{\frac{a}{\nu}}\left(1+\frac{1}{\beta}\right)g'(0) \\
&= \frac{\sqrt{a}\sqrt{\nu}}{\sqrt{U_w^2}}\left(1+\frac{1}{\beta}\right)g'(0) \\
&= \frac{1}{\sqrt{Re_x}}\left(1+\frac{1}{\beta}\right)g'(0). \\
\Rightarrow\quad (Re_x)^{1/2}C_{fy} &= \left(1+\frac{1}{\beta}\right)g'(0).
\end{aligned}
\tag{3.27}
$$

Here $Re_x = \frac{U_w^2}{a\nu}$ denotes the local Reynolds number.

Local Nusselt number is defined as follows:

$$
Nu_x = \frac{U_w q_w}{ak(T_w - T_\infty)}. \tag{3.28}
$$

where

$$
q_w = k\left(\frac{\partial T}{\partial z}\right)_{z=0} + (q_r)_w
$$

and

$$(q_r)_w = \left(-\frac{16\sigma^* T^3}{3k^*} \left(\frac{\partial T}{\partial z}\right)_{z=0} \right)_w. \tag{3.29}$$

The dimensionless form of Nu_x is produced by the following steps:

$$\begin{aligned}
Nu_x &= -U_w(T_w - T_\infty)\left[\frac{-k\theta'(0) - \frac{16\sigma^* k T_\infty^3}{3kk^*}\left(1 + (\theta_w - 1)\theta\right)_w^3 \theta'(0)}{ak(T_w - T_\infty)}\right]\sqrt{\frac{a}{\nu}} \\
&= -U_w\theta'(0)\left[\frac{-1 - Rd\left(1 + (\theta_w - 1)\theta\right)_w^3}{a}\right]\sqrt{\frac{a}{\nu}} \\
&= -\sqrt{\frac{U_w^2}{a\nu}}\left[-1 - Rd\left(1 + (\theta_w - 1)\theta\right)_w^3\right]\theta'(0) \\
&= -(Re_x)^{1/2}\left[-1 - Rd\left(1 + (\frac{T_w - T_\infty}{T_\infty})\left(\frac{T - T_\infty}{T_w - T_\infty}\right)\right)_w^3\right]\theta'(0) \\
\Rightarrow \quad Re_x^{-1/2} Nu_x &= -\left[1 + Rd\left(\theta_w\right)^3\right]\theta'(0).
\end{aligned}$$

The Local Sherwood number Sh_x is termed as:

$$Sh_x = \frac{xq_m}{D_B(C_w - C_\infty)}. \tag{3.30}$$

where

$$q_m = -D_B\left(\frac{\partial C}{\partial z}\right)_{z=0}. \tag{3.31}$$

The dimensionless form of Sh_x can be produced through the following steps:

$$\begin{aligned}
Sh_x &= -\frac{xD_B(C_w - C_\infty)\phi'(0)\sqrt{\frac{a}{\nu}}}{D_B(C_w - C_\infty)} \\
&= -\frac{x\phi'(0)\sqrt{a}}{\sqrt{\nu}} \\
&= -\sqrt{\frac{U_w^2}{a\nu}}\phi'(0). \\
\Rightarrow \quad Re_x^{-1/2} Sh_x &= -\phi'(0).
\end{aligned}$$

3.3 Numerical Method for Solution

The ordinary differential equations (3.17) and (3.18) have been solved numerically by using the shooting technique. For this purpose, the following notations have been taken:

$$
\begin{aligned}
&f = Z_1, \qquad f' = Z_1' = Z_2, \qquad f'' = Z_1'' = Z_2' = Z_3,\\
&g = Z_4, \qquad g' = Z_4' = Z_5.
\end{aligned}
$$

The momentum equations are then transformed into the following system of first-order ODEs:

$$
\begin{aligned}
Z_1' &= Z_2, && Z_1(0) = 0.\\
Z_2' &= Z_3, && Z_2(0) = 1.\\
Z_3' &= \frac{\beta}{1+\beta}\left(Z_2^2 - Z_1 Z_3 - 2Z_4\gamma_1 + MZ_2\right), && Z_3(0) = r.\\
Z_4' &= Z_5, && Z_4(0) = 0.\\
Z_5' &= \frac{\beta}{1+\beta}\left(-Z_1 Z_5 + Z_2 Z_4 - 2Z_2\gamma_1 + MZ_4\right), && Z_5(0) = m.
\end{aligned}
$$

RK-4 method has been applied for solving the above IVP.
The domain of the problem is considered to be bounded i.e. $[0,\ \eta_\infty]$, where η_∞ represents as a +ve real number, for which the variation in the solution is ignorable after $\eta = \eta_\infty$. The missing conditions r and m are to be chosen such that.

$$
Z_2(\eta_\infty, r, m) = 0, \qquad Z_4(\eta_\infty, r, m) = 0.
$$

Newton's method will be used to find r and m. This method has the following iterative scheme:

$$
\begin{bmatrix} r \\ m \end{bmatrix}_{(n+1)} = \begin{bmatrix} r \\ m \end{bmatrix}_{(n)} - \begin{bmatrix} \frac{\partial Z_2}{\partial r} & \frac{\partial Z_2}{\partial m} \\ \frac{\partial Z_4}{\partial r} & \frac{\partial Z_4}{\partial m} \end{bmatrix}^{-1}_{(n)} \begin{bmatrix} Z_2 \\ Z_4 \end{bmatrix}_{(n)}
$$

Now introducing the following notations:

$$\frac{\partial Z_1}{\partial r} = Z_6, \quad \frac{\partial Z_2}{\partial r} = Z_7, \quad \frac{\partial Z_3}{\partial r} = Z_8, \quad \frac{\partial Z_4}{\partial r} = Z_9, \quad \frac{\partial Z_5}{\partial r} = Z_{10},$$
$$\frac{\partial Z_1}{\partial m} = Z_{11}, \quad \frac{\partial Z_2}{\partial m} = Z_{12}, \quad \frac{\partial Z_3}{\partial m} = Z_{13}, \quad \frac{\partial Z_4}{\partial m} = Z_{14}, \quad \frac{\partial Z_5}{\partial m} = Z_{15}.$$

The iterative scheme of Newton method is, by using the results of above notations as follows:

$$\begin{bmatrix} r \\ m \end{bmatrix}_{(n+1)} = \begin{bmatrix} r \\ m \end{bmatrix}_{(n)} - \begin{bmatrix} Z_7 & Z_{12} \\ Z_9 & Z_{14} \end{bmatrix}^{-1}_{(n)} \begin{bmatrix} Z_2 \\ Z_4 \end{bmatrix}_{(n)}.$$

The last set of five first order ODEs in terms of r and m are differentiated to get another system of ODEs, as follows:

$$Z_6' = Z_7, \qquad Z_6(0) = 0.$$
$$Z_7' = Z_8, \qquad Z_7(0) = 0.$$
$$Z_8' = \frac{\beta}{1+\beta}\bigg(2Z_2Z_7 - Z_6Z_3 - Z_1Z_8 - 2Z_9\gamma_1 + MZ_7\bigg), \qquad Z_8(0) = 1.$$
$$Z_9' = Z_{10}, \qquad Z_9(0) = 0.$$
$$Z_{10}' = \frac{\beta}{1+\beta}\bigg(- Z_6Z_5 - Z_1Z_10 + Z_7Z_4 + Z_2Z_9 - 2Z_7\gamma_1 + MZ_9\bigg), \qquad Z_{10}(0) = 0.$$
$$Z_{11}' = Z_{12}, \qquad Z_{11}(0) = 0.$$
$$Z_{12}' = Z_{13}, \qquad Z_{12}(0) = 0.$$
$$Z_{13}' = \frac{\beta}{1+\beta}\bigg(2Z_2Z_{12} - Z_{11}Z_3 - Z_1Z_{13} - 2Z_{14}\gamma_1 + MZ_{12}\bigg), \qquad Z_{13}(0) = 0.$$
$$Z_{14}' = Z_{15}, \qquad Z_{14}(0) = 0.$$
$$Z_{15}' = \frac{\beta}{1+\beta}\bigg(- Z_{11}Z_5 - Z_1Z_{15} + Z_{12}Z_4 + Z_2Z_{14} - 2Z_12\gamma_1 + MZ_{14}\bigg), \quad Z_{15}(0) = 1.$$

For the Newton's technique, the stopping criteria is as follows:

$$max\{\mid Z_2(\eta_\infty, r^n, m^n) \mid, \mid Z_4(\eta_\infty, r^n, m^n) \mid\} < \epsilon,$$

where $\epsilon > 0$ is an arbitrarily small number, which has been considered as 10^{-10}.

The ordinary differential equations (3.19) and (3.20) will be approximated by using the shooting technique, assuming f and g as known functions.
Consider equations (3.19)−(3.20) in the following form:

$$\theta'' = \frac{1}{\Big(1 + Rd\Big(1 + (\theta_w - 1)\theta\Big)^3\Big)}\Bigg[-3Rd(\theta_w - 1)\theta'^2\Big(1 + (\theta_w - 1)\theta\Big)^2$$
$$- Pr\Big[f\theta' + N_b\theta'\phi' + N_t\theta'^2 + Ec\Big(\Big(1 + \frac{1}{\beta}\Big)\Big(f''^2 + g'^2\Big)$$
$$+ M\Big(f'^2 + g^2\Big)\Big)\Big]\Bigg] \tag{3.32}$$

$$\phi'' = -Scf\phi' - \Big(\frac{Nt}{Nb}\Big)\frac{1}{\Big[1 + Rd\Big(1 + (\theta_w - 1)\theta\Big)^3\Big]}\Bigg[-3Rd(\theta_w - 1)\theta'^2$$
$$\Big(1 + (\theta_w - 1)\theta\Big)^2 Pr\Big[f\theta' + N_b\theta'\phi' + N_t\theta'^2 + Ec\Big(\Big(1 + \frac{1}{\beta}\Big)\Big(f''^2 + g'^2\Big)$$
$$+ M\Big(f'^2 + g^2\Big)\Big)\Big]\Bigg]. \tag{3.33}$$

To apply the shooting method, we utilize the following notions:

$$\theta = Y_1, \qquad \theta' = Y_1' = Y_2,$$
$$\phi = Y_3, \qquad \phi' = Y_3' = Y_4.$$

The above equations are then transformed into the set of first-order ODEs:

$$Y_1' = Y_2, \qquad Y_1(0) = 1.$$
$$Y_2' = \frac{1}{\Big(1 + Rd\Big(1 + (\theta_w - 1)Y_1\Big)^3\Big)}\Bigg[-3Rd(\theta_w - 1)Y_2^2\Big(1 + (\theta_w - 1)Y_1\Big)^2$$
$$- Pr\Big[PrfY_2 + N_bY_2Y_4 + N_tY_2^2 + Ec\Big(\Big(1 + \frac{1}{\beta}\Big)\Big(f''^2 + g'^2\Big)$$

$$+M\left(f'^2+g^2\right)\Bigg)\Bigg]\Bigg], \qquad Y_2(0)=l.$$

$$Y_3' = Y_4, \qquad Y_3(0)=1.$$

$$Y_4' = -ScfY_4 - \left(\frac{Nt}{Nb}\right)\frac{1}{\left(1+Rd\left(1+(\theta_w-1)Y_1\right)^3\right)}\Bigg[-3Rd(\theta_w-1)Y_2^2$$

$$\left(1+(\theta_w-1)Y_1\right)^2 - Pr\Bigg[PrfY_2 + N_bY_2Y_4 + N_tY_2^2$$

$$+Ec\left(\left(1+\frac{1}{\beta}\right)\left(f''^2+g'^2\right)+M\left(f'^2+g^2\right)\right)\Bigg]\Bigg],$$

RK-4 method is applied for solving numerically, the last IVP.

l and p are to be chosen as missing conditions:

$$Y_1(\eta_\infty, l, p) = 0, \qquad Y_3(\eta_\infty, l, p) = 0. \tag{3.34}$$

Newton method is used to solve the above equations with the iterative scheme as follows:

$$\begin{bmatrix} l \\ p \end{bmatrix}_{(n+1)} = \begin{bmatrix} l \\ p \end{bmatrix}_{(n)} - \begin{bmatrix} \frac{\partial Y_1}{\partial l} & \frac{\partial Y_1}{\partial p} \\ \frac{\partial Y_3}{\partial l} & \frac{\partial Y_3}{\partial p} \end{bmatrix}^{-1}_{(n)} \begin{bmatrix} Y_1 \\ Y_3 \end{bmatrix}_{(n)}$$

Introducing the following further notations:

$$\frac{\partial Y_1}{\partial l} = Y_5, \quad \frac{\partial Y_2}{\partial l} = Y_6, \quad \frac{\partial Y_3}{\partial l} = Y_7, \quad \frac{\partial Y_4}{\partial l} = Y_8,$$
$$\frac{\partial Y_1}{\partial p} = Y_9, \quad \frac{\partial Y_2}{\partial p} = Y_{10}, \quad \frac{\partial Y_3}{\partial p} = Y_{11}, \quad \frac{\partial Y_4}{\partial p} = Y_{12}.$$

The form of Newton iterative scheme is, by using the results of above notations are as follows:

$$\begin{bmatrix} l \\ p \end{bmatrix}_{(n+1)} = \begin{bmatrix} l \\ p \end{bmatrix}_{(n)} - \begin{bmatrix} Y_5 & Y_9 \\ Y_7 & Y_{11} \end{bmatrix}^{-1}_{(n)} \begin{bmatrix} Y_1 \\ Y_3 \end{bmatrix}_{(n)}$$

The last set of four first order ODEs in terms of l and p are differentiated to get another system of ODEs, as follows:

$$Y_5' = Y_6, \qquad Y_5(0) = 0.$$

$$Y_6' = \frac{1}{\left(1 + Rd\left(1 + (\theta_w - 1)Y_1\right)^3\right)}\Bigg[- 3Rd(\theta_w - 1)2Y_2Y_6\left(1 + (\theta_w - 1)Y_1\right)^2$$

$$- 6Rd(\theta_w - 1)^2 Y_5 Y_2^2\left(1 + (\theta_w - 1)Y_1\right)$$

$$- Pr\left[PrfY_6 + N_bY_6Y_4 + N_bY_2Y_8 + 2N_tY_2Y_6\right]\Bigg]$$

$$- \frac{3Rd(\theta_w - 1)Y_5\left(1 + (\theta_w - 1)Y_1\right)^2}{\left(1 + Rd\left(1 + (\theta_w - 1)Y_1\right)^3\right)^2}\Bigg[- 3Rd(\theta_w - 1)Y_2^2\left(1 + (\theta_w - 1)Y_1\right)^2$$

$$- Pr\Bigg[PrfY_2 + N_bY_2Y_4 + N_tY_2^2 + Ec\Bigg(\left(1 + \frac{1}{\beta}\right)\left(f''^2 + g'^2\right)$$

$$+ M\left(f'^2 + g^2\right)\Bigg)\Bigg]\Bigg], \qquad Y_6(0) = 1.$$

$$Y_7' = Y_8, \qquad Y_7(0) = 0.$$

$$Y_8' = -ScfY_4 - \left(\frac{Nt}{Nb}\right)\frac{1}{\left(1 + Rd\left(1 + (\theta_w - 1)Y_1\right)^3\right)}\Bigg[- 3Rd(\theta_w - 1)2Y_2Y_6$$

$$\left(1 + (\theta_w - 1)Y_1\right)^2 - 6Rd(\theta_w - 1)^2Y_5Y_2^2\left(1 + (\theta_w - 1)Y_1\right) - Pr\Bigg[PrfY_6$$

$$+ N_bY_6Y_4 + N_bY_2Y_8 + 2N_tY_2Y_6\Bigg]\Bigg] + \frac{3Rd(\theta_w - 1)Y_5\left(1 + (\theta_w - 1)Y_1\right)^2}{\left(1 + Rd\left(1 + (\theta_w - 1)Y_1\right)^3\right)^2}$$

$$\left(\frac{Nt}{Nb}\right)\Bigg[- 3Rd(\theta_w - 1)Y_2^2\left(1 + (\theta_w - 1)Y_1\right)^2 - Pr\Bigg[PrfY_2 + N_bY_2Y_4$$

$$+ N_tY_2^2 + Ec\Bigg(\left(1 + \frac{1}{\beta}\right)\left(f''^2 + g'^2\right) + M\left(f'^2 + g^2\right)\Bigg)\Bigg]\Bigg], \qquad Y_8(0) = 0.$$

$$Y_9' = Y_{10}, \qquad Y_9(0) = 0.$$

$$Y_{10}' = \frac{1}{\left(1 + Rd\left(1 + (\theta_w - 1)Y_1\right)^3\right)}\Bigg[- 3Rd(\theta_w - 1)2Y_2Y_5\left(1 + (\theta_w - 1)Y_1\right)^2$$

$$
\begin{aligned}
&- 6Rd(\theta_w - 1)^2 Y_9 Y_2^2\Big(1 + (\theta_w - 1)Y_1\Big) - Pr\Big[PrfY_{10} \\
&+ N_b Y_{10} Y_4 + N_b Y_2 Y_{12} + 2N_t Y_2 Y_{10}\Big]\Big] - \frac{3Rd(\theta_w - 1)Y_9\Big(1 + (\theta_w - 1)Y_1\Big)^2}{\Big(1 + Rd\Big(1 + (\theta_w - 1)Y_1\Big)^3\Big)^2} \\
&\Big[- 3Rd(\theta_w - 1)Y_2^2\Big(1 + (\theta_w - 1)Y_1\Big)^2 - Pr\Big[PrfY_2 + N_b Y_2 Y_4 + N_t Y_2^2 \\
&+ Ec\Big(\Big(1 + \frac{1}{\beta}\Big)\Big(f''^2 + g'^2\Big) + M\Big(f'^2 + g^2\Big)\Big)\Big]\Big], \qquad Y_{10}(0) = 0. \\
Y_{11}' &= Y_{12}, \qquad Y_{11}(0) = 0. \\
Y_{12}' &= -ScfY_{12} - \frac{1}{\Big(1 + Rd\Big(1 + (\theta_w - 1)Y_1\Big)^3\Big)}\Big(\frac{Nt}{Nb}\Big)\Big[- 3Rd(\theta_w - 1)2Y_2 Y_{10} \\
&\Big(1 + (\theta_w - 1)Y_1\Big)^2 - 6Rd(\theta_w - 1)^2 Y_9 Y_2^2\Big(1 + (\theta_w - 1)Y_1\Big) - Pr\Big[PrfY_{10} \\
&+ N_b Y_{10} Y_4 + N_b Y_2 Y_{12} + 2N_t Y_2 Y_{10}\Big]\Big] + \frac{3Rd(\theta_w - 1)Y_9\Big(1 + (\theta_w - 1)Y_1\Big)^2}{\Big(1 + Rd\Big(1 + (\theta_w - 1)Y_1\Big)^3\Big)^2} \\
&\Big(\frac{Nt}{Nb}\Big)\Big[- 3Rd(\theta_w - 1)Y_2^2\Big(1 + (\theta_w - 1)Y_1\Big)^2 - Pr\Big[PrfY_2 + N_b Y_2 Y_4 \\
&+ N_t Y_2^2 + Ec\Big(\Big(1 + \frac{1}{\beta}\Big)\Big(f''^2 + g'^2\Big) + M\Big(f'^2 + g^2\Big)\Big)\Big]\Big], \qquad Y_{12}(0) = 1.
\end{aligned}
$$

The Newton's method stopping criteria is established as:

$$
max\{\mid Y_1(\eta_\infty, l^n, p^n) \mid, \mid Y_3(\eta_\infty, l^n, p^n) \mid\} < \epsilon.
$$

3.4 Results and Discussion of Graphs and Tables

In this section, we will thoroughly discuss the influence of the dimensionless parameters on the skin friction coefficients $Re_x^{\frac{1}{2}} C_{f_x}$, $Re_y^{\frac{1}{2}} C_{f_y}$, Nusselt number $Re_x^{-\frac{1}{2}} Nu_x$ and Sherwood number $Re_x^{-\frac{1}{2}} Sh_x$ through different graphs and tables. Table 3.1

shows the effect of Casson parameter β, rotation parameter γ_1 and magnetic parameter M on $Re_x^{\frac{1}{2}}C_{f_x}$ and $Re_y^{\frac{1}{2}}C_{f_y}$. For accelerating the values of Casson parameter β, $Re_x^{\frac{1}{2}}C_{f_x}$ and $Re_x^{\frac{1}{2}}C_{f_y}$ increase. Table 3.1 expresses the intervals I_f and I_g from where the missing conditions r and m can be chosen respectively. Analysis conducted regarding the Nusselt number, shows a great flexibility in the choice of missing initial conditions.Table 3.2 explains the impact of Casson parameter β, rotation parameter γ_1, magnetic parameter M, radiation parameter Rd, temprature ratio parameter, θ_w, Prandtl number Pr, Brownian parameter Nb, thermophoresis parameter Nt, Eckert number Ec and Schmidt number Sc on $Re_x^{-\frac{1}{2}}Nu_x$ and Sherwood number $Re_x^{-\frac{1}{2}}Sh_x$. A decreasing behaviour is observed in $Re_x^{-\frac{1}{2}}Nu_x$ and $Re_x^{-\frac{1}{2}}Sh_x$ by rising Casson parameter β.

Figure 3.2 illustrates how the velocity profile f' decreases as the Casson parameter β increases. From a tangible perspective, the Casson parameter is impacted by the yield stress. This stress, in turn, creates an opposing force that results in a decrease in the velocity of the fluid with the progressive rise of β values.
Figure 3.3 gives perception into the alike parameter correlated to the lateral velocity profile $g(\eta)$ in the y-direction. The velocity $g(\eta)$ exhibits an upward trend with respect to β. Within this framework, $g(\eta)$ adopts the configuration like parabolic, signifying that the flow transpires in the negative direction due to its negative values. The influence of M in the temperature profile θ is manifestly observed in Figure 3.4. It demonstrates that an escalation of this parameter leads to an elevation in the temperature profile, driven by the Lorentz force generated in the presence of a magnetic field.

The influence of the parameter γ_1 on $f^{'}$ and g is portrayed in Figures 3.5 and 3.6. It has been observed that an increase in the rotation parameter leads to a deterioration of velocity along the x-direction. In a physical sense, higher values of this parameter correspond to lower stretching rates along the x-direction. This parameter causes a decrease in the velocity along the x-direction. The results indicate that as the value of Nt is increased, both the temperature distribution and the concentration profile rise, as shown in Figures 3.7 and 3.8. This parameter signifies the availability of nanoparticles within the fluid.

The consequences of altering Magnetic parameter M for the velocity profiles $f^{'}$ and g is visualized in Figures 3.9 and 3.10, showcasing a decrease in $f^{'}$ and an increase in g with an increase in M. This occurs because a drag force which is temred as Lorentz force get raised due to applied magnetic field generated by the motion of charges. This force causes a decrease in the magnitude of velocity along the x-direction. Distinct values of θ_w illustrate the temperature profile θ increment in Figure 3.11. As this parameter increases, the temperature also experiences a corresponding increase.

A decline in the concentration profile ϕ is evident as the value of the Schmidt parameter Sc increases, as illustrated in Figure 3.12. Given that the Schmidt number is influenced by the Brownian diffusion coefficient, rise in Schmidt number leads to a decrease in the Brownian diffusion coefficient. Consequently, this suggests a reduction in nanoparticle concentration due to the diminished diffusion behavior. The effect of Nb is illustrated in Figures 3.13 and 3.14. As Nb increases, the temperature distribution rises, while the concentration profile decreases. The occurrence of Brownian motion in the fluid is attributed to the presence of nanoparticles. With an increase in Nb, this motion undergoes changes, leading to a subsequent decrease in the thickness of the concentration boundary layer for the nanoparticles.

Figure 3.15 reveals that due to an increment in γ_1, the temperature distribution also increases. In Figure 3.16, the impact of the radiation parameter Rd on the temperature distribution θ is depicted. As the radiation parameter boosts, it leads to the emit of more heat energy into the flow, resulting in an uplifted temperature profile. Figure 3.17 displays the impact of the Prandtl number Pr on the temperature distribution θ. Both the thickness of the thermal boundary layer and the temperature are functions that decrease as the Prandtl number Pr increases.
Certainly, the influence of the Eckert number Ec on the temperature distribution θ showcases a rising pattern in θ as the value of Ec increases, as illustrated in Figure 3.18. The temperature distribution escalates as the value of Eckert number goes up. This outcome arises from the fact that the Eckert number is dependent on kinetic energy, which, upon being converted to heat energy within the fluid,

results in a temperature increase. The impact of the Brownian parameter Nb in conjunction with the thermophoresis parameter Nt on the Sherwood number $Re^{-\frac{1}{2}}xShx$ is depicted in Figure 3.19. It has been observed that an increase in the value of Nb leads to a decreasing trend in the Sherwood number $Re^{-\frac{1}{2}}xShx$. Conversely, the Sherwood number exhibits an increasing trend as the value of Nt rises. The influence of the Brownian parameter Nb and the thermophoresis parameter Nt on the Nusselt number $Re^{-\frac{1}{2}}xNux$ is illustrated in Figure 3.20. It has been noted that an increase in the value of Nb leads to a decreasing trend in the Nusselt number $Re^{-\frac{1}{2}}xNux$. While, the Nusselt number exhibits a decreasing trend as the value of Nt rises.

Table 3.1: Results of $Re_x^{\frac{1}{2}}C_{fx}$ and $Re_x^{\frac{1}{2}}C_{fy}$ for various parameters

β	γ_1	M	$Re_x^{\frac{1}{2}}C_{fx}$	$Re_x^{\frac{1}{2}}C_{fy}$	I_f	I_g
0.5	0.5	0.5	-2.25599	-0.74306	[-2.60, -0.80]	[-1.90, -0.40]
0.8			-1.95536	-0.64464	[-1.90, -0.05]	[-2.10, -0.70]
1.0			-1.84389	-0.60783	[-1.50, -0.30]	[-3.30, -2.50]
	0.3		-2.17631	-0.46452	[-2.30, -2.20]	[-2.10, -1.70]
	0.6		-2.30372	-0.86977	[-2.00, -1.80]	[-1.96, -1.60]
	0.9		-2.48950	-1.20444	[-2.70, -2.00]	[-1.90, -1.80]
		0	-1.96303	-0.89072	[-2.20, -2.10]	[-3.40, -1.10]
		0.4	-2.10783	-0.76799	[-2.70, -1.70]	[-2.20, -1.60]
		0.8	-2.42690	-0.67951	[-2.20, -1.60]	[-3.30, -2.20]

TABLE 3.2: Results of $Re_x^{-\frac{1}{2}}Nu_x$ and $Re_x^{-\frac{1}{2}}Sh_x$ for various parameters

β	γ_1	M	Rd	θ_w	Pr	Nb	Nt	Ec	Sc	$Re_x^{-\frac{1}{2}}Nu_x$	$Re_x^{-\frac{1}{2}}Sh_x$
0.5	0.5	0.5	0.2	1.5	2.0	0.5	0.5	0.2	5.0	0.14108	1.77018
0.8										0.14565	1.72238
1.0										0.14675	1.70095
	0.3									0.19374	1.74255
	0.6									0.14098	1.74147
		0.0								0.26108	1.72395
		0.4								0.18124	1.73817
			0.4							0.25770	1.70134
			0.5							0.29915	1.68865
				1.2						0.11804	1.76998
				1.4						0.14631	1.75114
					0.0					0.20289	1.64514
					0.5					0.22277	1.63901
						0.2				0.27343	1.78912
						0.4				0.19469	1.75236
							0.2			0.22871	1.66604
							0.4			0.18207	1.71491
								0.0		0.46312	1.60693
								0.05		0.38878	1.63960
									3.0	0.17080	1.31038
									4.0	0.16415	1.54173

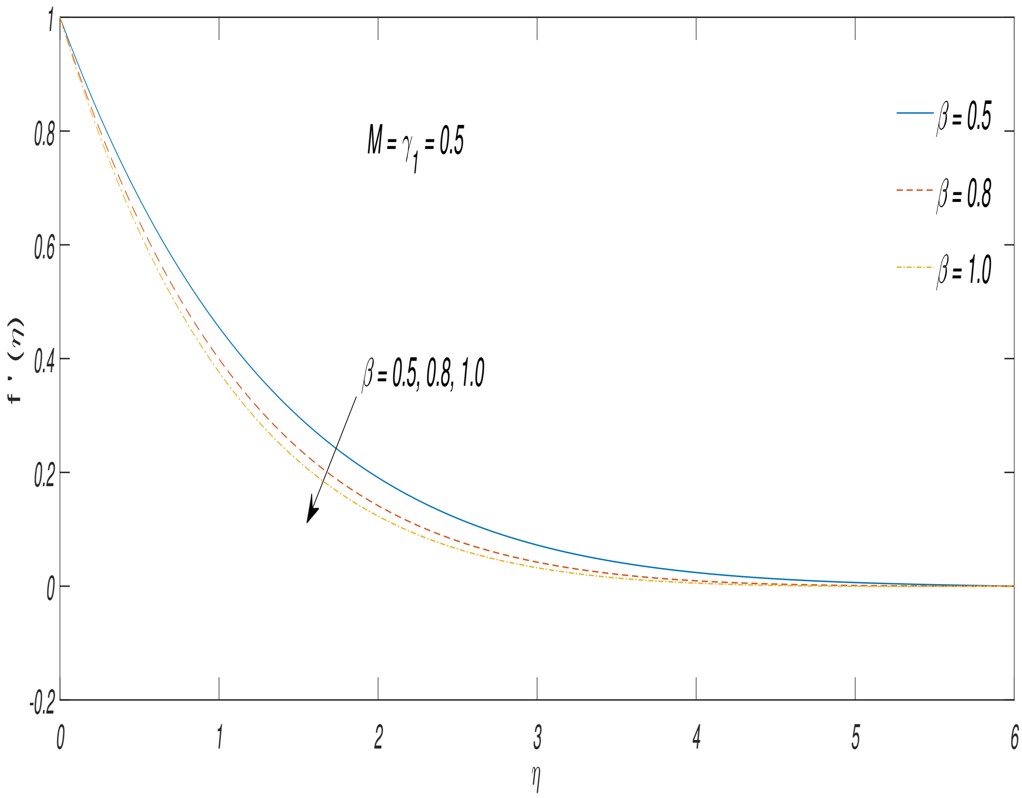

FIGURE 3.2: Velocity f'(η) discrepancy against β

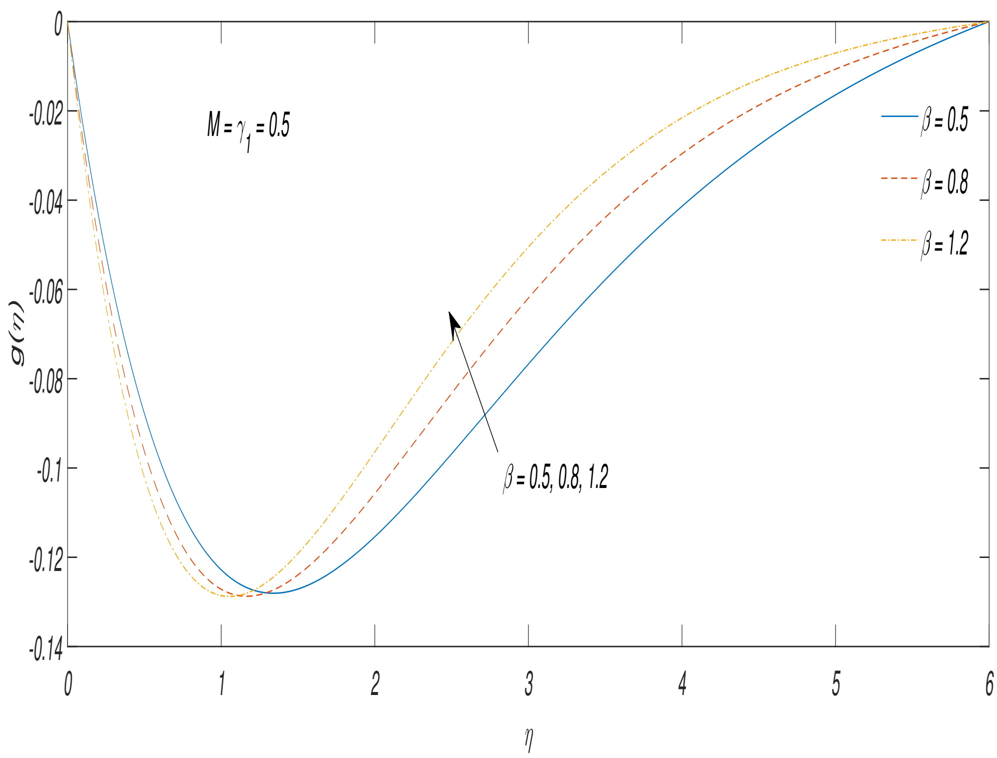

FIGURE 3.3: Velocity g(η) discrepancy against β

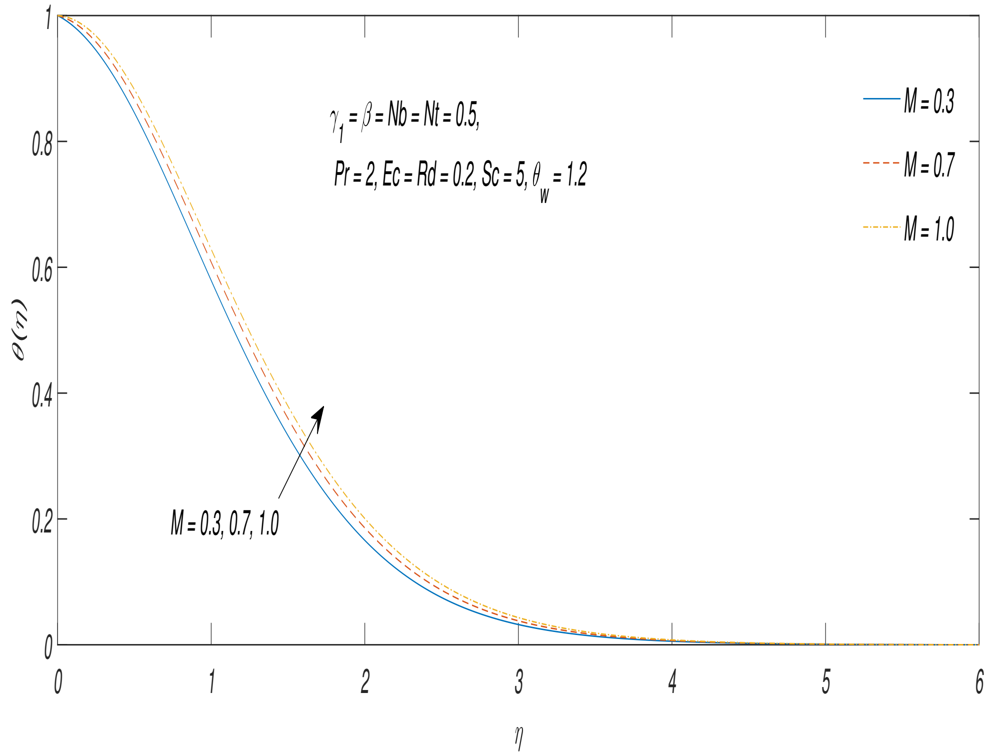

Figure 3.4: Temperature $\theta(\eta)$ discrepancy against M

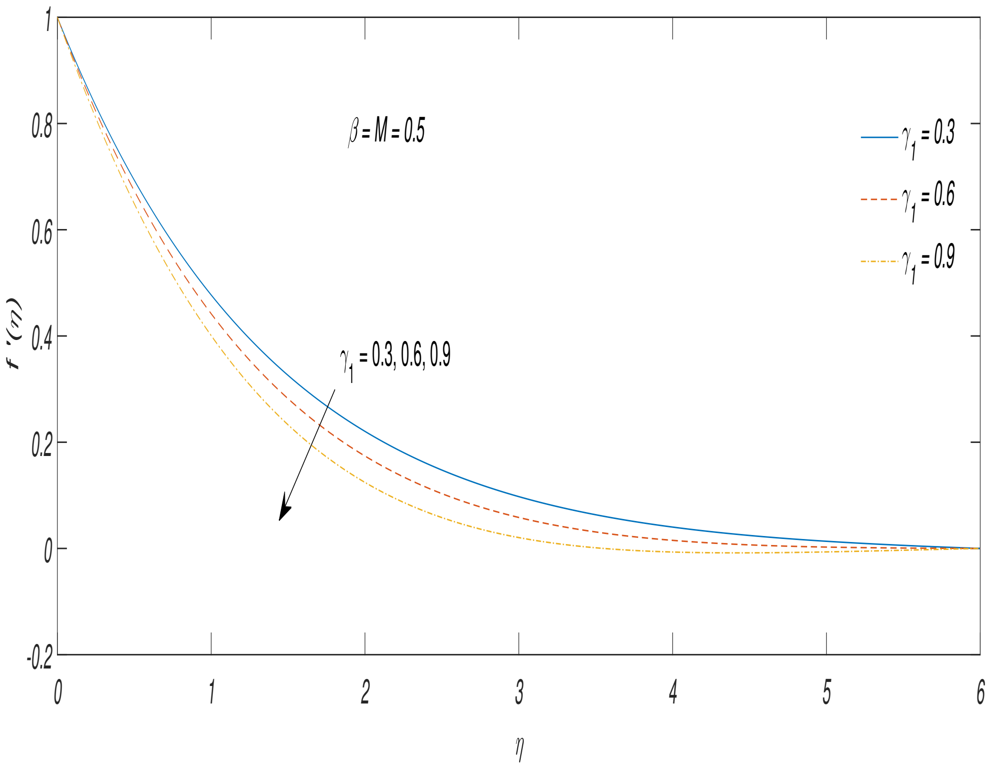

Figure 3.5: Velocity f'(η) discrepancy against γ_1

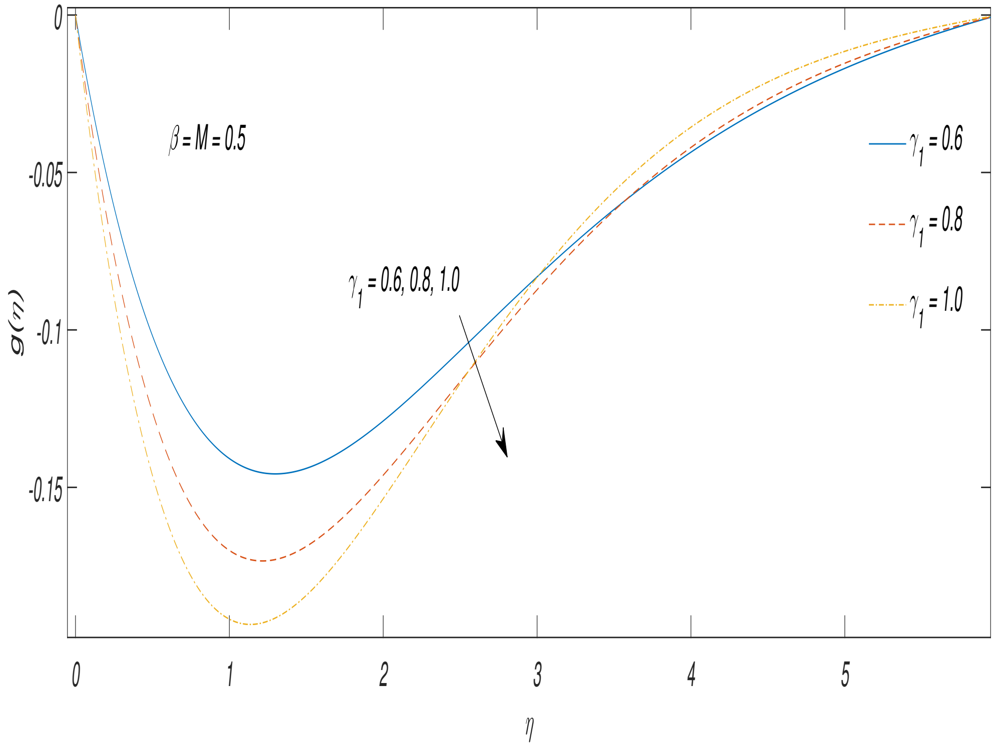

FIGURE 3.6: Velocity g(η) discrepancy against γ_1

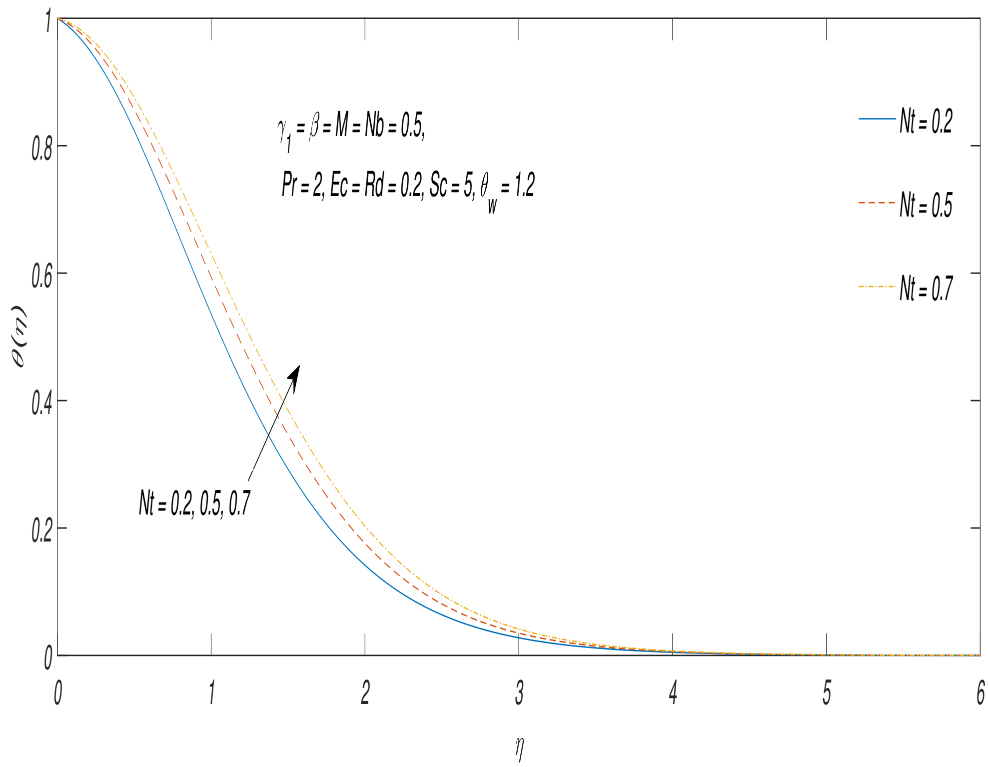

FIGURE 3.7: Temperature $\theta(\eta)$ discrepancy against Nt

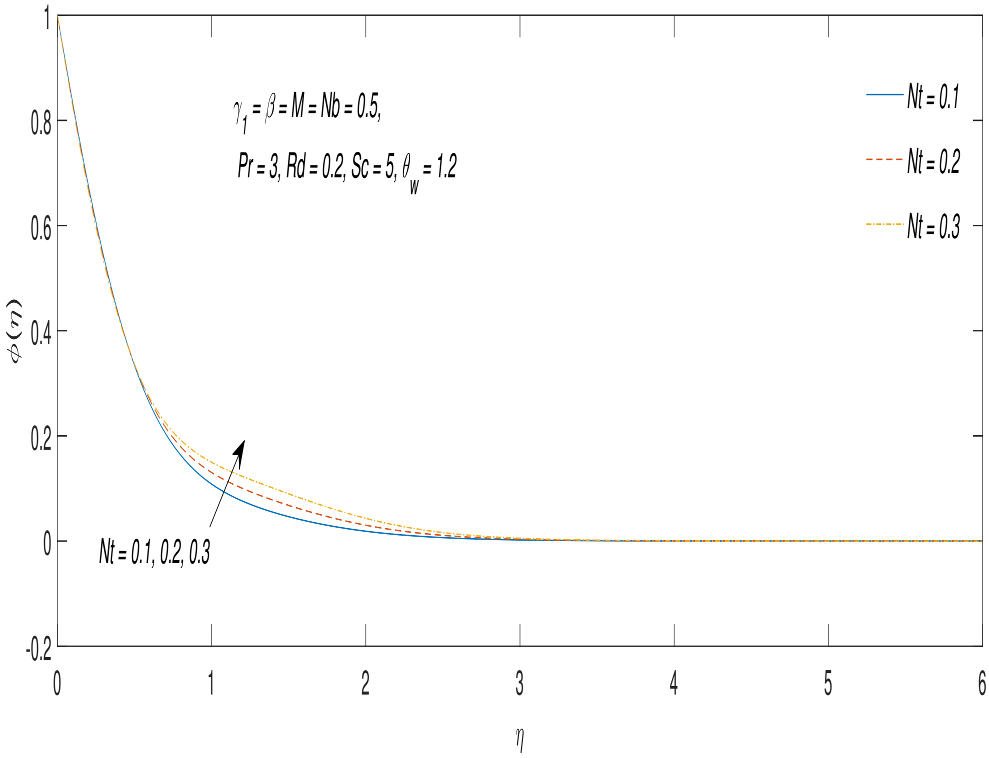

FIGURE 3.8: Concentration $\phi(\eta)$ discrepancy against Nt

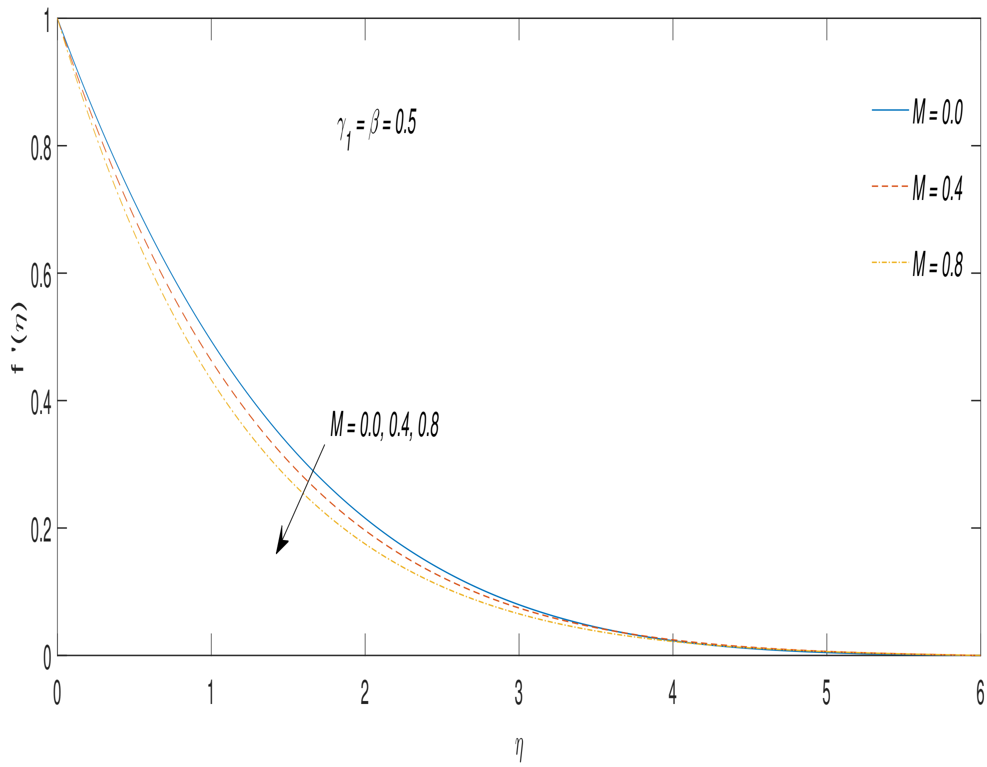

FIGURE 3.9: Velocity f'(η) discrepancy against M

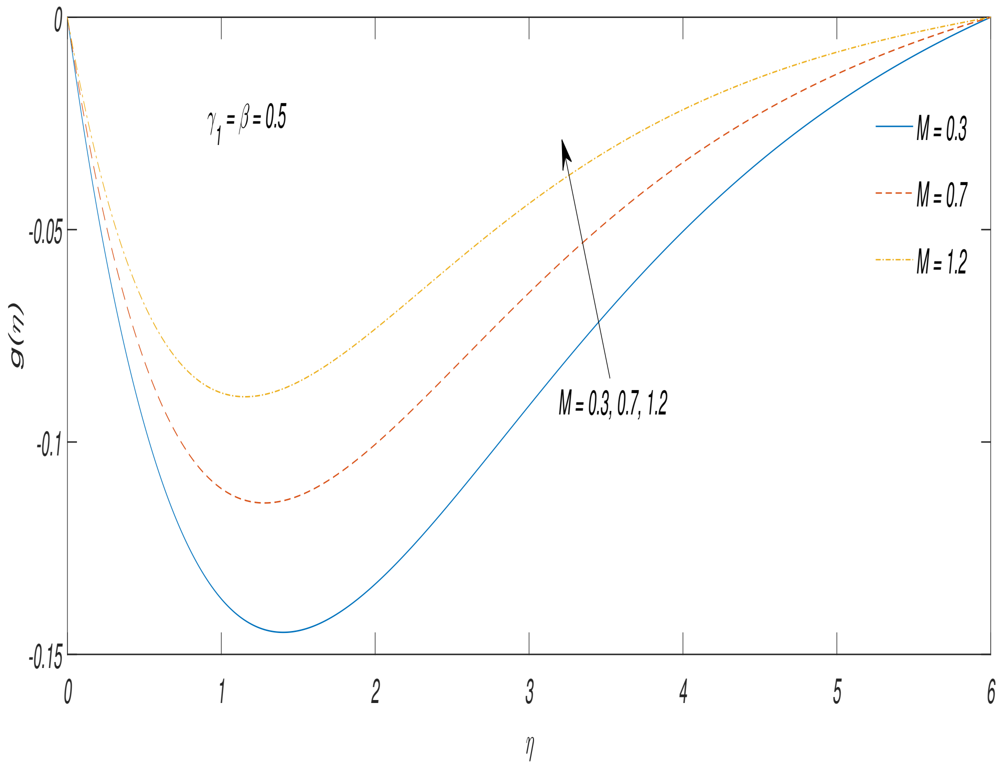

FIGURE 3.10: Velocity g(η) discrepancy against M

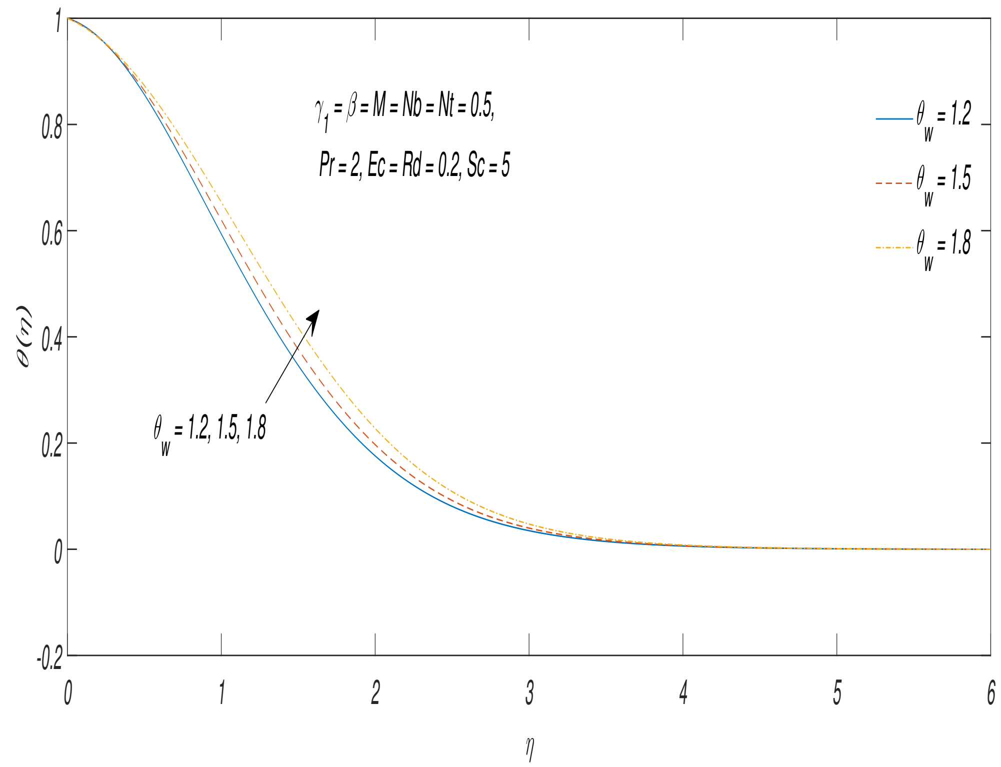

FIGURE 3.11: Temperature $\theta(\eta)$ discrepancy against θ_w

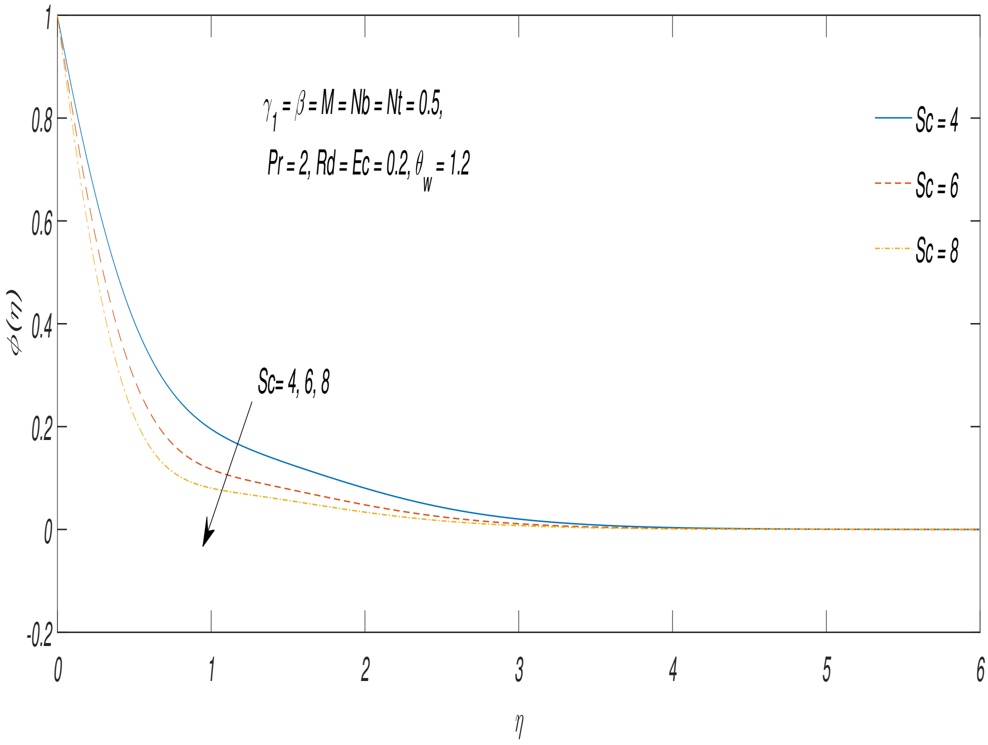

FIGURE 3.12: Concentration $\phi(\eta)$ discrepancy against Sc

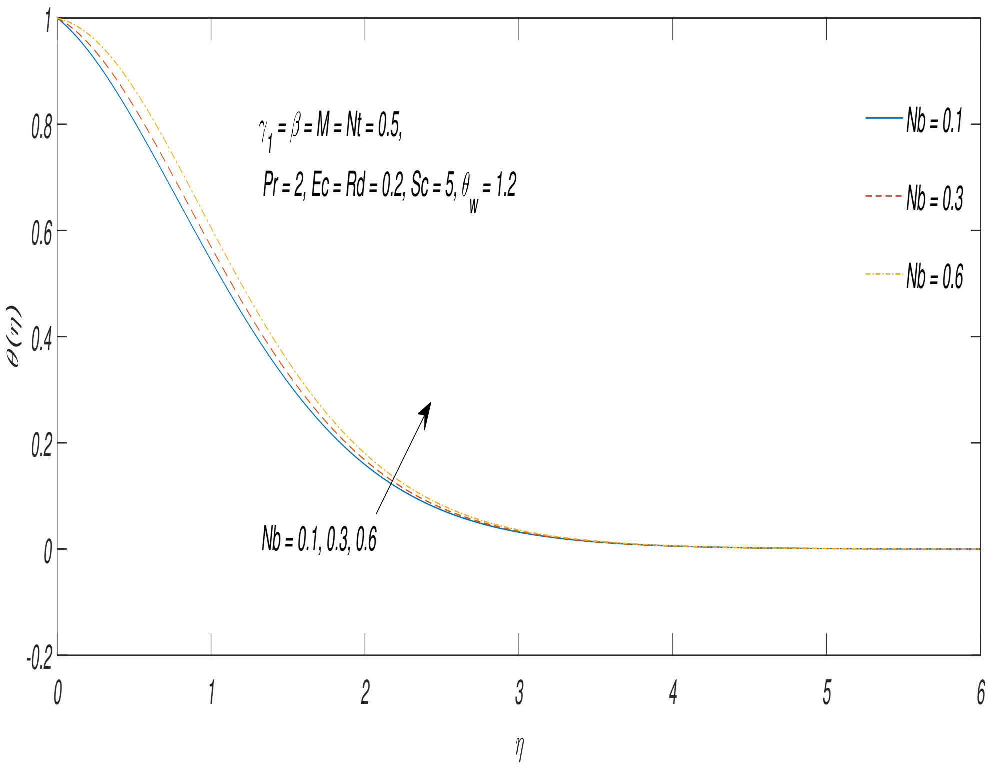

FIGURE 3.13: Temperature $\theta(\eta)$ discrepancy against Nb

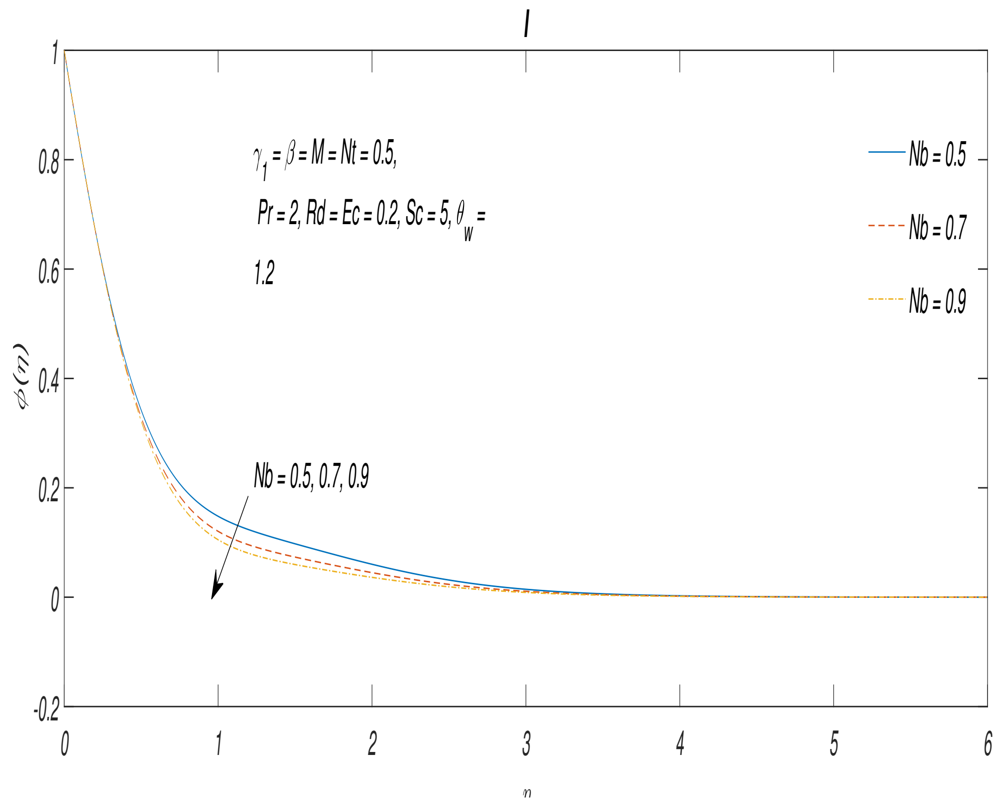

FIGURE 3.14: Concentration $\phi(\eta)$ discrepancy against Nb

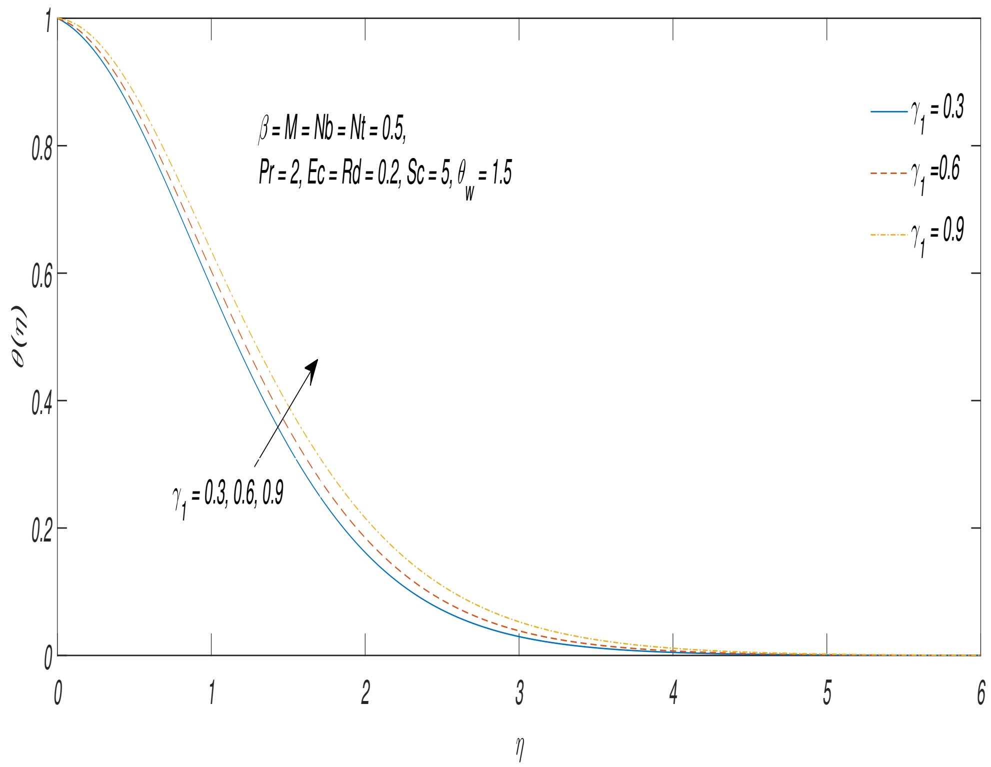

FIGURE 3.15: Temperature $\theta(\eta)$ discrepancy against γ_1

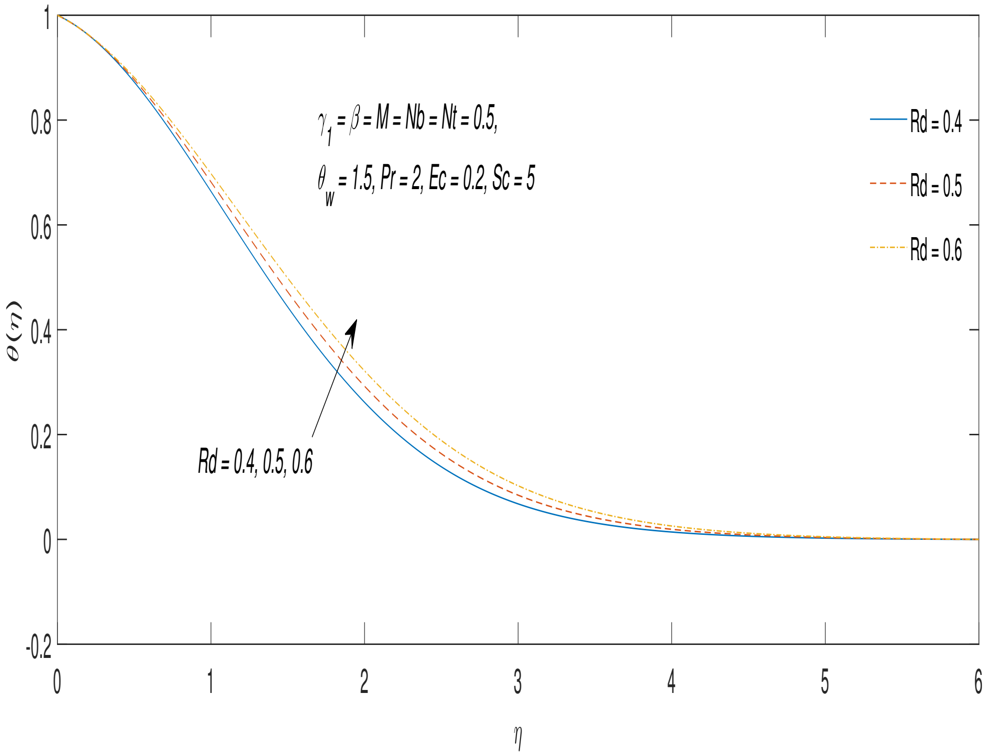

FIGURE 3.16: Temperature $\theta(\eta)$ discrepancy against Rd

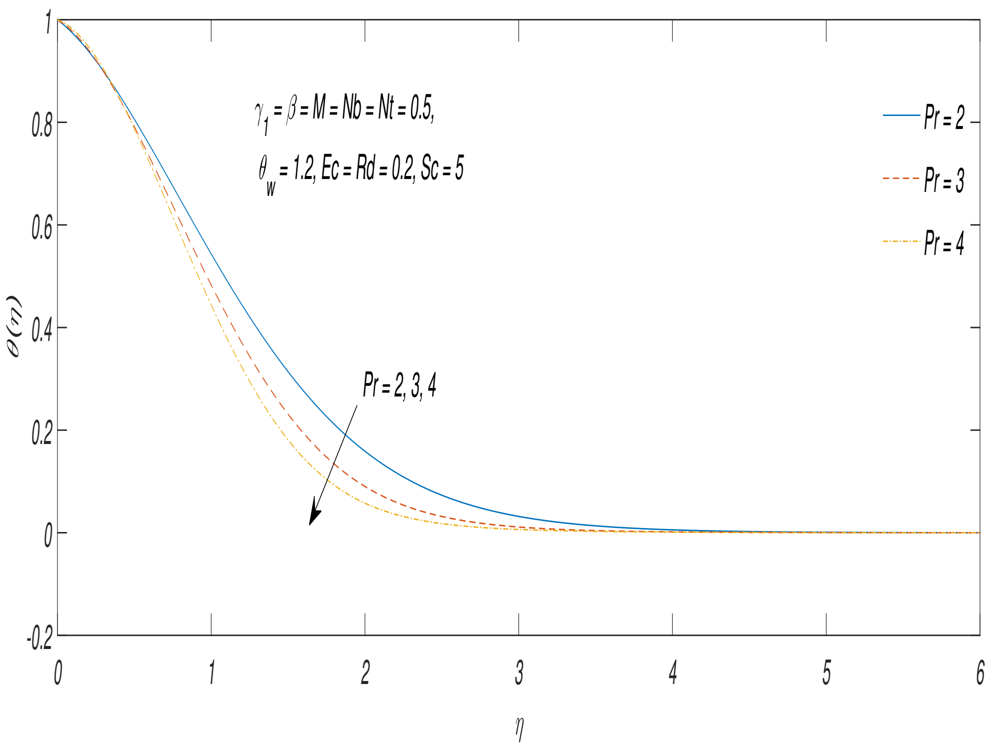

FIGURE 3.17: Temperature $\theta(\eta)$ discrepancy against Pr

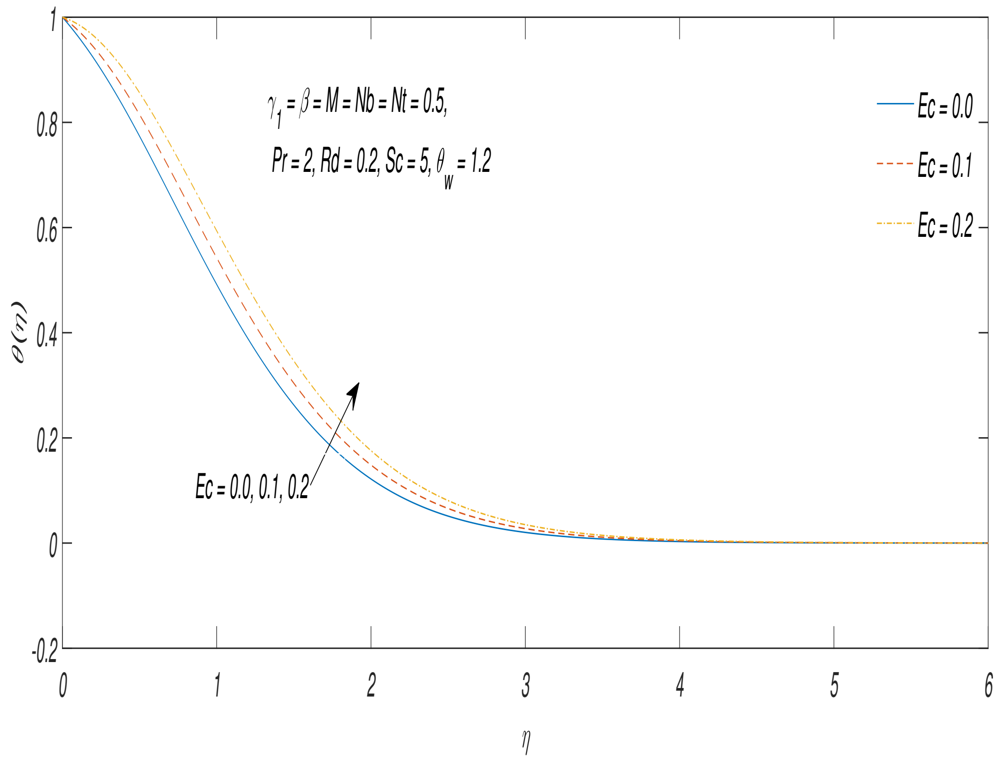

FIGURE 3.18: Temperature $\theta(\eta)$ discrepancy against Ec

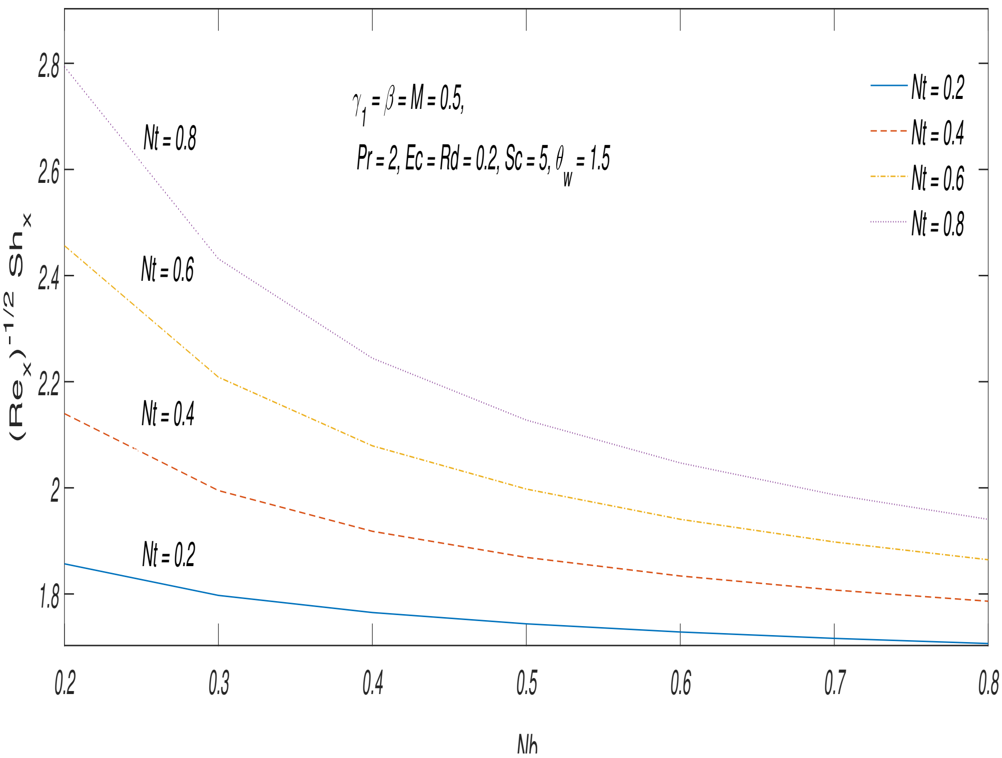

FIGURE 3.19: Sherwood number Sh_x discrepancy against Nb and Nt

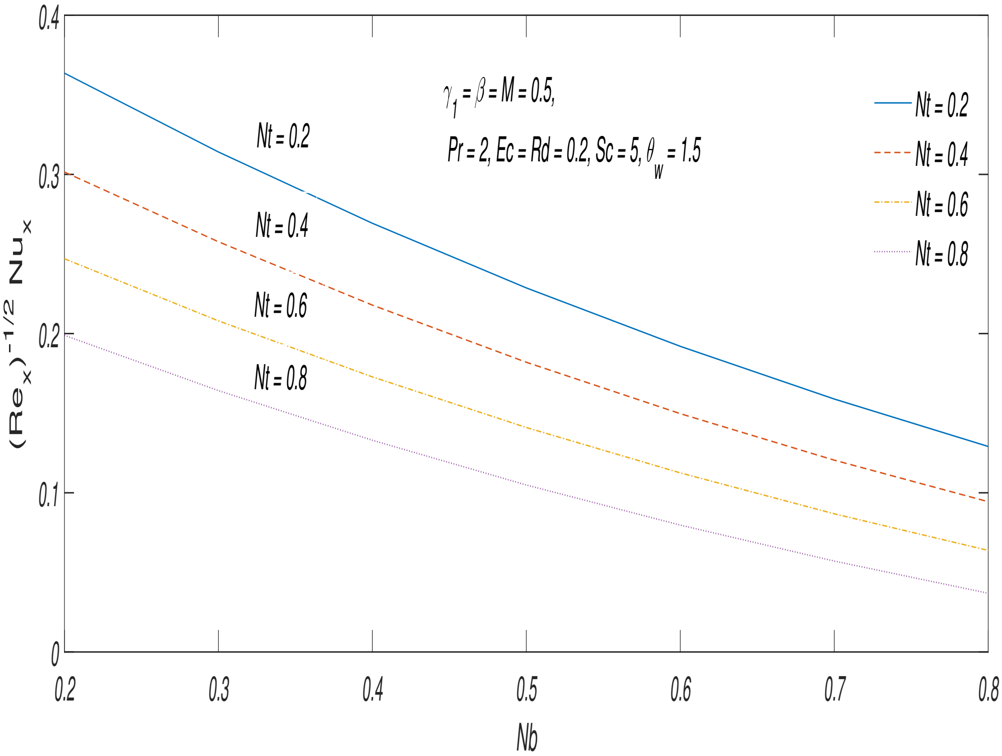

FIGURE 3.20: Nusselt number Nu_x discrepancy against Nb and Nt

Chapter 4

The Impact of Cattaneo-Christov Double Diffusion, Thermal Radiation on a Rotating Flow of Casson Nanofluid

4.1 Introduction

The model which is discussed in Chapter 3 has been extended in this chapter by taking an inclined magnetic field to account of the momentum equation. The effect of Cattaneo-Christov double diffusion has been taken for temperature and concentration equations. In this chapter, we will execute numerical analysis of the Cattaneo-Christov double diffusion Casson nanofluid flow on a linearly extending sheet. By employing similarity transformations, the governing nonlinear partial differential equations are converted into a set of dimensionless ODEs. Using the shooting technique as a numerical method, we compute the numerical solution for the ODEs.

4.2 Mathematical Modeling

Consider a three-dimensional steady, laminar flow of an incompressible Casson nanofluid along stretching sheet surface. In this study, the fluid has been considered to rotate around the z-axis with an angular velocity Ω within a flow region where z is restricted to values ≥ 0. Assume that the velocity of extending sheet is represented by $U_w(x) = ax$. An inclined magnetic field of magnitude B_0 is applied in z- axis. Energy transport phenomenon has been assumed in the presence of thermal radiation, heat generation, and Cattaneo-Christov double diffusion.

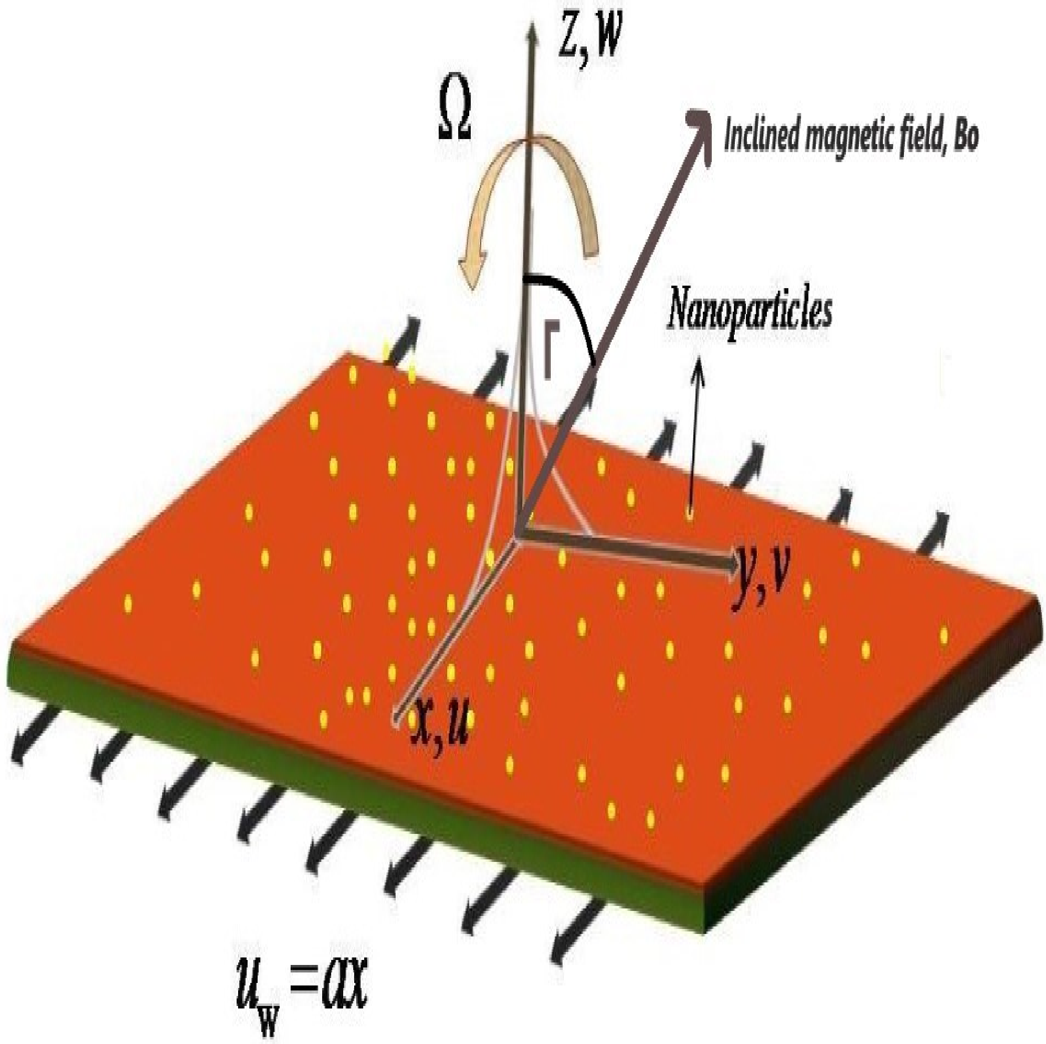

Figure 4.1: Methodical display of the tangible system.

By considering the above assumptions, the goverining PDEs become:

$$\frac{\partial u}{\partial x}+\frac{\partial v}{\partial y}+\frac{\partial w}{\partial z}=0, \tag{4.1}$$

$$u\frac{\partial u}{\partial x}+v\frac{\partial u}{\partial y}+w\frac{\partial u}{\partial z}-2\Omega v=\nu\left(1+\frac{1}{\beta}\right)\frac{\partial^2 u}{\partial z^2}-\frac{\mu}{\rho_f}\frac{u}{k}-\frac{\sigma B_0^2}{\rho_f}usin^2(\Gamma), \tag{4.2}$$

$$u\frac{\partial v}{\partial x}+v\frac{\partial v}{\partial y}+w\frac{\partial v}{\partial z}+2\Omega u=\nu\left(1+\frac{1}{\beta}\right)\frac{\partial^2 v}{\partial z^2}-\frac{\mu}{\rho_f}\frac{v}{k}-\frac{\sigma B_0^2}{\rho_f}vsin^2(\Gamma), \tag{4.3}$$

$$\begin{aligned}
&u\frac{\partial T}{\partial x}+v\frac{\partial T}{\partial y}+w\frac{\partial T}{\partial z}+\Gamma_e\Bigg[u^2\frac{\partial^2 T}{\partial x^2}+v^2\frac{\partial^2 T}{\partial y^2}+w^2\frac{\partial^2 T}{\partial z^2}+2uv\frac{\partial^2 T}{\partial x\partial y}\\
&\quad+2vw\frac{\partial^2 T}{\partial y\partial z}+2uw\frac{\partial^2 T}{\partial x\partial z}+\left(u\frac{\partial u}{\partial x}+v\frac{\partial u}{\partial y}+w\frac{\partial u}{\partial z}\right)\frac{\partial T}{\partial x}\\
&\quad+\left(u\frac{\partial v}{\partial x}+v\frac{\partial v}{\partial y}+w\frac{\partial v}{\partial z}\right)\frac{\partial T}{\partial y}+\left(u\frac{\partial w}{\partial x}+v\frac{\partial w}{\partial y}+w\frac{\partial w}{\partial z}\right)\frac{\partial T}{\partial z}\Bigg]\\
&=\frac{\partial}{\partial z}\left[\left(\alpha+\frac{16\sigma^* T^3}{3K^*\left(\rho c_p\right)_f}\right)\frac{\partial T}{\partial z}\right]+\tau\left[D_B\frac{\partial T}{\partial z}\frac{\partial C}{\partial z}+\frac{D_T}{T_\infty}\left(\frac{\partial T}{\partial z}\right)^2\right]\\
&\quad+\frac{\mu}{\left(\rho c_p\right)_f}\left(1+\frac{1}{\beta}\right)\left(\left(\frac{\partial u}{\partial z}\right)^2+\left(\frac{\partial v}{\partial z}\right)^2\right)\\
&\quad+\frac{\sigma B_0^2}{\left(\rho c_p\right)_f}\left(u^2+v^2\right)sin^2(\Gamma)+\frac{Q}{\left(\rho c_p\right)_f}(T-T_\infty),
\end{aligned} \tag{4.4}$$

$$\begin{aligned}
&u\frac{\partial C}{\partial x}+v\frac{\partial C}{\partial y}+w\frac{\partial C}{\partial z}+\Gamma_c\Bigg[u^2\frac{\partial^2 C}{\partial x^2}+v^2\frac{\partial^2 C}{\partial y^2}+w^2\frac{\partial^2 C}{\partial z^2}+2uv\frac{\partial^2 C}{\partial x\partial y}\\
&\quad+2vw\frac{\partial^2 C}{\partial y\partial z}+2uw\frac{\partial^2 C}{\partial x\partial z}+\left(u\frac{\partial u}{\partial x}+v\frac{\partial u}{\partial y}+w\frac{\partial u}{\partial z}\right)\frac{\partial C}{\partial x}\\
&\quad+\left(u\frac{\partial v}{\partial x}+v\frac{\partial v}{\partial y}+w\frac{\partial v}{\partial z}\right)\frac{\partial C}{\partial y}+\left(u\frac{\partial w}{\partial x}+v\frac{\partial w}{\partial y}+w\frac{\partial w}{\partial z}\right)\frac{\partial C}{\partial z}\Bigg]\\
&=D_B\frac{\partial^2 C}{\partial z^2}+\frac{D_T}{T_\infty}\frac{\partial^2 T}{\partial z^2}-K_c^*(C-C_\infty).
\end{aligned} \tag{4.5}$$

The associated BCs have been taken as:

$$\left.\begin{array}{l}
u=U_w(x),\quad v=0,\quad w=0,\quad T=T_w,\quad C=C_w\quad at\quad z=0,\\
u\to 0,\quad v\to 0\quad T\to T_\infty,\quad C\to C_\infty\quad as\quad z\to\infty.
\end{array}\right\} \tag{4.6}$$

For the conversion of the mathematical model in the form of partial differential equations (4.1)-(4.5) into the ODEs, the following similarity transformation is used:

$$\left.\begin{aligned} &u = axf^{'}, \quad v = axg, \quad w = -\sqrt{a\nu}f, \\ &T = T_{\infty}\left(1 + (\theta_w - 1)\,\theta(\eta)\right), \quad \phi = \frac{C - C_{\infty}}{C_w - C_{\infty}}, \quad \eta = z\sqrt{\frac{a}{\nu}}. \end{aligned}\right\} \tag{4.7}$$

where $\theta_w = \frac{T_w}{T_\infty}$, $\theta_w > 1$ denotes the temperature ratio parameter.

The identical satisfaction of (4.1) is already mentioned in Chapter 3.

The dimensionless momentum equation (4.2) is achieved by using the derivatives which have been discussed earlier in Chapter 3.

$$\begin{aligned} &u\frac{\partial u}{\partial x} + v\frac{\partial u}{\partial y} + w\frac{\partial u}{\partial z} - 2\Omega v = \nu\left(1 + \frac{1}{\beta}\right)\frac{\partial^2 u}{\partial z^2} - \frac{\mu}{\rho_f}\frac{u}{k} - \frac{\sigma B_0^2}{\rho_f}usin^2(\Gamma). \\ \Rightarrow\;& a^2xf'^2 - a^2xff'' - 2\gamma_1 a^2xg = \nu\left(1 + \frac{1}{\beta}\right)\left(\frac{a^2}{\nu}xf^{'''}\right) \\ &- \frac{\nu a^2xf^{'}}{ak} - \frac{a^2x\sigma B_0^2f^{'}}{a\rho_f}sin^2(\Gamma). \\ \Rightarrow\;& f'^2 - ff'' - 2\gamma_1 g = \nu\left(1 + \frac{1}{\beta}\right)\left(\frac{1}{\nu}f^{'''}\right) - \frac{\nu f^{'}}{ak} - \frac{\sigma B_0^2 f^{'}}{a\rho_f}sin^2(\Gamma). \end{aligned}$$

Finally, The momentum equation in the dimensionless form is as follows:

$$\left(1 + \frac{1}{\beta}\right)f^{'''} - f'^2 + ff^{''} + 2\gamma_1 g - Kf' - Mf'sin^2(\Gamma) = 0. \tag{4.8}$$

The following dimensionless parameters are used in equation (4.8):

$$\gamma_1 = \tfrac{\Omega}{a}, \quad M = \tfrac{\sigma B_0^2}{\rho a}, \quad K = \tfrac{\nu}{ak}.$$

Similarly, the momentum equation (4.3) in the dimensionless form is written as:

$$\begin{aligned} &u\frac{\partial v}{\partial x} + v\frac{\partial v}{\partial y} + w\frac{\partial v}{\partial z} + 2\Omega u = \nu\left(1 + \frac{1}{\beta}\right)\frac{\partial^2 v}{\partial z^2} - \frac{\mu}{\rho_f}\frac{v}{k} - \frac{\sigma B_0^2}{\rho_f}vsin^2(\Gamma). \\ \Rightarrow\;& a^2xf'g - a^2xg'f + 2\gamma_1 a^2xf' = \nu\left(1 + \frac{1}{\beta}\right)\left(\frac{a^2}{\nu}xg^{''}\right) - \frac{\nu a^2xg}{ak} - \frac{a^2x\sigma B_0^2 g}{a\rho_f}. \\ \Rightarrow\;& f'g - g'f + 2\gamma_1 f' = \nu\left(1 + \frac{1}{\beta}\right)\left(\frac{1}{\nu}g^{''}\right) - \frac{\nu g}{ak} - \frac{\sigma B_0^2 g}{a\rho_f}. \end{aligned}$$

$$\left(1 + \frac{1}{\beta}\right)g^{''} + fg^{'} - f^{'}g - 2\gamma_1 f^{'} - Kg - Mgsin^2(\Gamma) = 0. \tag{4.9}$$

The equation (4.4) is transformed, by using the derivatices below:

$$\frac{\partial^2 T}{\partial z^2} = (T_w - T_\infty)\theta'' \frac{a}{\nu}. \tag{4.10}$$

$$w^2 \frac{\partial^2 T}{\partial z^2} = a\nu f^2 (T_w - T_\infty)\theta'' \frac{a}{\nu}. \tag{4.11}$$

$$u\frac{\partial T}{\partial x} = v\frac{\partial T}{\partial y} = 0. \tag{4.12}$$

$$u^2\frac{\partial^2 T}{\partial x^2} = v^2\frac{\partial^2 T}{\partial y^2} = 0. \tag{4.13}$$

$$2uv\frac{\partial^2 T}{\partial x \partial y} = 2vw\frac{\partial^2 T}{\partial y \partial z} = 2uw\frac{\partial^2 T}{\partial x \partial z} = 0. \tag{4.14}$$

$$w\frac{\partial w}{\partial z} = a\sqrt{a\nu} f f'. \tag{4.15}$$

The governing equation (4.4) for the conservation of energy gets the following dimensionless form, through the procedure shown below:

$$\begin{aligned}
& u\frac{\partial T}{\partial x} + v\frac{\partial T}{\partial y} + w\frac{\partial T}{\partial z} + \Gamma_e\Bigg[u^2\frac{\partial^2 T}{\partial x^2} + v^2\frac{\partial^2 T}{\partial y^2} + w^2\frac{\partial^2 T}{\partial z^2} + 2uv\frac{\partial^2 T}{\partial x \partial y} \\
& + 2vw\frac{\partial^2 T}{\partial y \partial z} + 2uw\frac{\partial^2 T}{\partial x \partial z} + \left(u\frac{\partial u}{\partial x} + v\frac{\partial u}{\partial y} + w\frac{\partial u}{\partial z}\right)\frac{\partial T}{\partial x} \\
& + \left(u\frac{\partial v}{\partial x} + v\frac{\partial v}{\partial y} + w\frac{\partial v}{\partial z}\right)\frac{\partial T}{\partial y} + \left(u\frac{\partial w}{\partial x} + v\frac{\partial w}{\partial y} + w\frac{\partial w}{\partial z}\right)\frac{\partial T}{\partial z}\Bigg] \\
& = \frac{\partial}{\partial z}\left[\left(\alpha + \frac{16\sigma^* T^3}{3K^*\left(\rho c_p\right)_f}\right)\frac{\partial T}{\partial z}\right] + \tau\left[D_B\frac{\partial T}{\partial z}\frac{\partial C}{\partial z} + \frac{D_T}{T_\infty}\left(\frac{\partial T}{\partial z}\right)^2\right] \\
& + \frac{\mu}{(\rho c_p)_f}\left(1 + \frac{1}{\beta}\right)\left(\left(\frac{\partial u}{\partial z}\right)^2 + \left(\frac{\partial v}{\partial z}\right)^2\right) \\
& + \frac{\sigma B_0^2}{(\rho c_p)_f}\left(u^2 + v^2\right) sin^2(\Gamma) + \frac{Q}{(\rho c_p)_f}(T - T_\infty). \\
\Rightarrow \quad & - af(T_w - T_\infty)\theta' + \Gamma_e\Bigg[+ a\nu f^2\left((T_w - T_\infty)\theta''\frac{a}{\nu}\right) \\
& + a\sqrt{a\nu} f f'\left((T_w - T_\infty)\theta'(\sqrt{\frac{a}{\nu}})\right)\Bigg] \\
& = \frac{\alpha a}{\nu}\Bigg[(T_w - T_\infty)\theta'' + Rd(T_w - T_\infty)\theta'\Big(1 + (\theta_w - 1)\theta\Big)^3 \\
& + 3Rd(\theta_w - 1)(T_w - T_\infty)\theta'^2\Big(1 + (\theta_w - 1)\theta\Big)^2\Bigg] + aN_b(T_w - T_\infty)\theta'\phi' \\
& + aN_t(T_w - T_\infty)\theta'^2 + \frac{aU_w^2}{(c_p)_f}\left(1 + \frac{1}{\beta}\right)\left(f''^2 + g'^2\right)
\end{aligned}$$

$$
\begin{aligned}
& + \frac{a\sigma B_0^2 U_w^2}{a(\rho c_p)_f}\left(f^{'2} + g^2\right) + \frac{Q}{(\rho c_p)_f}(T - T_\infty). \\
\Rightarrow \quad & - f\theta^{'} + a\Gamma_e\left[+ f^2\theta^{''} + \sqrt{a\nu}ff'\theta'\sqrt{\frac{a}{\nu}}\right] = \frac{\alpha}{\nu}\left[\theta^{''} + Rd\theta^{'}\left(1 + (\theta_w - 1)\theta\right)^3\right. \\
& \left. + 3Rd(\theta_w - 1)\theta'^2\left(1 + (\theta_w - 1)\theta\right)^2\right] + N_b\theta^{'}\phi^{'} + N_t\theta'^2 \\
& + \frac{aU_w^2}{(T_w - T_\infty)(c_p)_f}\left(1 + \frac{1}{\beta}\right)\left(f^{''2} + g'^2\right) \\
& + \frac{\sigma B_0^2 U_w^2}{a(T_w - T_\infty)(\rho c_p)_f}\left(f^{'2} + g^2\right) + \frac{Q}{(\rho c_p)_f}\frac{(T - T_\infty)}{a(T_w - T_\infty} - Prf\theta^{'}. \\
\Rightarrow \quad & + Pr\lambda_E\left[f^2\theta'' + ff'\theta'\right] = \theta^{''} + Rd\theta^{''}\left(1 + (\theta_w - 1)\theta\right)^3 \\
& + 3Rd(\theta_w - 1)\theta'^2\left(1 + (\theta_w - 1)\theta\right)^2 + PrN_b\theta^{'}\phi^{'} + PrN_t\theta'^2 \\
& + PrEc\left(1 + \frac{1}{\beta}\right)\left(f^{''2} + g'^2\right) + PrEcM\left(f^{'2} + g^2\right) + Pr\epsilon\theta. \\
\Rightarrow \quad & \left(\left(1 + Rd\left(1 + (\theta_w - 1)\theta\right)^3\right)\theta^{'}\right)^{'} \\
& + Pr\left[+ Prf\theta^{'}N_b\theta^{'}\phi^{'} + N_t\theta'^2 + Ec\left(\left(1 + \frac{1}{\beta}\right)\left(f^{''2} + g^{'2}\right)\right.\right. \\
& \left.\left. + M\left(f^{'2} + g^2\right)\right) - \lambda_E\left[f^2\theta'' + ff'\theta'\right] - \epsilon\theta\right] = 0. \qquad (4.16)
\end{aligned}
$$

The dimensionless parameters used in equation (4.16) are:

$$
\begin{gathered}
M{=}\tfrac{\sigma B_0^2}{\rho a}, \quad Rd{=}\tfrac{16\sigma^* T_\infty^3}{3kk^*}, \quad Pr{=}\tfrac{\nu}{\alpha}, \quad Nb{=}\tfrac{\tau D_B(C_w - C_\infty)}{\nu}, \\
Nt{=}\tfrac{\tau D_T(T_w - T_\infty)}{\nu T_\infty}, \quad Ec{=}\tfrac{U_w^2}{(c_p)_f(T_w - T_\infty)}, \quad \epsilon = \tfrac{Q}{a(\rho c_p)_f}.
\end{gathered}
$$

Now, for the conversion of concentration equation (4.5), the following derivatives are required.

$$
\begin{aligned}
\phi &= \frac{C - C_\infty}{C_w - C_\infty} \\
\Rightarrow \quad C &= C_\infty + (C_w - C_\infty)\phi. \\
w\frac{\partial C}{\partial z} &= -af\left(C_w - C_\infty\right)\phi^{'}. \qquad (4.17) \\
\frac{\partial^2 C}{\partial z^2} &= \left(C_w - C_\infty\right)\phi^{''}\frac{a}{\nu}. \qquad (4.18)
\end{aligned}
$$

$$u\frac{\partial C}{\partial x}=v\frac{\partial C}{\partial y}=0. \tag{4.19}$$

$$u^2\frac{\partial^2 C}{\partial x^2}=v^2\frac{\partial^2 C}{\partial y^2}=0. \tag{4.20}$$

$$2uv\frac{\partial^2 C}{\partial x\partial y}=2vw\frac{\partial^2 C}{\partial y\partial z}=2uw\frac{\partial^2 C}{\partial x\partial z}=0. \tag{4.21}$$

$$w\frac{\partial w}{\partial z}=a\sqrt{a\nu}ff'. \tag{4.22}$$

The governing equation (4.5) for the conservation of concentration gets the following dimensionless form:

$$\begin{aligned}
&-af\Big(C_w-C_\infty\Big)\phi^{'}+\Gamma_c\Big[a\nu f^2\Big((C_w-C_\infty)\phi^{''}\frac{a}{\nu}\Big)\\
&+a\sqrt{a\nu}ff'\Big((C_w-C_\infty)\phi^{'}\sqrt{\frac{a}{\nu}}\Big)\Big]=D_B\Big(C_w-C_\infty\Big)\phi^{''}\frac{a}{\nu}\\
&+\frac{D_B}{T_\infty}\Big((T_w-T_\infty)\theta^{''}\frac{a}{\nu}\Big)-K_c^*(C-C_\infty).\\
\Rightarrow&-f\phi^{'}+a\Gamma_C\Big[f^2\phi^{''}+ff'\phi^{'}\Big]=\frac{D_B}{\nu}\phi^{''}\\
&+\frac{D_T}{T_\infty}\frac{(T_w-T_\infty)}{(C_w-C_\infty)}\frac{\theta^{''}}{\nu}-K_c^*\frac{(C-C_\infty)}{a(C_w-C_\infty)}.\\
\Rightarrow&-f\phi^{'}+\lambda_C\Big[f^2\phi^{''}+ff'\phi^{'}\Big]=\frac{D_B}{\nu}\phi^{''}\\
&+\frac{D_T}{T_\infty}\frac{(T_w-T_\infty)}{(C_w-C_\infty)}\frac{\theta^{''}}{\nu}-\frac{K_c^*}{a}\phi\\
&-\frac{\nu}{D_B}f\phi^{'}+\frac{\nu}{D_B}\lambda_C\Big[f^2\phi^{''}+ff'\phi^{'}\Big]=\phi^{''}\\
&+\frac{D_T}{T_\infty}\frac{\nu}{D_B}\frac{\tau(T_w-T_\infty)}{\tau(C_w-C_\infty)}\frac{\theta^{''}}{\nu}-\frac{\nu}{D_B}\frac{K_c^*}{a}\phi.\\
\Rightarrow&-Scf\phi^{'}+Sc\lambda_C\Big[f^2\phi^{''}+ff'\phi^{'}\Big]=\phi^{''}\\
&+\frac{N_t}{N_b}\theta^{''}-ScK_c\phi.
\end{aligned}$$

$$\phi^{''}+Sc\Big[f\phi^{'}-\lambda_C\Big(f^2\phi^{''}+ff'\phi^{'}\Big)-K_c\phi\Big]+\frac{N_t}{N_b}\theta^{''}=0. \tag{4.23}$$

The following dimensionless parameters are used in equation (4.32):

$$Nb{=}\tfrac{\tau D_B(C_w-C_\infty)}{\nu},\quad Nt{=}\tfrac{\tau D_T(T_w-T_\infty)}{\nu T_\infty},\quad Sc{=}\tfrac{\nu}{D_B}$$
$$\lambda_C{=}\mathrm{a}\Gamma_c,\quad K_c=\tfrac{K_c^*}{a}.$$

The related dimensionless BCs are converted by the following procedure.

$$u = U_w(x), \qquad at \quad z = 0.$$
$$\Rightarrow \quad axf'(\eta) = ax, \qquad at \quad \eta = 0.$$
$$\Rightarrow \quad f'(0) = 1,$$
$$v = 0, \qquad at \quad z = 0.$$
$$\Rightarrow \quad axg(\eta) = 0, \qquad at \quad \eta = 0.$$
$$\Rightarrow \quad g(0) = 0,$$
$$w = 0, \qquad at \quad z = 0.$$
$$\Rightarrow \quad -\sqrt{a\nu}f(\eta) = 0, \qquad at \quad \eta = 0.$$
$$\Rightarrow \quad f(0) = 0,$$
$$T = T_w, \qquad at \quad z = 0.$$
$$\Rightarrow \quad \theta(\eta)(T_w - T_\infty) + T_\infty = T_w, \qquad at \quad \eta = 0.$$
$$\Rightarrow \quad \theta(\eta)(T_w - T_\infty) = (T_w - T_\infty), \qquad at \quad \eta = 0.$$
$$\Rightarrow \quad \theta(0) = 1,$$
$$C = C_w, \qquad at \quad z = 0.$$
$$\Rightarrow \quad \phi(\eta)(C_w - C_\infty) = (C_w - C_\infty), \qquad at \quad \eta = 0.$$
$$\Rightarrow \quad \phi(0) = 1,$$
$$u \to 0, \qquad as \quad z \to \infty.$$
$$\Rightarrow \quad f'(\eta) \to 0, \qquad as \quad \eta \to \infty.$$
$$v \to 0, \qquad as \quad z \to \infty.$$
$$\Rightarrow \quad g(\eta) \to 0, \qquad as \quad \eta \to \infty.$$
$$w \to 0, \qquad as \quad z \to \infty.$$
$$\Rightarrow \quad f(\eta) \to 0, \qquad as \quad \eta \to \infty.$$
$$T \to T_\infty, \qquad as \quad z \to \infty.$$
$$\Rightarrow \quad \theta(\eta) \to 0, \qquad as \quad \eta \to \infty.$$
$$C \to C_\infty, \qquad as \quad z \to \infty.$$
$$\Rightarrow \quad \phi(\eta) \to 0, \qquad as \quad \eta \to \infty.$$

The ultimate governing model into dimensionless is:

$$\left(1+\frac{1}{\beta}\right)f^{'''}-f^{\prime 2}+ff^{''}+2\gamma_1 g-\kappa f'-Mf'sin^2(\Gamma)=0, \tag{4.24}$$

$$\left(1+\frac{1}{\beta}\right)g^{''}+fg^{'}-f^{'}g-2\gamma_1 f^{'}-\kappa g-Mgsin^2(\Gamma)=0, \tag{4.25}$$

$$\begin{aligned}&\left(\left(1+Rd\left(1+(\theta_w-1)\theta\right)^3\right)\theta^{'}\right)^{'}+Pr\Bigg[+Prf\theta^{'}+N_b\theta^{'}\phi^{'}\\&+N_t\theta^{\prime 2}+Ec\left(\left(1+\frac{1}{\beta}\right)\left(f^{\prime\prime 2}+g^{'2}\right)+M\left(f^{'2}+g^2\right)\right)\\&-\lambda_E\left[f^2\theta''+ff'\theta'\right]+\epsilon\theta\Bigg]=0.\end{aligned} \tag{4.26}$$

$$\phi^{''}+Sc\left[f\phi^{'}-\lambda_C\left(f^2\phi^{''}+ff'\phi^{'}\right)-K_c\phi\right]+\frac{N_t}{N_b}\theta^{''}=0. \tag{4.27}$$

The dimensionless form for the related BCs (4.6) are:

$$\left.\begin{aligned}&f(0)=0,\quad g(0)=0,\quad f'(0)=1,\quad \theta(0)=0,\quad \phi(0)=0,\quad as\quad \eta\to 0.\\&f^{'}\to 0,\quad g\to 0,\quad \theta\to 0,\quad \phi\to 0,\quad as\quad \eta\to\infty.\end{aligned}\right\} \tag{4.28}$$

The dimensionless numbers are same as discussed in Chapter 3, as the following:

$$C_{fx}=\frac{\tau_{wx}}{\rho_f U_w^2}, \tag{4.29}$$

$$C_{fy}=\frac{\tau_{wy}}{\rho_f U_w^2}, \tag{4.30}$$

$$Re_x^{-\frac{1}{2}}Nu_x=\frac{U_w q_w}{ak(T_w-T_\infty)}. \tag{4.31}$$

Now, the local Sherwood number is defined as:

$$Sh_x=\frac{xq_m}{D_B(C_w-C_\infty)}, \tag{4.32}$$

where

$$q_m=-D_B\left(\frac{\partial C}{\partial z}\right)_{z=0}.$$

Therefore

$$Sh_x = -\frac{xD_B(C_w - C_\infty)\phi^{'}(0)\sqrt{\frac{a}{\nu}}}{D_B(C_w - C_\infty)}$$

$$\begin{aligned} &= -\frac{x\phi^{'}(0)\sqrt{a}}{\sqrt{\nu}} \\ &= -\sqrt{\frac{U_w^2}{a\nu}}\phi^{'}(0) \\ \Rightarrow \quad Re_x^{-1/2}Sh_x &= -\phi^{'}(0). \end{aligned} \tag{4.33}$$

4.3 Numerical Method for Solution

The ordinary differential equations (4.24) and (4.25)have been resolved using the shooting method.

$$\begin{aligned} f^{'''} &= \frac{1}{\left(1+\frac{1}{\beta}\right)}\left[f'^2 - ff^{''} - 2\gamma_1 g + \kappa f' + Mf'sin^2(\Gamma)\right], \\ g^{''} &= \frac{1}{\left(1+\frac{1}{\beta}\right)}\left[-fg' + f'g + 2\gamma_1 f' + \kappa g + Mgsin^2(\Gamma)\right]. \end{aligned}$$

For this purpose, the following notations have been taken:

$$\begin{aligned} &f = Z_1, \qquad f' = Z_1' = Z_2, \qquad f'' = Z_1'' = Z_2' = Z_3, \\ &g = Z_4, \qquad g' = Z_4' = Z_5. \end{aligned}$$

The momentum equations are then transformed into the following system of first-order ODEs:

$$\begin{aligned} &Z_1' = Z_2, && Z_1(0) = 0. \\ &Z_2' = Z_3, && Z_2(0) = 1. \\ &Z_4' = Z_5, && Z_4(0) = 0. \end{aligned}$$

$$Z_5' = \frac{\beta}{1+\beta}\Bigg(- Z_1 Z_5 + Z_2 Z_4 + 2\gamma_1 Z_2 + \kappa Z_4 + M Z_4 sin^2(\Gamma)\Bigg), \qquad Z_5(0) = m.$$

RK-4 method is applied to compute the above IVP.

The domain of the problem is considered to be bounded i.e. $[0,\ \eta_\infty]$, where η_∞ represents as a +ve real number, in which variation in the solution is ignorable after $\eta = \eta_\infty$. The missing conditions r and m are to be chosen such that:

$$Z_2(\eta_\infty, r, m) = 0, \qquad Z_4(\eta_\infty, r, m) = 0.$$

Newton's method will be used to find r and m. This method has the following iterative scheme:

$$\begin{bmatrix} r \\ m \end{bmatrix}_{(n+1)} = \begin{bmatrix} r \\ m \end{bmatrix}_{(n)} - \begin{bmatrix} \frac{\partial Z_2}{\partial r} & \frac{\partial Z_2}{\partial m} \\ \frac{\partial Z_4}{\partial r} & \frac{\partial Z_4}{\partial m} \end{bmatrix}^{-1}_{(n)} \begin{bmatrix} Z_2 \\ Z_4 \end{bmatrix}_{(n)} \tag{4.34}$$

We further introduce the following notations:

$$\begin{aligned} &\frac{\partial Z_1}{\partial r} = Z_6, \quad \frac{\partial Z_2}{\partial r} = Z_7, \quad \frac{\partial Z_3}{\partial r} = Z_8, \quad \frac{\partial Z_4}{\partial r} = Z_9, \quad \frac{\partial Z_5}{\partial r} = Z_{10}, \\ &\frac{\partial Z_1}{\partial m} = Z_{11}, \quad \frac{\partial Z_2}{\partial m} = Z_{12}, \quad \frac{\partial Z_3}{\partial m} = Z_{13}, \quad \frac{\partial Z_4}{\partial m} = Z_{14}, \quad \frac{\partial Z_5}{\partial m} = Z_{15}. \end{aligned}$$

The iterative scheme of Newton method is, by using the results of above notations as follows:

$$\begin{bmatrix} r \\ m \end{bmatrix}_{(n+1)} = \begin{bmatrix} r \\ m \end{bmatrix}_{(n)} - \begin{bmatrix} Z_7 & Z_{12} \\ Z_9 & Z_{14} \end{bmatrix}^{-1}_{(n)} \begin{bmatrix} Z_2 \\ Z_4 \end{bmatrix}_{(n)}. \tag{4.35}$$

The last set of five first order ODEs in terms of r and m are differentiated to get another system of ODEs, as follows:

$$Z_6' = Z_7, \qquad Z_6(0) = 0.$$

$$Z_7' = Z_8, \qquad Z_7(0) = 0.$$

$$Z_8' = \frac{\beta}{1+\beta}\left(2Z_2Z_7 - Z_6Z_3 - Z_1Z_8 - 2Z_9\gamma_1 + \kappa Z_7 + MZ_7 sin^2(\Gamma)\right), \quad Z_8(0) = 1.$$

$$Z_9' = Z_{10}, \qquad Z_9(0) = 0.$$

$$Z_{10}' = \frac{\beta}{1+\beta}\left(-Z_6Z_5 - Z_1Z_10 + Z_7Z_4 + Z_2Z_9 - 2Z_7\gamma_1 + \kappa Z_9 + MZ_9 sin^2(\Gamma)\right),$$

$$Z_{10}(0) = 0.$$

$$Z_{11}' = Z_{12}, \qquad Z_{11}(0) = 0.$$

$$Z_{12}' = Z_{13}, \qquad Z_{12}(0) = 0.$$

$$Z_{13}' = \frac{\beta}{1+\beta}\left(2Z_2Z_{12} - Z_{11}Z_3 - Z_1Z_{13} - 2Z_{14}\gamma_1 + \kappa Z_{12} + MZ_{12} sin^2(\Gamma)\right),$$

$$Z_{13}(0) = 0.$$

$$Z_{14}' = Z_{15}, \qquad Z_{14}(0) = 0.$$

$$Z_{15}' = \frac{\beta}{1+\beta}\left(-Z_{11}Z_5 - Z_1Z_{15} + Z_{12}Z_4 + Z_2Z_{14} - 2Z_12\gamma_1 + \kappa Z_{14} + MZ_{14} sin^2(\Gamma)\right),$$

$$Z_{15}(0) = 1.$$

For the Newton's technique, the stopping criteria is as follows:

$$max\{\mid Z_2(\eta_\infty, r^n, m^n) \mid, \mid Z_4(\eta_\infty, r^n, m^n) \mid\} < \epsilon,$$

where $\epsilon > 0$ is a sufficiently small number, which has been considered as 10^{-10}. The ordinary differential equations (4.26) and (4.27) will be approximated by using the shooting technique assuming f and g as the known functions. Consider equations (4.26)−(4.27) in the following form:

$$\theta'' = \frac{1}{\left(1 - Pr\lambda_E f^2 + Rd\left(1+(\theta_w-1)\theta\right)^3\right)}\Bigg[-3Rd(\theta_w-1)\theta'^2\left(1+(\theta_w-1)\theta\right)^2 + M\left(f'^2 + g^2\right)\Bigg) - \lambda_E\left(ff'\theta'\right) + \epsilon\theta\Bigg]\Bigg], \tag{4.36}$$

$$\phi'' = \frac{1}{1 - Sc\lambda_C f^2(\eta)}\Bigg\{-Sc\Bigg[f\phi' - \lambda_C\left(ff'\phi'\right) - K_c\phi\Bigg]$$

$$\Bigg[-3Rd(\theta_w-1)\theta'^2\Big(1+(\theta_w-1)\theta\Big)^2-Pr\Big[f\theta'+N_b\theta'\phi'+N_t\theta'^2$$
$$+Ec\Bigg(\Big(1+\frac{1}{\beta}\Big)\Big(f''^2+g'^2\Big)+M\Big(f'^2+g^2\Big)\Bigg)-\lambda_E\Big(ff'\theta'\Big)+\epsilon\theta\Big]\Big]\Bigg]\Bigg\}. \tag{4.37}$$

The notations below has been taken into consideration:

$$\theta = Y_1, \qquad \theta' = Y_1' = Y_2,$$
$$\phi = Y_3, \qquad \phi' = Y_3' = Y_4.$$

The equations (4.26)−(4.27) are then transformed into the following system of first-order ODEs:

$$Y_1' = Y_2, \qquad Y_1(0) = 1.$$
$$Y_2' = \frac{1}{\Big(1-Pr\lambda_E f^2+Rd\Big(1+(\theta_w-1)Y_1\Big)^3\Big)}$$
$$\Bigg[-3Rd(\theta_w-1)Y_2^2\Big(1+(\theta_w-1)Y_1\Big)^2-Pr\Big[fY_2+N_bY_2Y_4+N_tY_2^2$$
$$+Ec\Bigg(\Big(1+\frac{1}{\beta}\Big)\Big(f''^2+g'^2\Big)+M\Big(f'^2+g^2\Big)\Bigg)-\lambda_E\Big(ff'Y_2\Big)+\epsilon Y_1\Big]\Bigg],$$
$$Y_2(0) = l.$$
$$Y_3' = Y_4, \qquad Y_3(0) = 1.$$
$$Y_4' = \frac{1}{1-Sc\lambda_C f^2(\eta)}\Bigg[-Sc\Big[fY_4-\lambda_C\Big(ff'Y_4\Big)-K_cY_3\Big]$$
$$-\frac{N_t}{N_b}\Bigg\{\frac{1}{\Big(1-Pr\lambda_E f^2+Rd\Big(1+(\theta_w-1)Y_1\Big)^3\Big)}$$
$$\Bigg[-3Rd(\theta_w-1)Y_2^2\Big(1+(\theta_w-1)Y_1\Big)^2-Pr\Big[fY_2+N_bY_2Y_4+N_tY_2^2$$
$$+Ec\Bigg(\Big(1+\frac{1}{\beta}\Big)\Big(f''^2+g'^2\Big)+M\Big(f'^2+g^2\Big)\Bigg)-\lambda_E\Big(ff'Y_2\Big)+\epsilon Y_1\Big]\Big]\Bigg\}\Bigg]$$
$$, \quad Y_4(0) = p.$$

RK-4 method is applied for solving numerically, the last IVP. l and p are to be chosen as missing conditions as follows:

$$Y_1(\eta_\infty, l, p) = 0, \qquad Y_3(\eta_\infty, l, p) = 0.$$

Newton method is applied for solving the above equations with the iterative scheme as follows:

$$\begin{bmatrix} l \\ p \end{bmatrix}_{(n+1)} = \begin{bmatrix} l \\ p \end{bmatrix}_{(n)} - \begin{bmatrix} \frac{\partial Y_1}{\partial l} & \frac{\partial Y_1}{\partial p} \\ \frac{\partial Y_3}{\partial l} & \frac{\partial Y_3}{\partial p} \end{bmatrix}^{-1}_{(n)} \begin{bmatrix} Y_1 \\ Y_3 \end{bmatrix}_{(n)}. \tag{4.38}$$

We further introduce the following notations:

$$\frac{\partial Y_1}{\partial l} = Y_5, \quad \frac{\partial Y_2}{\partial l} = Y_6, \quad \frac{\partial Y_3}{\partial l} = Y_7, \quad \frac{\partial Y_4}{\partial l} = Y_8,$$
$$\frac{\partial Y_1}{\partial p} = Y_9, \quad \frac{\partial Y_2}{\partial p} = Y_{10}, \quad \frac{\partial Y_3}{\partial p} = Y_{11}, \quad \frac{\partial Y_4}{\partial p} = Y_{12}.$$

The form of Newton iterative scheme is, by using the results of above notations are as follows:

$$\begin{bmatrix} l \\ p \end{bmatrix}_{(n+1)} = \begin{bmatrix} l \\ p \end{bmatrix}_{(n)} - \begin{bmatrix} Y_5 & Y_9 \\ Y_7 & Y_{11} \end{bmatrix}^{-1}_{(n)} \begin{bmatrix} Y_1 \\ Y_3 \end{bmatrix}_{(n)}. \tag{4.39}$$

The last set of four first order ODEs in terms of l and p are differentiated to get another system of ODEs, as follows:

$$Y_5' = Y_6, \qquad Y_5(0) = 0.$$

$$\begin{aligned} Y_6' = & \frac{1}{\left(1 - Pr\lambda_E f^2 + Rd\left(1 + (\theta_w - 1)Y_1\right)^3\right)} \\ & - 6Rd(\theta_w - 1)^2 Y_5 Y_2^2 \left(1 + (\theta_w - 1)Y_1\right) - Pr\Big[fY_6 + N_b Y_6 Y_4 + N_b Y_2 Y_8 \\ & + 2N_t Y_2 Y_6 - \lambda_E \left(ff'Y_6\right) + \epsilon Y_5\Big]\Big] - \frac{3Rd(\theta_w - 1)Y_5\left(1 + (\theta_w - 1)Y_1\right)^2}{\left(1 - Pr\lambda_E f^2 + Rd\left(1 + (\theta_w - 1)Y_1\right)^3\right)^2} \end{aligned}$$

$$\left[-3Rd(\theta_w-1)Y_2^2\left(1+(\theta_w-1)Y_1\right)^2-Pr\left[fY_2+N_bY_2Y_4+N_tY_2^2\right.\right.$$

$$\left.\left.+Ec\left(\left(1+\frac{1}{\beta}\right)\left(f''^2+g'^2\right)+M\left(f'^2+g^2\right)\right)-\lambda_E\left(ff'Y_2\right)+\epsilon Y_1\right]\right],$$

$$Y_6(0)=1.$$

$$Y_7'=Y_8, \qquad Y_7(0)=0.$$

$$Y_8'=\frac{1}{1-Sc\lambda_C f^2(\eta)}\left[-Sc\left[fY_8-\lambda_C\left(ff'Y_8\right)-K_cY_7\right]\right.$$

$$-\frac{N_t}{N_b}\left\{\frac{1}{\left(1-Pr\lambda_E f^2+Rd\left(1+(\theta_w-1)y_1\right)^3\right)}\right.$$

$$\left[-6Rd(\theta_w-1)Y_2Y_6\left(1+(\theta_w-1)Y_1\right)^2\right.$$

$$-6Rd(\theta_w-1)^2Y_5Y_2^2\left(1+(\theta_w-1)Y_1\right)$$

$$\left.-Pr\left[fY_6+N_bY_6Y_4+N_bY_2Y_8+2N_tY_2Y_6-\lambda_E\left(ff'Y_6\right)+\epsilon Y_5\right]\right]$$

$$-\frac{3Rd(\theta_w-1)Y_5\left(1+(\theta_w-1)Y_1\right)^2}{\left(1-Pr\lambda_E f^2+Rd\left(1+(\theta_w-1)Y_1\right)^3\right)^2}$$

$$\left(-3Rd(\theta_w-1)Y_2^2\left(1+(\theta_w-1)Y_1\right)^2-Pr\left[fY_2+N_bY_2Y_4+N_tY_2^2\right.\right.$$

$$\left.\left.\left.\left.+Ec\left(\left(1+\frac{1}{\beta}\right)\left(f''^2+g'^2\right)+M\left(f'^2+g^2\right)\right)-\lambda_E\left(ff'Y_2\right)+\epsilon Y_1\right]\right)\right\}\right],$$

$$Y_8(0)=0.$$

$$Y_9'=Y_{10}, \qquad Y_9(0)=0.$$

$$Y_{10}'=\frac{1}{\left(1-Pr\lambda_E f^2+Rd\left(1+(\theta_w-1)Y_1\right)^3\right)}$$

$$\left[-6Rd(\theta_w-1)Y_2Y_{10}\left(1+(\theta_w-1)Y_1\right)^2\right.$$

$$-6Rd(\theta_w-1)^2Y_9Y_2^2\left(1+(\theta_w-1)Y_1\right)-Pr\left[fY_{10}\right.$$

$$\left.\left.+N_bY_{10}Y_4+N_bY_2Y_{12}+2N_tY_2Y_{10}-\lambda_E\left(ff'Y_{10}\right)+\epsilon Y_9\right]\right]$$

$$
\begin{aligned}
&-\frac{3Rd(\theta_w-1)Y_9\Big(1+(\theta_w-1)Y_1\Big)^2}{\bigg(1-Pr\lambda_E f^2+Rd\Big(1+(\theta_w-1)Y_1\Big)^3\bigg)^2}\\
&\bigg[-3Rd(\theta_w-1)Y_2^2\Big(1+(\theta_w-1)Y_1\Big)^2-Pr\Big[fY_2+N_bY_2Y_4+N_tY_2^2\\
&+Ec\bigg(\Big(1+\frac{1}{\beta}\Big)\Big(f''^2+g'^2\Big)+M\Big(f'^2+g^2\Big)\bigg)-\lambda_E\Big(ff'Y_2\Big)+\epsilon Y_1\Big]\bigg],\\
&\hspace{25em} Y_{10}(0)=0.
\end{aligned}
$$

$$
Y_{11}'=Y_{12}, \qquad Y_{11}(0)=0.
$$

$$
\begin{aligned}
Y_{12}'=&\frac{1}{1-Sc\lambda_C f^2(\eta)}\bigg[-Sc\Big[fY_{12}-\lambda_C\Big(ff'Y_{12}\Big)-K_cY_{11}\Big]\\
&-\frac{N_t}{N_b}\Bigg\{\frac{1}{\bigg(1-Pr\lambda_E f^2+Rd\Big(1+(\theta_w-1)Y_1\Big)^3\bigg)}\\
&\bigg[-6Rd(\theta_w-1)Y_2Y_{10}\Big(1+(\theta_w-1)Y_1\Big)^2\\
&-6Rd(\theta_w-1)^2Y_9Y_2^2\Big(1+(\theta_w-1)Y_1\Big)-Pr\Big[fY_{10}+N_bY_{10}Y_4\\
&+N_bY_2Y_{12}+2N_tY_2Y_{10}-\lambda_E\Big(ff'Y_{10}\Big)+\epsilon Y_9\Big]\bigg]\\
&-\left[\frac{3Rd(\theta_w-1)Y_9\Big(1+(\theta_w-1)Y_1\Big)^2}{\bigg(1-Pr\lambda_E f^2+Rd\Big(1+(\theta_w-1)Y_1\Big)^3\bigg)^2}\right]\\
&\bigg[-3Rd(\theta_w-1)Y_2^2\Big(1+(\theta_w-1)Y_1\Big)^2-Pr\Big[fY_2\\
&+N_bY_2Y_4+N_tY_2^2+Ec\bigg(\Big(1+\frac{1}{\beta}\Big)\Big(f''^2+g'^2\Big)+M\Big(f'^2+g^2\Big)\bigg)\\
&-\lambda_E\Big(ff'Y_2\Big)+\epsilon Y_1\Big]\bigg]\Bigg\}\bigg], \qquad Y_{12}(0)=1.
\end{aligned}
$$

For the Newton's method the stopping criteria is set as:

$$
max\{\mid Y_1(\eta_\infty,l^n,p^n)\mid,\mid Y_3(\eta_\infty,l^n,p^n)\mid\}<\epsilon.
$$

where $\epsilon > 0$ is a sufficiently small number, which has been considered as 10^{-10}.

4.4 Representation of Graphs and Tables

In this section, we thoroughly discuss the influence of the dimensionless parameters on the skin friction coefficient $Re_x^{\frac{1}{2}}C_{f_x}$, $Re_y^{\frac{1}{2}}C_{f_y}$, Nusselt number $Re_x^{-\frac{1}{2}}Nu_x$ and sherwood number $Re_x^{-\frac{1}{2}}Sh_x$ through different graphs and tables. Table 4.1, shows the effect of Casson parameter β, rotation parameter γ_1, magnetic parameter M, porous medium parameter K and inclination angle Γ on $Re_x^{\frac{1}{2}}C_{f_x}$ and $Re_y^{\frac{1}{2}}C_{f_y}$. For accelerating the values of Casson parameter β, $Re_x^{\frac{1}{2}}C_{f_x}$, $Re_x^{\frac{1}{2}}C_{f_y}$ increase. Table 4.1 expresses the intervals I_f and I_g from where the missing conditions r and m can be chosen. Observation made on the Nusselt number, shows a great flexibility of the choice of missing initial conditions. Table 4.2 explains the impact of Casson parameter β, rotation parameter γ_1 magnetic parameter M, porous medium parameter K, inclination angle Γ, radiation parameter Rd, temprature ratio parameter θ_w, Prandtl number Pr, Brownian parameter Nb, thermophoresis parameter Nt, Eckert number Ec and Schmidt number Sc, time relaxtaion parameter of temperature λ_E, time relaxtaion parameter of concentration λ_C, heat generation/absorption parameter ϵ and chemical reaction parameter K_c.

Figure 4.2 shows a decreasing behaviour of the velocity f' when increasing the Casson parameter β. From a tangible perspective, the Casson parameter is impacted by the yield stress. This stress, in turn, creates an opposing force that results in a decrease in the velocity of the fluid with a gradual increase in β values. The identical parameter concerned with the velocity distribution $g(\eta)$ together with y-axis is absorbed by Figure 4.3. The velocity distribution $g(\eta)$ reveals an upward trend with respect to β is mentioned in figure. Within this framework, the function $g(\eta)$ adopts a parabolic configuration, signifying that the flow transpires in the negative direction due to its negative values.

The influence of M in the temperature profile θ is manifestly observed in Figure 4.4. It demonstrates that an escalation of this parameter leads to an elevation in the temperature profile, driven by the Lorentz force generated in the presence of a magnetic field. The influence of the parameter γ_1 on f' and g is portrayed in Figures 4.5 and 4.6. It has been observed that an increase in the rotation parameter leads to a deterioration of velocity along the x-direction. The results indicate that as the value of Nt is increased, both the temperature distribution and the concentration profile rise, as shown in Figures 4.7 and 4.8. The consequences of altering Magnetic parameter M for the velocity profiles f' and g is visualized in Figures 4.9 and 4.10, showcasing a decrease in $f^{'}$ and an increase in g with an increase in M. This occurs because a drag force which is termed as Lorentz force get raised due to applied magnetic field generated by the motion of charges. This force causes a decrease in the magnitude of velocity along the x-direction.

Distinct values of θ_w illustrate the temperature profile θ increment in Figure 4.11. As this parameter increases, the temperature also experiences a corresponding increase. A decline in the concentration profile ϕ is evident as the value of the Schmidt parameter Sc increases, as illustrated in Figure 4.12. Given that the Schmidt number is influenced by the Brownian diffusion coefficient, rise in Schmidt number leads to a decrease in the Brownian diffusion coefficient. Consequently, this suggests a reduction in nanoparticle concentration due to the diminished diffusion behavior. Figures 4.13 and 4.14 depict the velocity profiles for varying values of the porous medium parameter K. The profile denoted as f' exhibits a decreasing trend as K increases, while the profile represented by g demonstrates an increase with rising values of K. This occurs because, on increasing the permeability of a porous medium will increase the flow rate of fluid through it, assuming a constant pressure gradient.

Figures 4.15 and 4.16 demonstrate the influence of Nb. As Nb increases, the temperature distribution rises, while the concentration profile decreases. The occurrence of Brownian motion in the fluid is attributed to the presence of nanoparticles. With an increase in Nb, this motion undergoes changes, leading to a subsequent decrease in the thickness of the concentration boundary layer for the nanoparticles. Through the analysis of Figures 4.17 and 4.18 for various distinct values of Γ, it has been noted that f' exhibits a decreasing trend, while g demonstrates an increasing trend. It demonstrates that for the inclined angles, the gravitational force opposes the stretching effect, potentially delaying the flow initiation and altering the boundary layer structure. Figure 4.19 reveals that with an increase in the value of γ_1, the temperature distribution also increases.

Figure 4.20 illustrates that as the value of the chemical reaction parameter K_c increases, there is a noticeable decreasing trend in the concentration discrepancy ϕ. This occurs because when the chemical reaction parameter is increased, the concentration distribution decreases owing to the accelerated movement of fluid molecules. Figure 4.21 reflects the variation in temperature profile θ due to a parameter Rd. As the radiation parameter boosts, it leads to the emit of more heat energy into the flow, resulting in an uplifted temperature profile. Figure 4.22 shows the relation between relaxation time parameter of concentration λ_C and ϕ, where ϕ decreases by increasing λ_C. Genuinely, an elevated λ_C value induces a diminished mass diffusivity, leading to a concentration distribution with a narrower profile.

Figure 4.23 displays the impact of the Prandtl number Pr on the temperature distribution θ. Both the thickness of the thermal boundary layer and the temperature are functions that decrease as the Prandtl number Pr increases. Certainly, the influence of the Eckert number Ec on the temperature distribution θ showcases a rising pattern in θ as the value of Ec increases, as mentioned in Figure 4.24. The temperature distribution escalates as the value of Eckert number goes up. This outcome arises from the fact that the Eckert number is dependent on the kinetic energy, which upon being converted to the heat energy within the fluid, results in a temperature increase. The Figure 4.25 indicates that on rising the Casson parameter β the temperature discrepancy θ shows a rising behaviour. Figure 4.26 expresses the relation between relaxation time parameter of temperature λ_E and temperature discrepancy θ, where θ has decreasing trend by rising λ_E. visibly, when λ_E attains higher values, the system manifests non-conductive features, which in turn leads to a contraction of the thermal distribution.

For increasing the values of heat generation/absorption ϵ, Figure 4.27 depicts that the temperature discrepancy θ is increasing. The impact of the Brownian parameter Nb in conjunction with the thermophoresis parameter Nt on the Sherwood number $Re_x^{-\frac{1}{2}} Sh_x$ is depicted in Figure 4.28. It has been observed that an increase in the value of Nb leads to a decreasing trend in the Sherwood number $Re_x^{-\frac{1}{2}} Sh_x$. Conversely, the Sherwood number exhibits an increasing trend as the value of Nt rises. In Figure 4.29, increasing the magnetic parameter M has been noted to result in an increase in the skin friction $Re_x^{\frac{1}{2}} C_{f_y}$, whereas for higher values of γ_1, $Re_x^{\frac{1}{2}} C_{f_y}$ exhibits a declining trend.

TABLE 4.1: Results of $Re_x^{\frac{1}{2}} C_{fx}$ and $Re_x^{\frac{1}{2}} C_{fy}$ for various parameters

β	γ_1	M	K	Γ	$Re_x^{\frac{1}{2}} C_{fx}$	$Re_x^{\frac{1}{2}} C_{fy}$	I_f	I_g
0.5	0.5	0.5	0.4	$\pi/2$	-2.48263	-0.66128	[-1.70, 1.90]	[-2.30, 1.70]
0.8					-2.15059	-0.57329	[-1.90, 1.60]	[-2.50, 1.90]
1.0					-2.02772	-0.54057	[-1.80, 2.30]	[-2.70, 0.60]
	0.3				-2.42473	-0.40770	[-1.10, 2.60]	[-3.10, 2.20]
	0.6				-2.51875	-0.78023	[-2.20, 2.80]	[-2.60, 3.00]
	0.9				-2.64364	-1.10502	[-2.30, 3.10]	[-2.40, 1.70]
		0			-2.19783	-0.76779	[-1.20, 3.50]	[-2.80, 2.70]
		0.4			-2.42669	-0.67951	[-1.80, 3.30]	[-3.10, 3.30]
		0.8			-2.64515	-0.61357	[-1.80, 3.60]	[-2.00, 1.10]
			0.6		-2.59172	-0.62842	[-2.20, 3.80]	[-2.60, 3.10]
			0.8		-2.69784	-0.59963	[-2.30, 3.40]	[-1.90, 1.20]
			1.0		-2.80102	-0.57418	[-2.00, 3.30]	[-2.70, 3.30]
				$\pi/6$	-2.27046	-0.73718	[-2.50, 3.10]	[-3.10, 3.20]
				$\pi/4$	-2.34222	-0.70947	[-2.10, 2.70]	[-1.80, 1.50]
				$\pi/3$	-2.41297	-0.68427	[-2.20, 3.00]	[-3.20, 3.30]

TABLE 4.2: Results of $Re_x^{-\frac{1}{2}}Nu_x$ and $Re_x^{-\frac{1}{2}}Sh_x$ for various parameters

β	γ_1	M	K	Γ	Rd	θ_w	Pr	Nb	Nt	Ec	Sc	λ_E	ϵ	λ_C	K_c	$Re_x^{-\frac{1}{2}}Nu_x$	$Re_x^{-\frac{1}{2}}Sh_x$
0.5	0.5	0.5	0.4	$\pi/2$	0.2	1.5	2.0	0.5	0.5	0.2	5.0	0.1	0.2	0.1	0.2	0.01724	1.96539
0.6																0.01285	1.95535
	0.2															0.06499	1.96819
	0.3															0.05309	1.96747
		0.0														0.14902	1.96936
		0.3														0.06959	1.96686
			0.3													0.02879	1.96765
			0.5													0.00547	1.96319
				$\pi/6$												0.11585	1.96828
				$\pi/4$												0.08277	1.96726
					0.4											0.06359	1.95224
					0.5											0.07338	1.94802
						1.6										0.02836	1.96224
						1.7										0.03901	1.95920
							1.0									0.05238	1.93649
							1.5									0.04469	1.95296

TABLE 4.2: Results of $Re_x^{-\frac{1}{2}}Nu_x$ and $Re_x^{-\frac{1}{2}}Sh_x$ for various parameters

β	γ_1	M	K	Γ	Rd	θ_w	Pr	Nb	Nt	Ec	Sc	λ_E	ϵ	λ_C	K_c	$Re_x^{-\frac{1}{2}}Nu_x$	$Re_x^{-\frac{1}{2}}Sh_x$
								0.2								0.08835	2.00692
								0.3								0.05054	1.97964
									0.0							0.05179	1.90933
									0.05							0.03431	1.93689
										0.0						0.40286	1.92442
										0.05						0.30721	1.93453
											3.0					0.00517	1.49949
											4.0					0.01153	1.74717
												0.2				0.03533	1.96580
												0.3				0.05267	1.96630
													0.0			0.26899	1.94262
													0.1			0.15202	1.95344
														0.13		0.01758	1.97309
														0.15		0.01782	1.97828
															0.1	0.01203	1.69165
															0.0	0.01479	1.83341

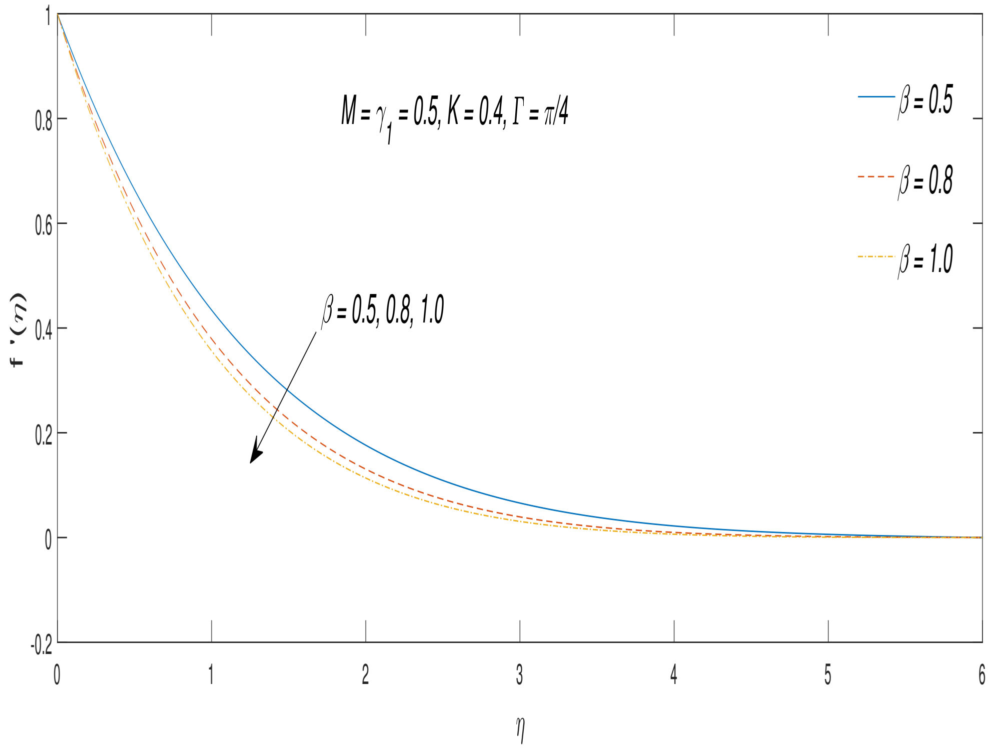

FIGURE 4.2: Velocity f'(η) discrepancy against β

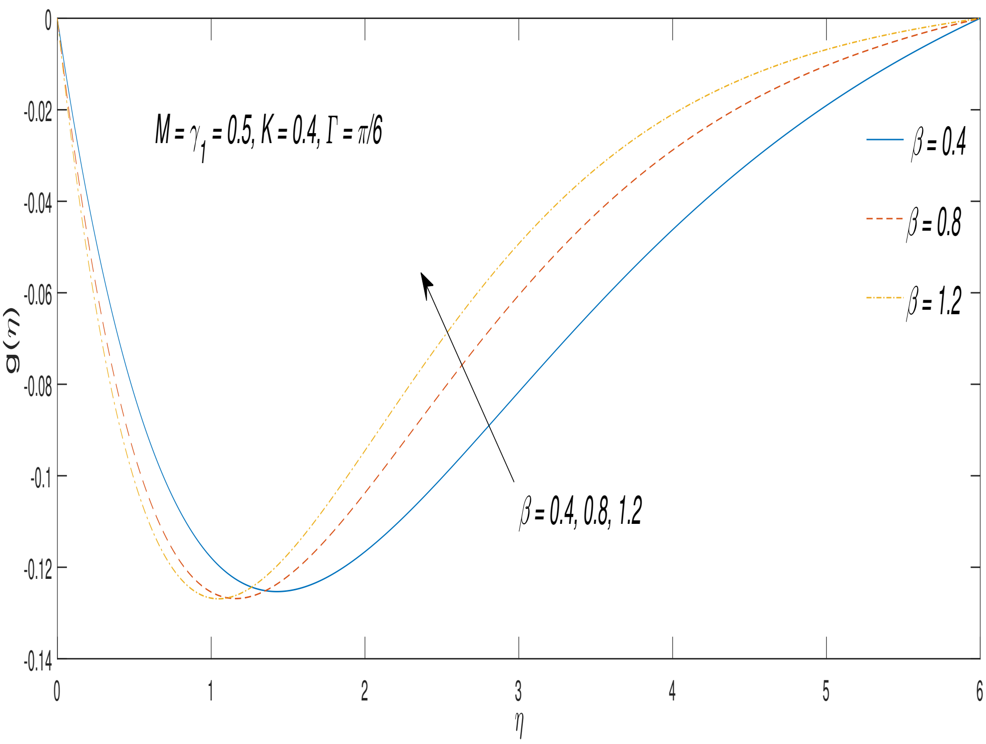

FIGURE 4.3: Velocity g(η) discrepancy against β

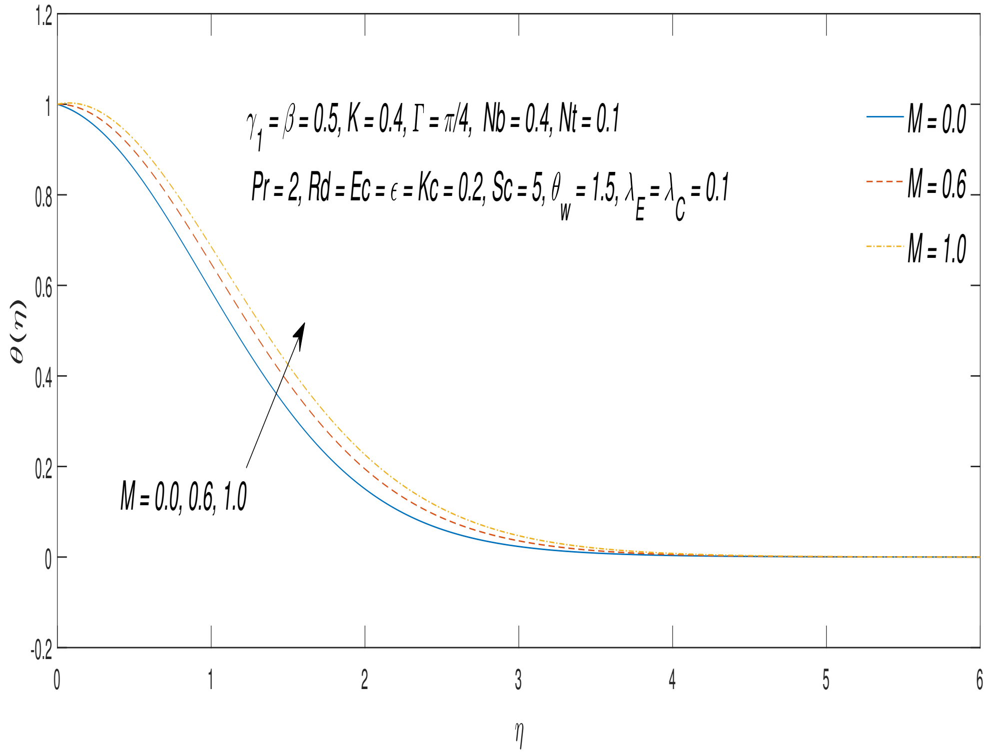

FIGURE 4.4: Temperature $\theta(\eta)$ discrepancy against M

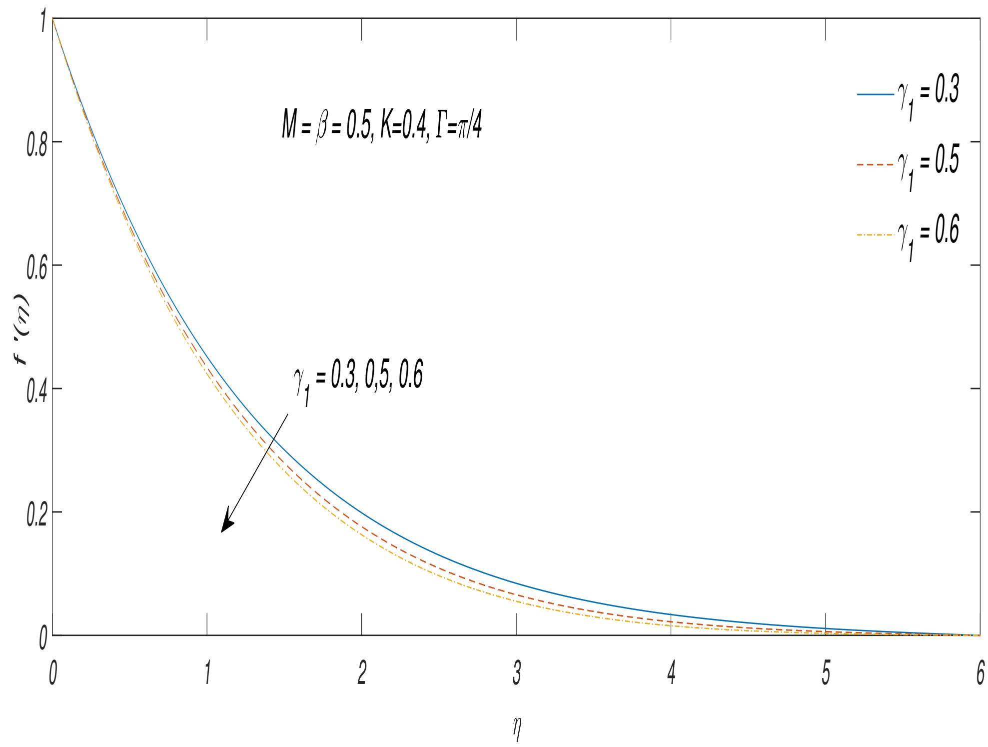

FIGURE 4.5: Velocity f'(η) discrepancy against γ_1

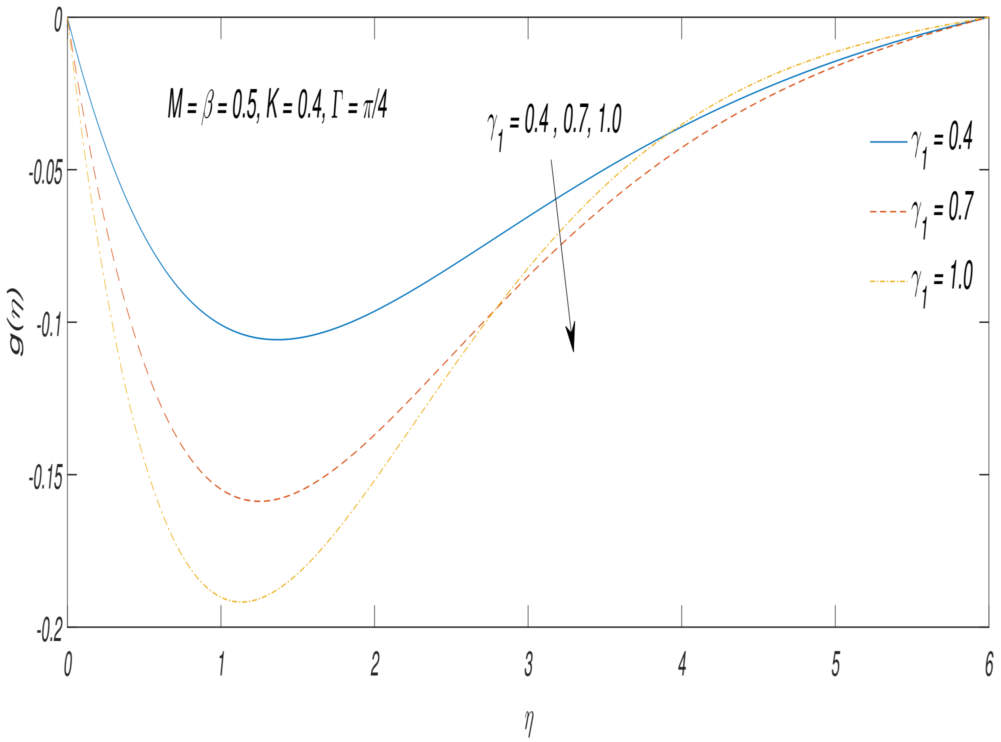

FIGURE 4.6: Velocity g(η) discrepancy against γ_1

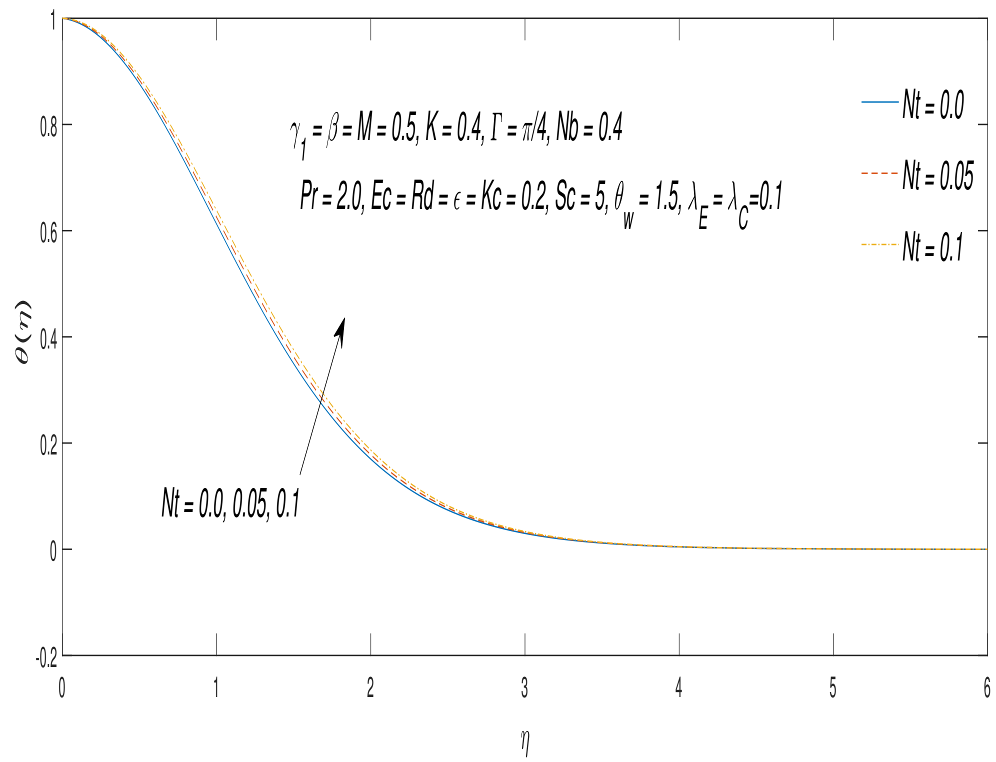

FIGURE 4.7: Temperature $\theta(\eta)$ discrepancy against Nt

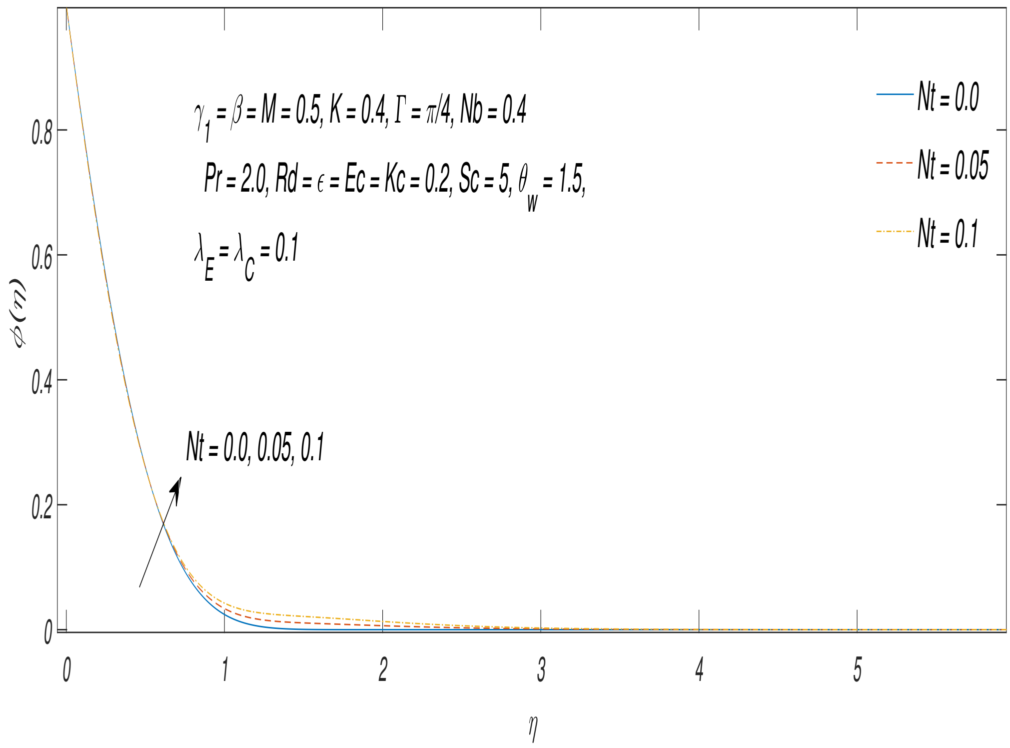

FIGURE 4.8: Concentration $\phi(\eta)$ discrepancy against Nt

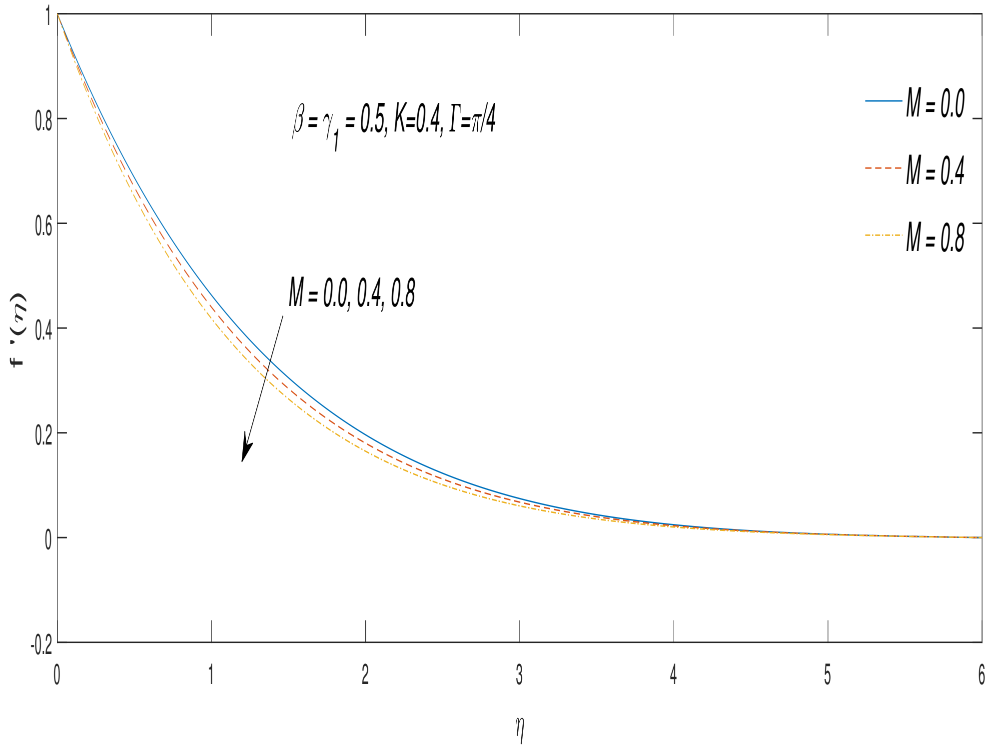

FIGURE 4.9: Velocity f'(η) discrepancy against M

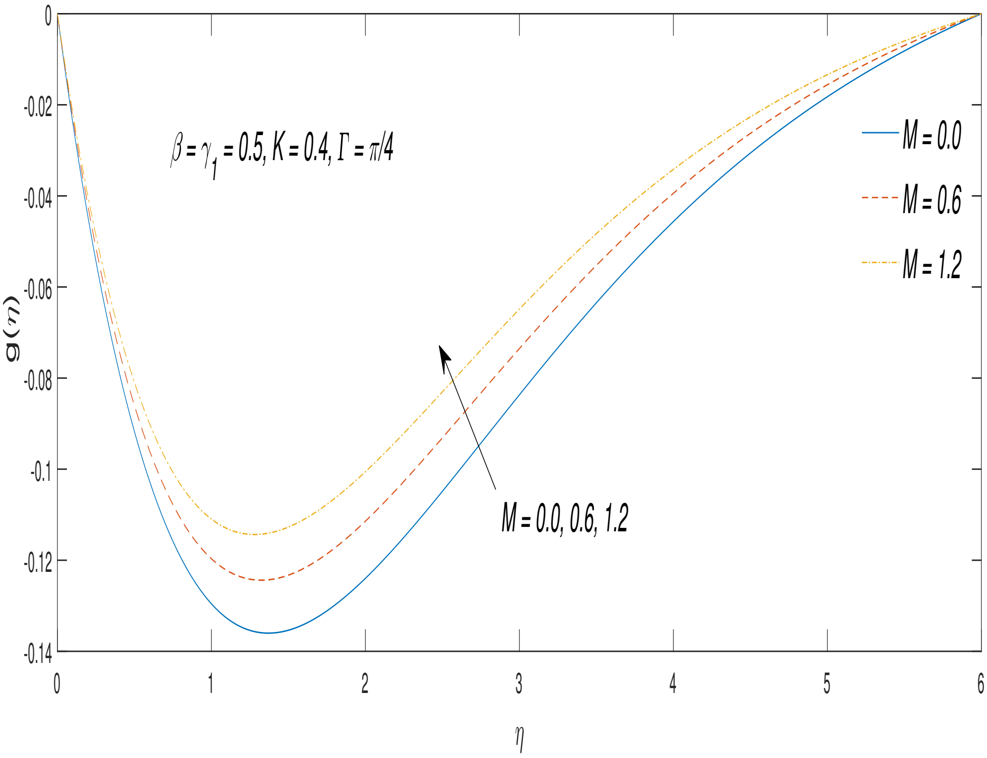

FIGURE 4.10: Velocity g(η) discrepancy against M

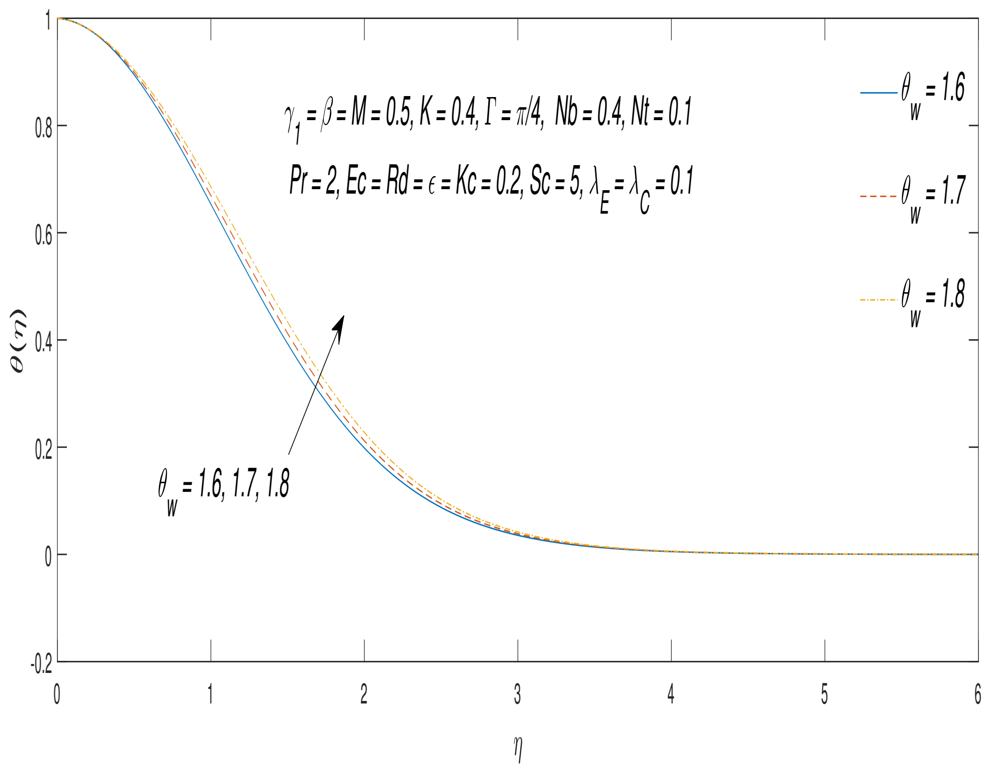

FIGURE 4.11: Temperature $\theta(\eta)$ discrepancy against θ_w

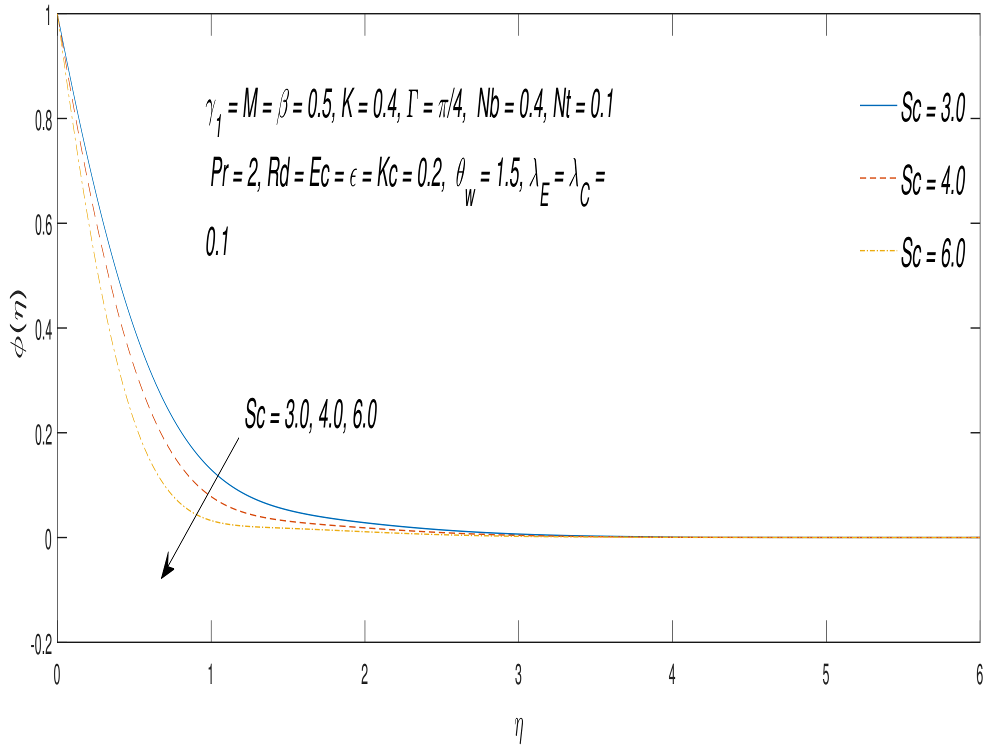

Figure 4.12: Concentration $\phi(\eta)$ discrepancy against Sc

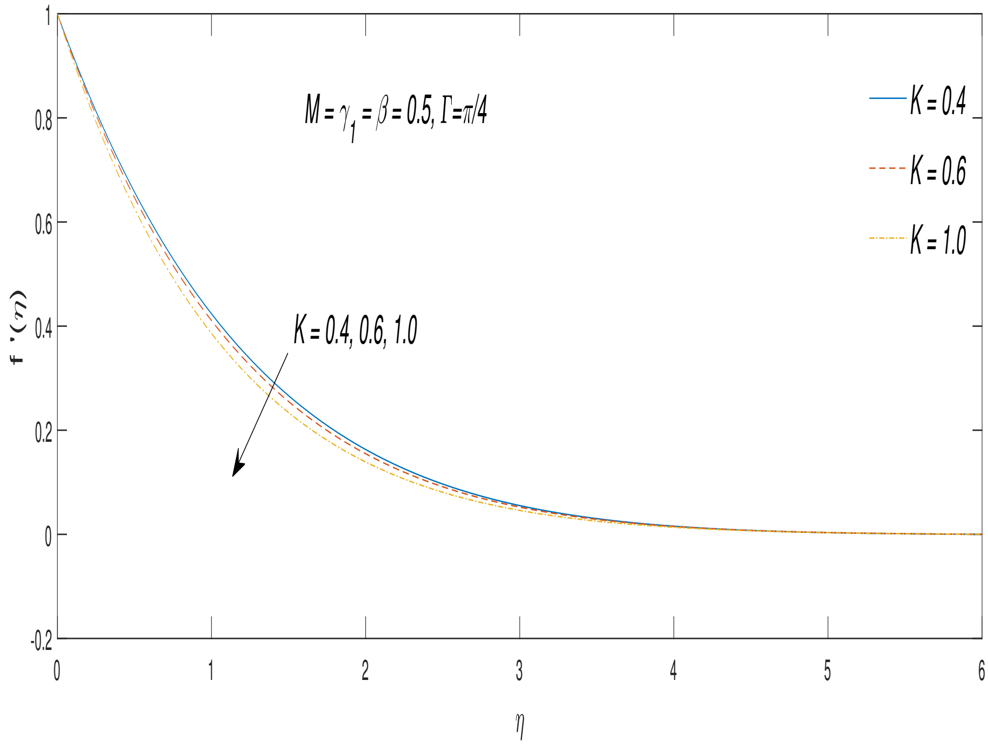

Figure 4.13: Velocity f'(η) discrepancy against K

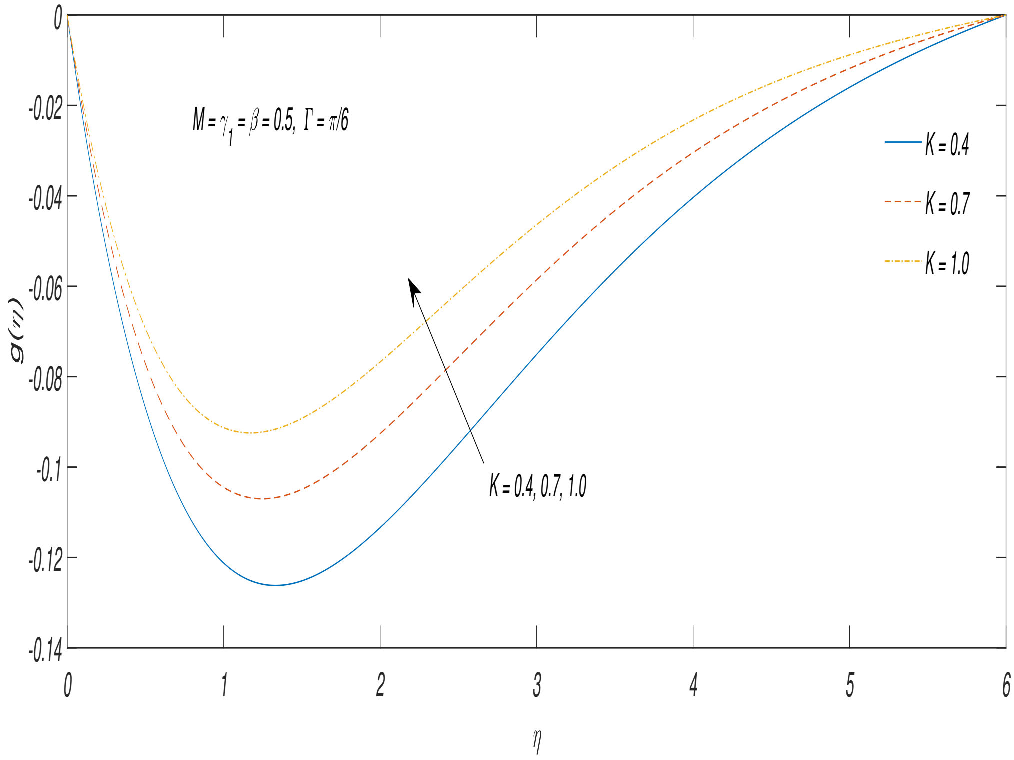

FIGURE 4.14: Velocity g(η) discrepancy against K

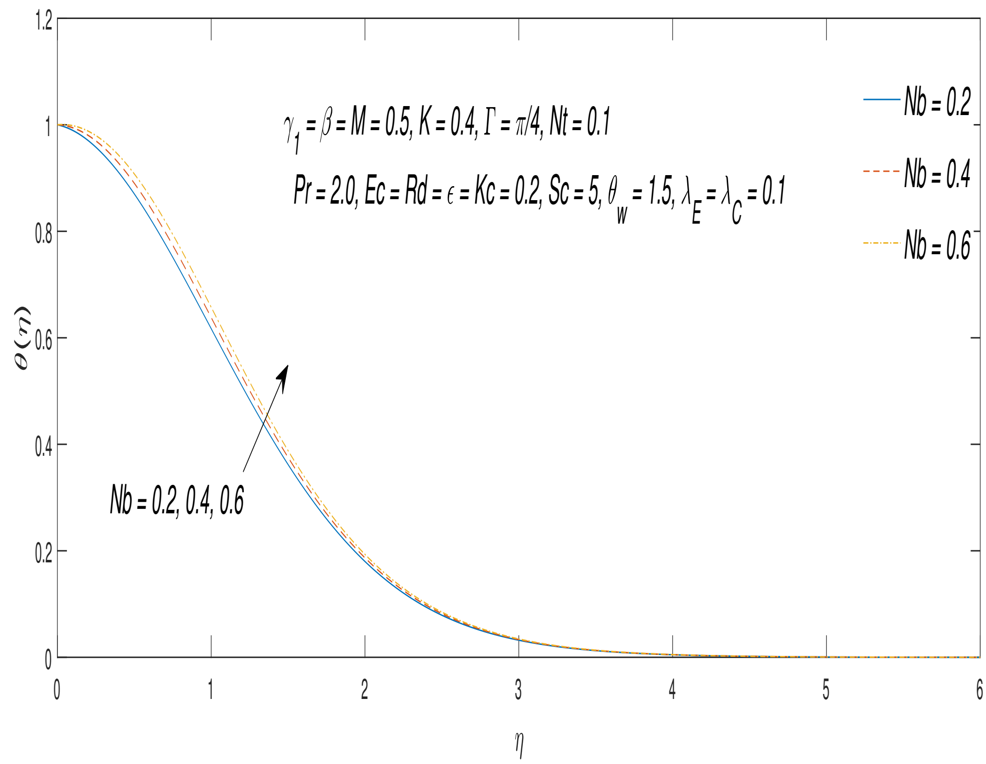

FIGURE 4.15: Temperature $\theta(\eta)$ discrepancy against Nb

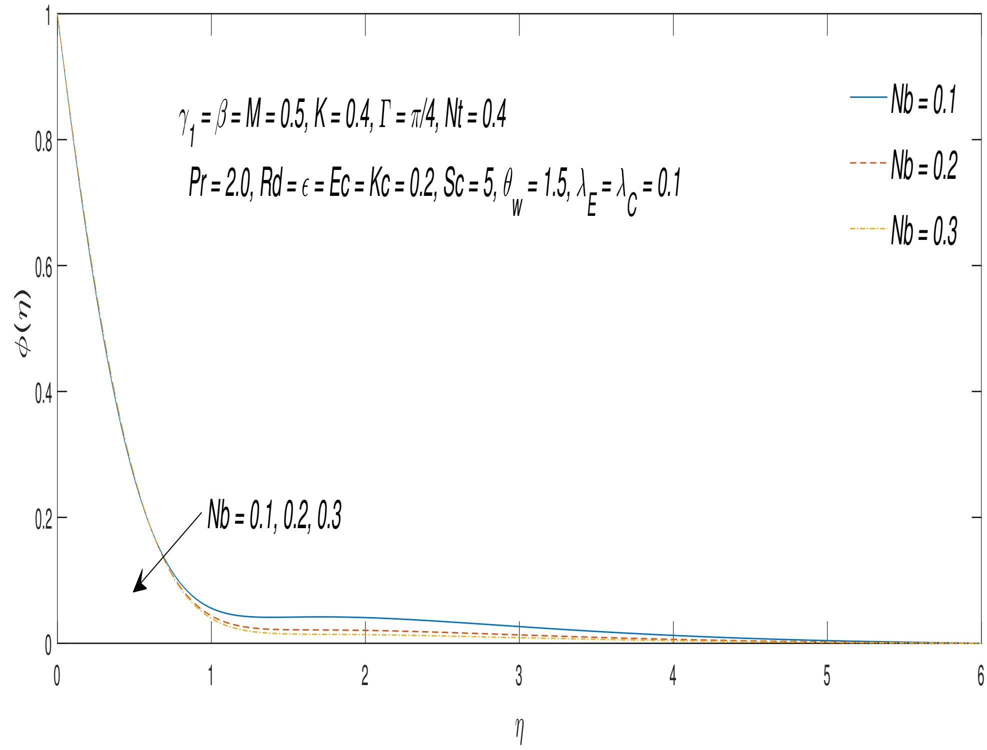

FIGURE 4.16: Concentration $\phi(\eta)$ discrepancy against Nb

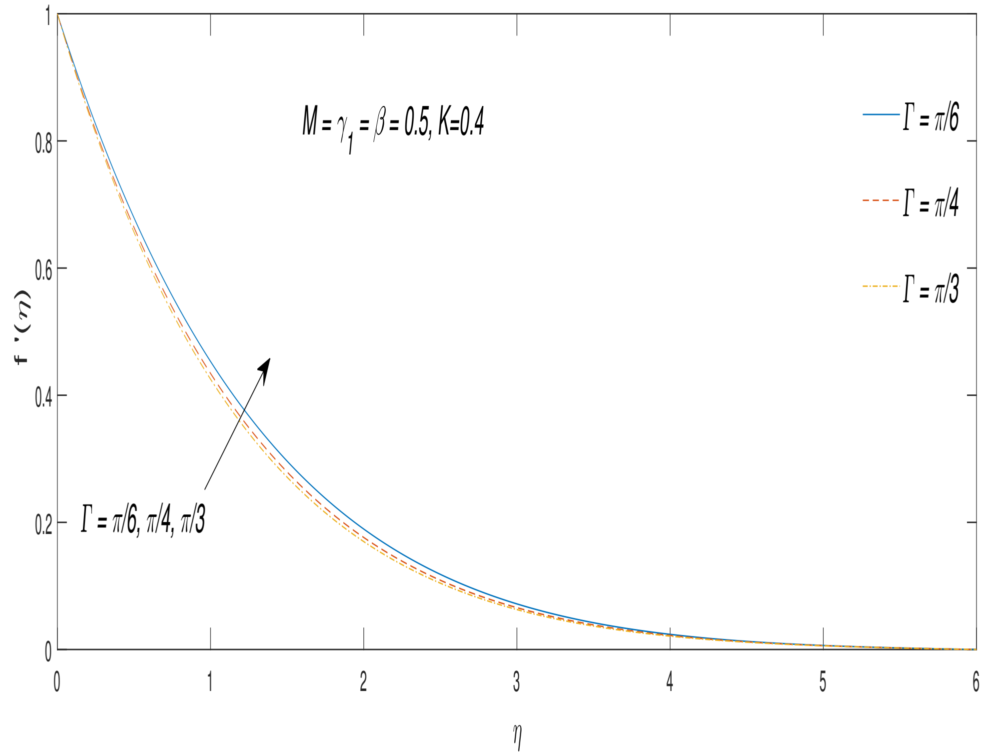

FIGURE 4.17: Velocity f'(η) discrepancy against Γ

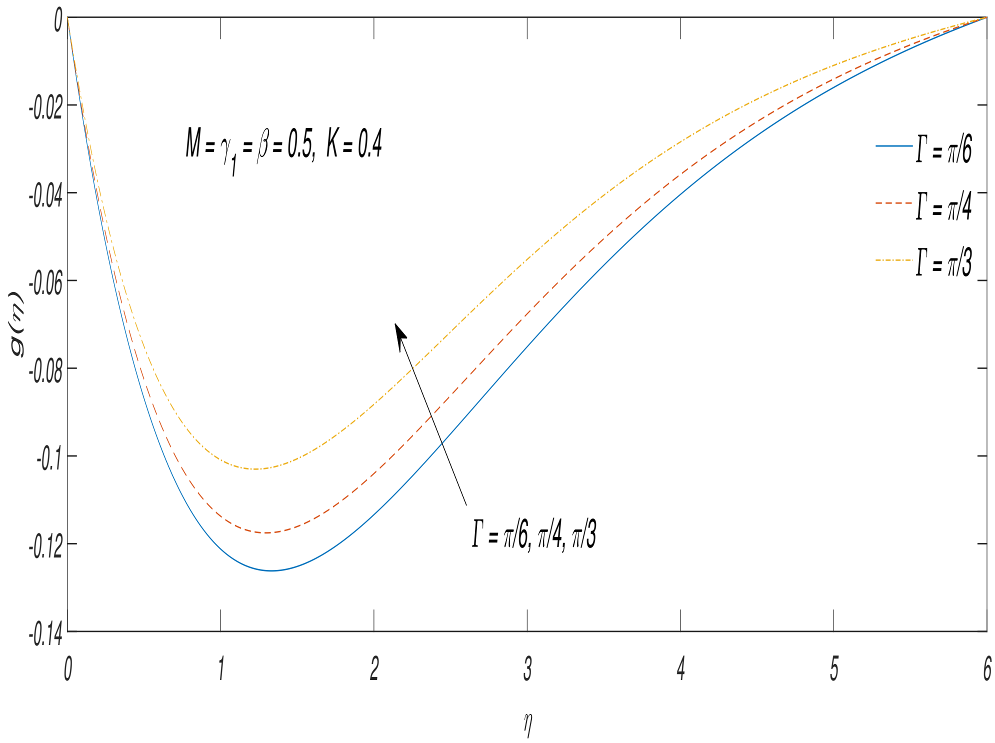

FIGURE 4.18: Velocity g(η) discrepancy against Γ

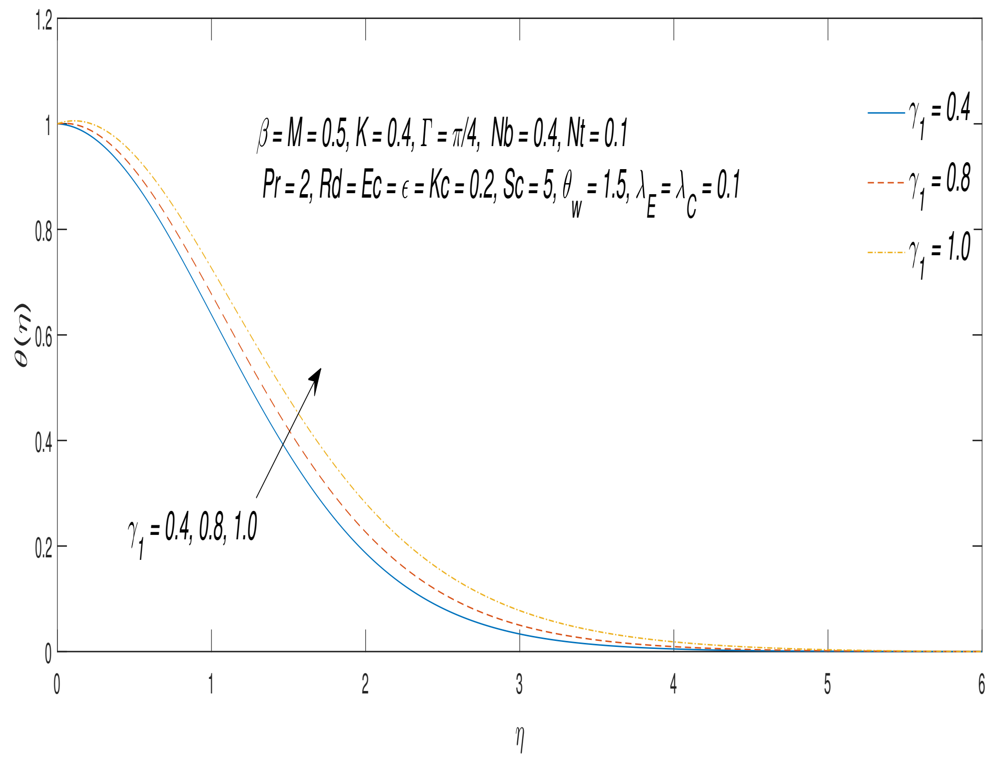

FIGURE 4.19: Temperature $\theta(\eta)$ discrepancy against γ_1

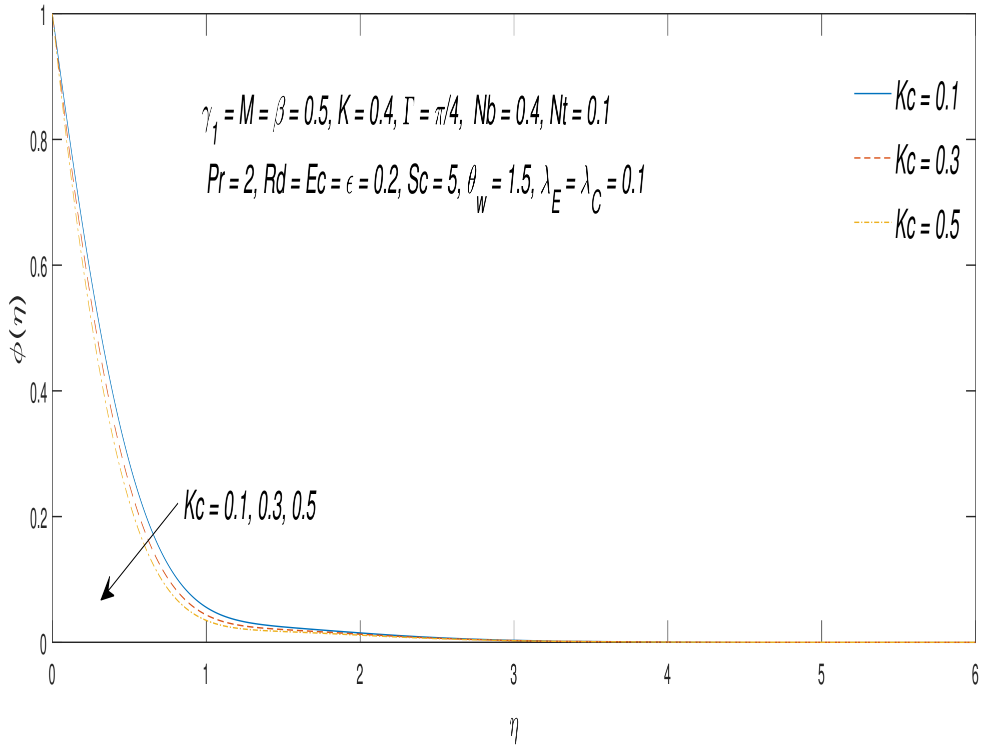

FIGURE 4.20: Concentration $\phi(\eta)$ discrepancy against K_c

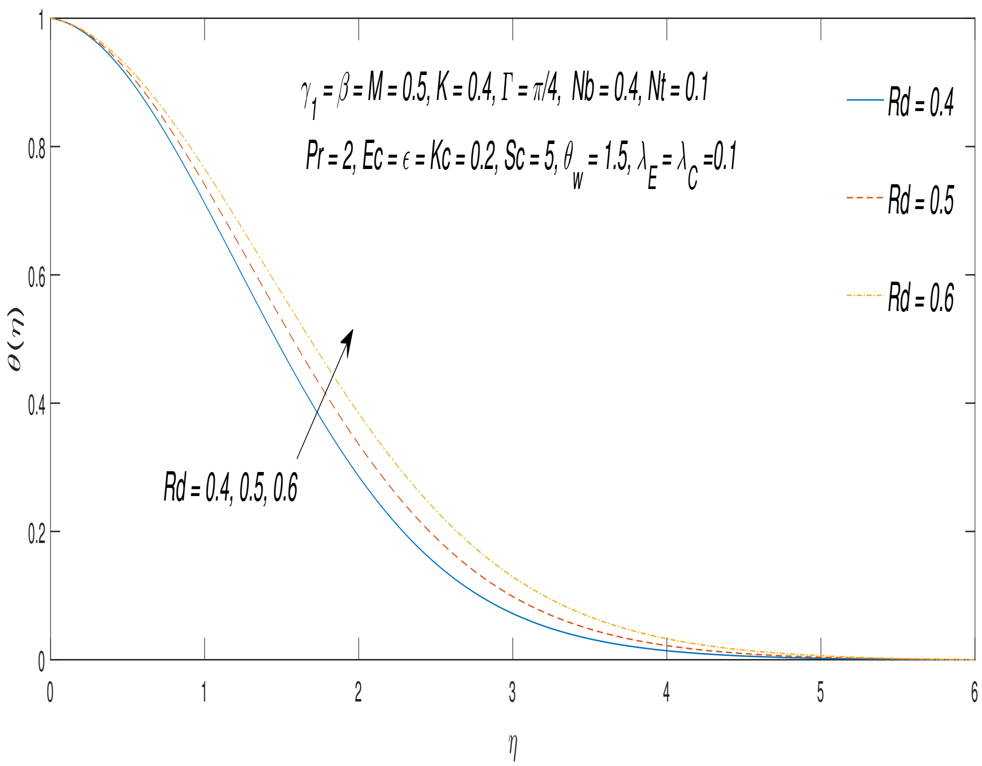

FIGURE 4.21: Temperature $\theta(\eta)$ discrepancy against Rd

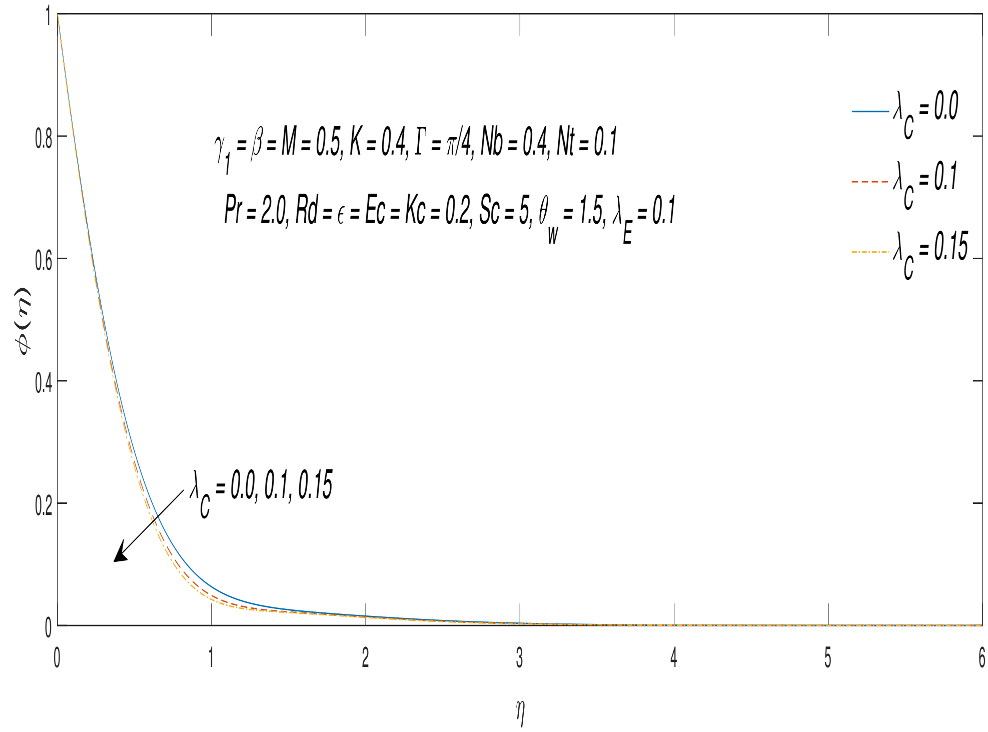

FIGURE 4.22: Concentration $\phi(\eta)$ discrepancy against λ_C

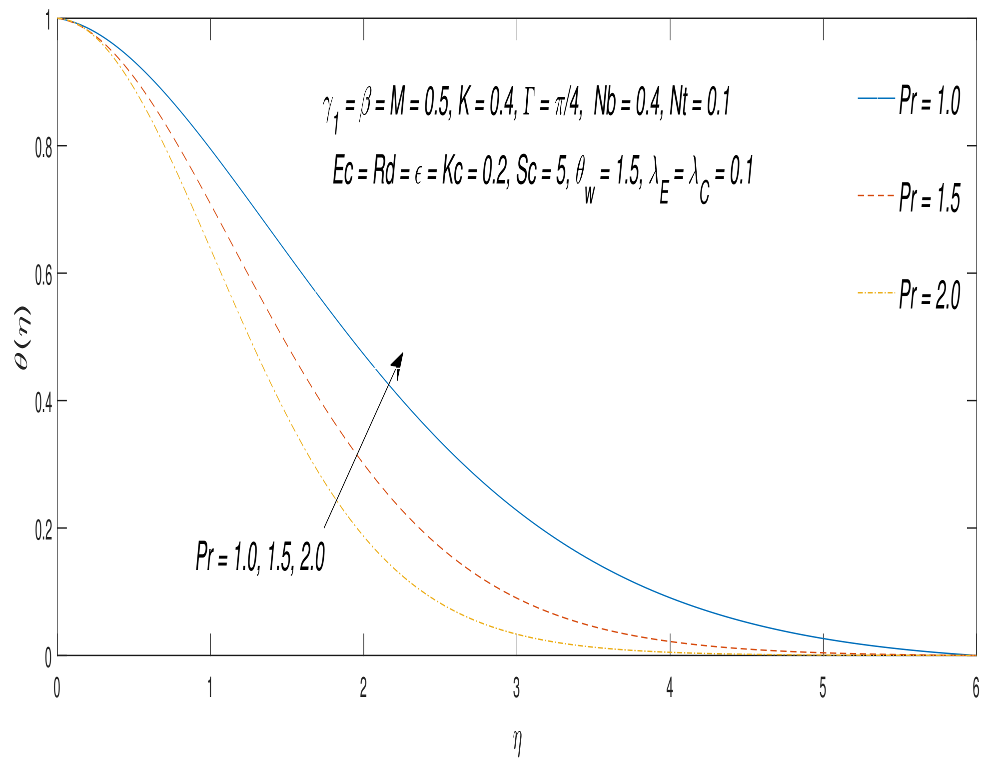

FIGURE 4.23: Temperature $\theta(\eta)$ discrepancy against Pr

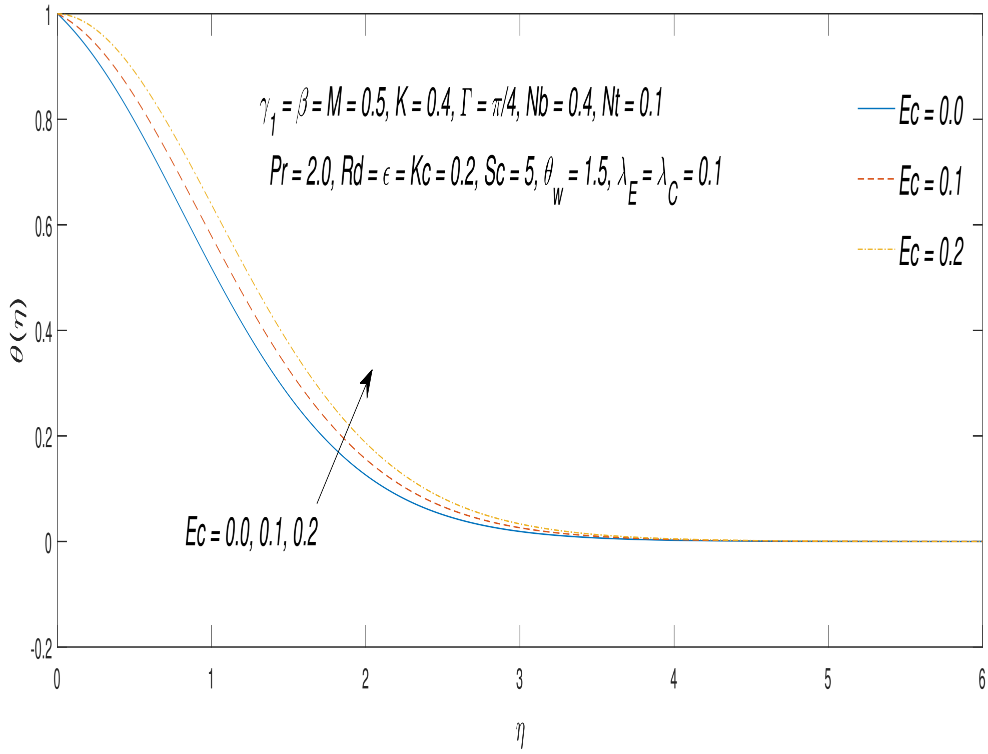

FIGURE 4.24: Temperature $\theta(\eta)$ discrepancy against Ec

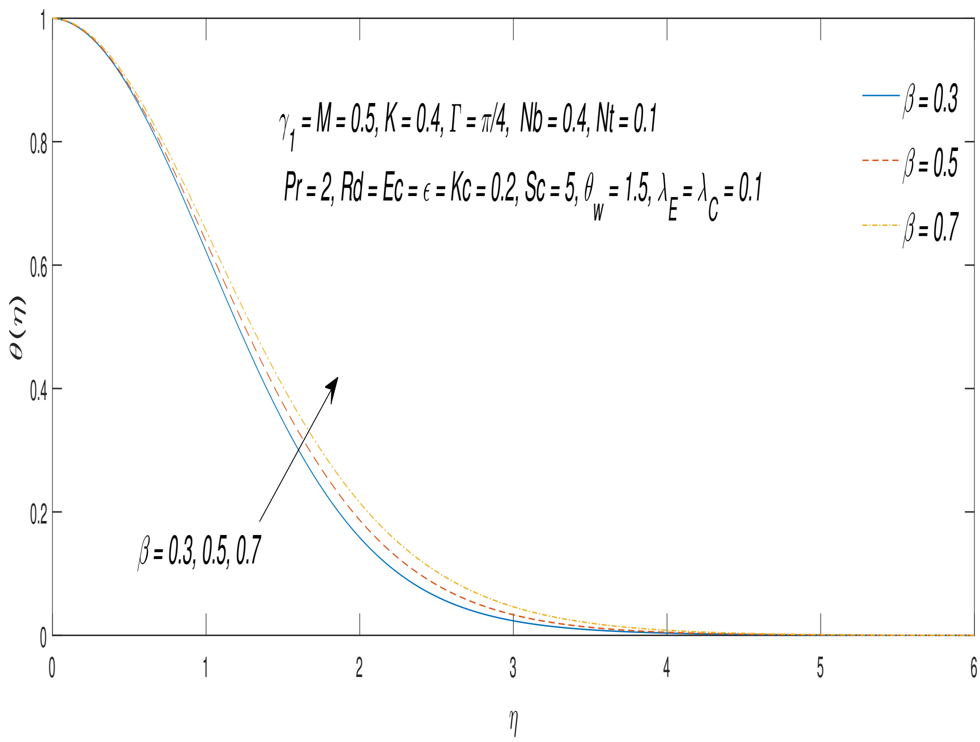

FIGURE 4.25: Temperature $\theta(\eta)$ discrepancy against β

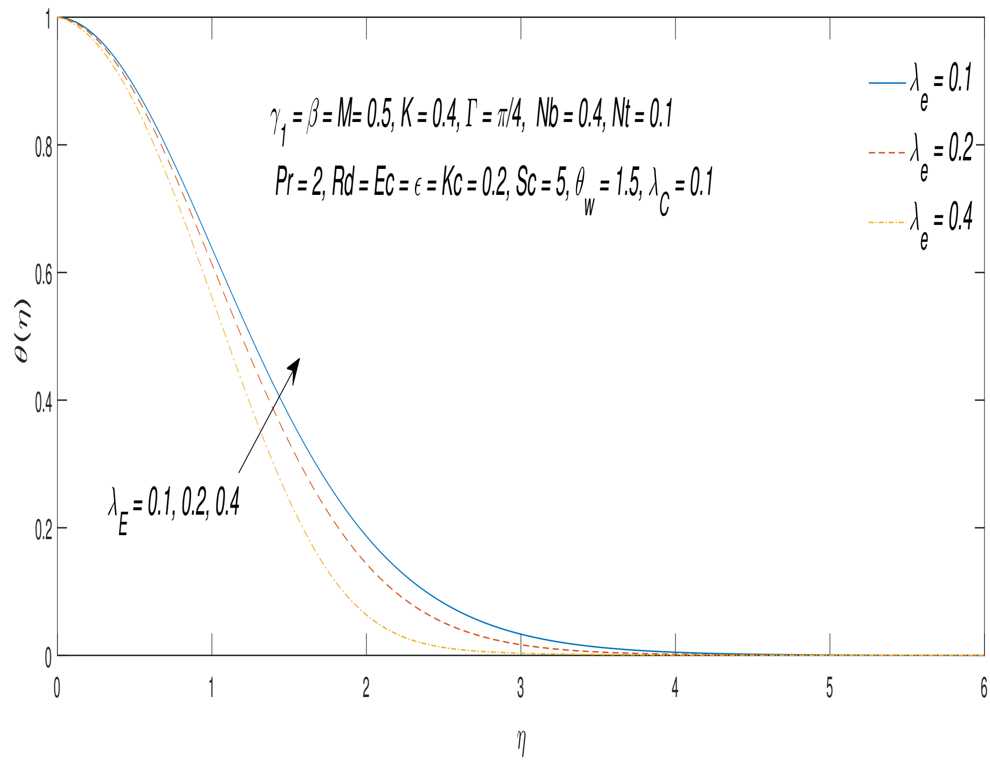

FIGURE 4.26: Temperature $\theta(\eta)$ discrepancy against λ_E

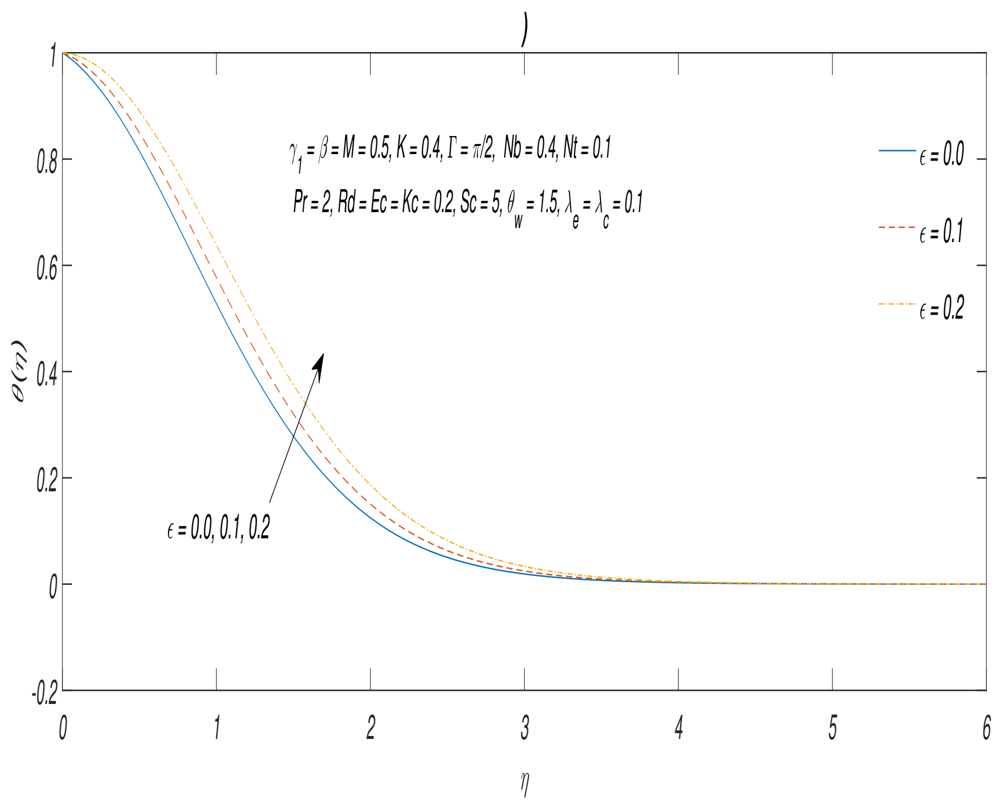

FIGURE 4.27: Temperature $\theta(\eta)$ discrepancy against ϵ

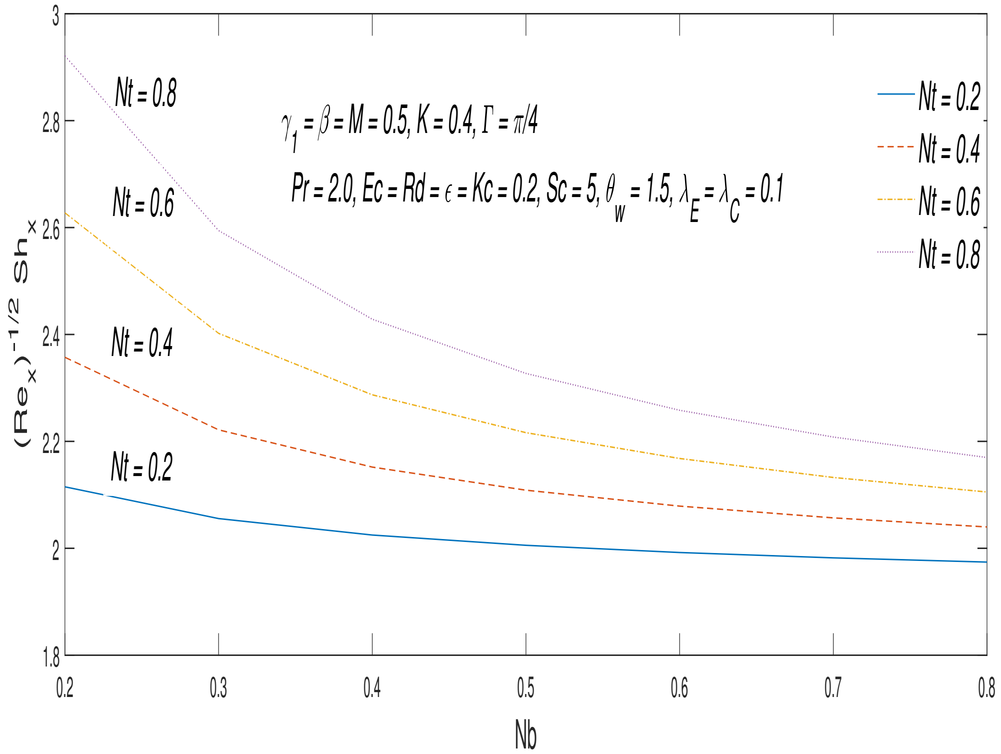

FIGURE 4.28: Sherwood number Sh_x discrepancy against Nb and Nt

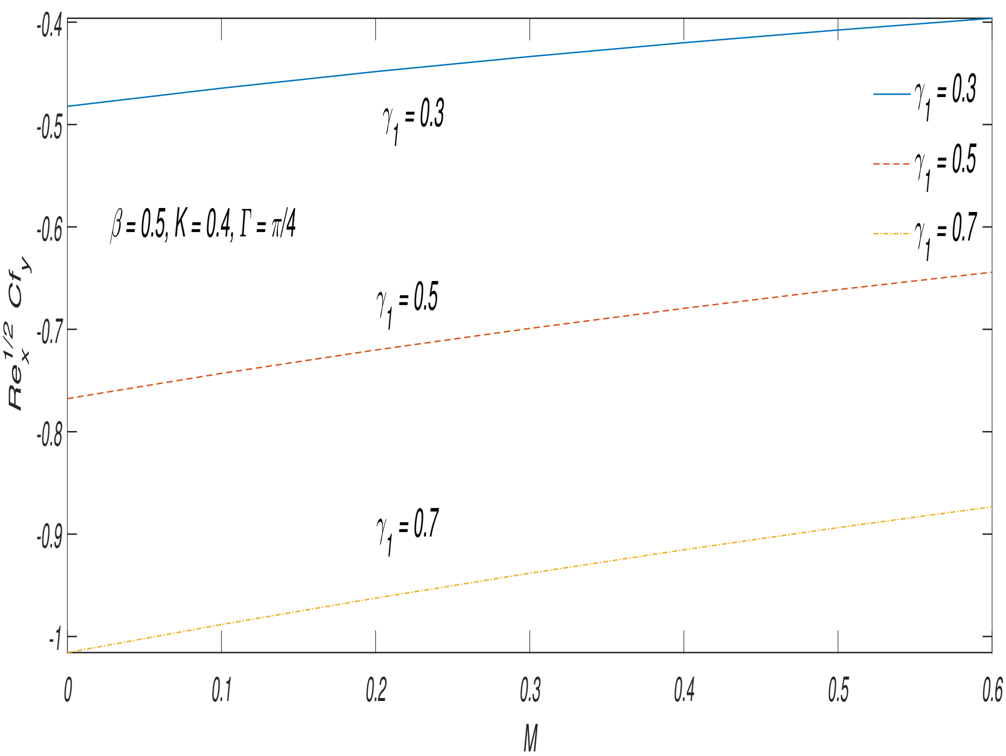

FIGURE 4.29: skin friction Cf_y discrepancy against γ_1 and M

Chapter 5

Conclusion

In this thesis, the work of Archana et al. [31] is reviewed and extended by Cattaneo-Christov double diffusion in the temperature equation and concentration equation as well. Firstly, by using similarity transformation, the momentum, energy and concentartion equations are altered into the ODEs. Through the application of the Shooting technique, numerical solutions for the transformed ODEs have been achieved. Utilizing diverse values for the governing parameters, we showcase the outcomes in the form of Tables and graphs for velocity, temperature, and concentration profiles. Following are the key results of current work:

- Increasing the values of M, the velocity profile $f'(\eta)$ decreases while the temperature distribution increases.
- The temperature distribution is showing decreasing trend by rising the Prandtl number.
- By increasing the values of Schmidt number, an increasing behaviour is observed in concentration distribution.
- Increasing values of the Casson parameter demonstrate an upward trend in both $g(\eta)$ and $\theta(\eta)$.
- The concentration distribution is decreasing on increasing the values of time relaxation parameter of concentration.

- An increase in the temperature distribution is observed as the values of the Eckert number 'Ec' are raised.

- Increasing values of chemical reaction parameter gives a decreasing trend in concentration distribution.

- The temperature distribution is decreasing on increasing the values of time relaxation parameter of temperature.

- By increasing the values of brownian parameter, the Sherwood number decreases, while sherwood number is showing increasing trend by rising the values of thermophoresis parameter.

Bibliography

[1] S. Zhao, X. Xu, and M. Collins, "The numerical analysis of fluid-solid interactions for blood flow in arterial structures part 2: development of coupled fluid-solid algorithms," *Proceedings of the Institution of Mechanical Engineers, Part H: Journal of Engineering in Medicine*, vol. 212, no. 4, pp. 241–252, 1998.

[2] Y. B. Li, Z. Q. Lin, S. J. Hu, and G. L. Chen, "Numerical analysis of magnetic fluid dynamics behaviors during resistance spot welding," *Journal of Applied Physics*, vol. 101, no. 5, 2007.

[3] H. Eisazadeh, M. Hamedi, and A. Halvaee, "New parametric study of nugget size in resistance spot welding process using finite element method," *Materials & Design*, vol. 31, no. 1, pp. 149–157, 2010.

[4] J. Wang, H.-P. Wang, F. Lu, B. E. Carlson, and D. R. Sigler, "Analysis of AL-steel resistance spot welding process by developing a fully coupled multiphysics simulation model," *International Journal of Heat and Mass Transfer*, vol. 89, pp. 1061–1072, 2015.

[5] S. U. Choi and J. A. Eastman, "Enhancing thermal conductivity of fluids with nanoparticles," tech. rep., Argonne National Lab.(ANL), Argonne, IL (United States), 1995.

[6] X.-Q. Wang and A. S. Mujumdar, "A review on nanofluids-part i: theoretical and numerical investigations," *Brazilian Journal of Chemical Engineering*, vol. 25, pp. 613–630, 2008.

[7] C. Yang, W. Li, Y. Sano, M. Mochizuki, and A. Nakayama, "On the anomalous convective heat transfer enhancement in nanofluids: a theoretical answer to the nanofluids controversy," *Journal of Heat Transfer*, vol. 135, no. 5, p. 054504, 2013.

[8] K. Jahani, M. Mohammadi, M. B. Shafii, and Z. Shiee, "Promising technology for electronic cooling: nanofluidic micro pulsating heat pipes," *Journal of Electronic Packaging*, vol. 135, no. 2, p. 021005, 2013.

[9] N. Casson, "Flow equation for pigment-oil suspensions of the printing ink-type," *Rheology of Disperse Systems*, pp. 84–104, 1959.

[10] S. Nadeem, R. Mehmood, and N. S. Akbar, "Oblique stagnation point flow of a Casson-nano fluid towards a stretching surface with heat transfer," *Journal of Computational and Theoretical Nanoscience*, vol. 11, no. 6, pp. 1422–1432, 2014.

[11] A. S. Butt, A. Ali, and A. Mehmood, "Study of flow and heat transfer on a stretching surface in a rotating Casson fluid," *Proceedings of the National Academy of Sciences, India Section A: Physical Sciences*, vol. 85, no. 3, pp. 421–426, 2015.

[12] R. S. R. Gorla and A. J. Chamkha, "Natural convective boundary layer flow over a horizontal plate embedded in a porous medium saturated with a non-Newtonian nanofluid," *International Journal of Microscale and Nanoscale thermal Fluid transport Phenomena*, vol. 2, pp. 211–227, 2011.

[13] S. Shehzad, F. Abbasi, T. Hayat, and F. Alsaadi, "Model and comparative study for peristaltic transport of water based nanofluids," *Journal of Molecular Liquids*, vol. 209, pp. 723–728, 2015.

[14] M. Sheikholeslami, M. Rashidi, T. Hayat, and D. Ganji, "Free convection of magnetic nanofluid considering MFD viscosity effect," *Journal of Molecular Liquids*, vol. 218, pp. 393–399, 2016.

[15] M. Sheikholeslami, "CVFEM for magnetic nanofluid convective heat transfer in a porous curved enclosure," *The European Physical Journal Plus*, vol. 131, no. 11, p. 413, 2016.

[16] M. Sheikholeslami, "CuO-water nanofluid free convection in a porous cavity considering Darcy law," *The European Physical Journal Plus*, vol. 132, no. 1, p. 55, 2017.

[17] M. Sheikholeslami, "Magnetic field influence on nanofluid thermal radiation in a cavity with tilted elliptic inner cylinder," *Journal of Molecular Liquids*, vol. 229, pp. 137–147, 2017.

[18] M. Sheikholeslami, "Influence of Lorentz forces on nanofluid flow in a porous cylinder considering Darcy model," *Journal of Molecular Liquids*, vol. 225, pp. 903–912, 2017.

[19] T. Hayat, M. I. Khan, M. Waqas, and A. Alsaedi, "Newtonian heating effect in nanofluid flow by a permeable cylinder," *Results in Physics*, vol. 7, pp. 256–262, 2017.

[20] C. Wang, "Stretching a surface in a rotating fluid," *Zeitschrift für angewandte Mathematik und Physik ZAMP*, vol. 39, no. 2, pp. 177–185, 1988.

[21] K. Zaimi, A. Ishak, and I. Pop, "Stretching surface in rotating viscoelastic fluid," *Applied Mathematics and Mechanics*, vol. 34, pp. 945–952, 2013.

[22] M. Rashidi, S. Abelman, and N. F. Mehr, "Entropy generation in steady mhd flow due to a rotating porous disk in a nanofluid," *International Journal of Heat and Mass transfer*, vol. 62, pp. 515–525, 2013.

[23] F. Mabood, S. Ibrahim, and W. Khan, "Framing the features of Brownian motion and thermophoresis on radiative nanofluid flow past a rotating stretching sheet with magnetohydrodynamics," *Results in Physics*, vol. 6, pp. 1015–1023, 2016.

[24] S. Das, R. Jana, and O. Makinde, "Transient hydromagnetic reactive Couette flow and heat transfer in a rotating frame of reference," *Alexandria Engineering Journal*, vol. 55, no. 1, pp. 635–644, 2016.

[25] A. O. Ali, O. D. Makinde, and Y. Nkansah-Gyekye, "Numerical study of unsteady mhd Couette flow and heat transfer of nanofluids in a rotating system with convective cooling," *International Journal of Numerical Methods for Heat & Fluid Flow*, vol. 26, no. 5, pp. 1567–1579, 2016.

[26] B. Prasannakumara, B. Gireesha, and P. Manjunatha, "Melting phenomenon in mhd stagnation point flow of dusty fluid over a stretching sheet in the presence of thermal radiation and non-uniform heat source/sink," *International Journal for Computational Methods in Engineering Science and Mechanics*, vol. 16, no. 5, pp. 265–274, 2015.

[27] S. Das, R. Jana, and O. Makinde, "Magnetohydrodynamic free convective flow of nanofluids past an oscillating porous flat plate in a rotating system with thermal radiation and Hall effects," *Journal of Mechanics*, vol. 32, no. 2, pp. 197–210, 2016.

[28] O. D. Makinde and A. S. Eegunjobi, "Entropy analysis of thermally radiating magnetohydrodynamic slip flow of Casson fluid in a microchannel filled with saturated porous media," *Journal of Porous Media*, vol. 19, no. 9, 2016.

[29] M. Sheikholeslami and S. Shehzad, "Thermal radiation of ferrofluid in existence of Lorentz forces considering variable viscosity," *International Journal of Heat and Mass Transfer*, vol. 109, pp. 82–92, 2017.

[30] T. Hayat, T. Muhammad, A. Alsaedi, and M. Alhuthali, "Magnetohydrodynamic three-dimensional flow of viscoelastic nanofluid in the presence of nonlinear thermal radiation," *Journal of Magnetism and Magnetic Materials*, vol. 385, pp. 222–229, 2015.

[31] M. Archana, B. Gireesha, B. Prasannakumara, and R. Gorla, "Influence of nonlinear thermal radiation on rotating flow of Casson nanofluid," *Nonlinear Engineering*, vol. 7, no. 2, pp. 91–101, 2018.

[32] R. W. Fox, A. McDonald, and P. Pitchard, "Introduction to Fluid Mechanics," 2006.

[33] R. Bansal, *A Textbook of Fluid Mechanics*. Firewall Media, 2005.

[34] J. N. Reddy and D. K. Gartling, *The Finite Element Methods in Heat Transfer and Fluid Dynamics*. CRC press, 2010.

[35] P. A. Davidson and A. Thess, *Magnetohydrodynamics*, vol. 418. Springer Science & Business Media, 2002.

[36] M. Gad-el Hak, *Advances in Fluid Mechanics Measurements*, vol. 45. Springer Science & Business Media, 2013.

[37] R. W. Lewis, P. Nithiarasu, and K. N. Seetharamu, *Fundamentals of the Finite Element Methods for Heat and Fluid Flow*. John Wiley & Sons, 2004.

[38] J. Kunes, *Dimensionless Physical Quantities in Science and Engineering*. Elsevier, 2012.

Turnitin Originality Report

The Impact of Cattaneo-Christov Double Diffusion, Thermal Radiation on a Rotating Flow of Casson Nanofluid by Muhammad Samiullah

turnitin

From Ms Theses (CUST Library)

- Processed on 23-Nov-2023 12:15 PKT
- ID: 2236777867
- Word Count: 16255

Graduate Studies Office

18%

Within Limits

Similarity Index
18%
Similarity by Source

Internet Sources:
13%
Publications:
12%
Student Papers:
8%

sources:

1. 1% match (student papers from 17-Feb-2016)
Submitted to Higher Education Commission Pakistan on 2016-02-17

2. 1% match (Frank Hawthorne. "The crystal structure of braithwaiteite", Journal of Coordination Chemistry, 2008)
Frank Hawthorne. "The crystal structure of braithwaiteite", Journal of Coordination Chemistry, 2008

3. 1% match (Internet from 12-Oct-2022)
http://studentsrepo.um.edu.my/11762/2/Nadhirah.pdf

4. 1% match (Internet from 07-Nov-2022)
https://dokumen.pub/applied-mathematics-and-scientific-computing-international-conference-on-advances-in-mathematical-sciences-vellore-india-december-2017-volume-ii-1st-ed-978-3-030-01122-2-978-3-030-01123-9.html

5. < 1% match (student papers from 03-Sep-2021)
Submitted to Higher Education Commission Pakistan on 2021-09-03

6. < 1% match (student papers from 21-Jan-2014)
Submitted to Higher Education Commission Pakistan on 2014-01-21

7. < 1% match (student papers from 22-Feb-2019)
Submitted to Higher Education Commission Pakistan on 2019-02-22

8. < 1% match (student papers from 02-May-2019)
Submitted to Higher Education Commission Pakistan on 2019-05-02

9. < 1% match (student papers from 02-Jan-2015)
Submitted to Higher Education Commission Pakistan on 2015-01-02

10. < 1% match (student papers from 24-Jun-2019)
Submitted to Higher Education Commission Pakistan on 2019-06-24

11. < 1% match (student papers from 27-Dec-2014)
Submitted to Higher Education Commission Pakistan on 2014-12-27

12. < 1% match (student papers from 29-Nov-2018)
Submitted to Higher Education Commission Pakistan on 2018-11-29

13. < 1% match (student papers from 16-Feb-2018)
Submitted to Higher Education Commission Pakistan on 2018-02-16

14. < 1% match (Internet from 02-Feb-2023)
https://thesis.cust.edu.pk/UploadedFiles/MMT183011-Muhammad%20Asif%20Khan.pdf

15. < 1% match (Internet from 15-Jan-2023)
https://thesis.cust.edu.pk/UploadedFiles/Naveeda%20Aziz-MMT153001.pdf